CORA Cork Open Research Archive
Cartlann Taighde Oscailte Chorcaí

Title	Design of bent quantum waveguides via shortcuts to adiabaticity
Authors	Odelli, Manuel
Publication date	2020-12
Original Citation	Odelli, M. 2020. Design of bent quantum waveguides via shortcuts to adiabaticity. MRes Thesis, University College Cork.
Type of publication	Masters thesis (Research)
Rights	© 2020, Manuel Odelli. - https://creativecommons.org/licenses/by-nc-nd/4.0/
Download date	2026-11-06 11:51:23
Item downloaded from	https://hdl.handle.net/10468/11298



UCC
University College Cork, Ireland
Coláiste na hOllscoile Corcaigh

NATIONAL UNIVERSITY OF IRELAND, CORK



ucc

Coláiste na hOllscoile Corcaigh, Éire
University College Cork, Ireland

Design of Bent Quantum Waveguides via Shortcuts to Adiabaticity

by

Manuel Odelli

A thesis submitted in fulfillment of the requirements for

the Master by Research

in the Department of Physics

Supervisor: Dr. Andreas RUSCHHAUPT

Head of Department: Prof. John McInerney

2020

Declaration of Authorship

This is to certify that the work I am submitting is my own and has not been submitted for another degree, either at University College Cork or elsewhere. All external references and sources are clearly acknowledged and identified within the contents. I have read and understood the regulations of University College Cork concerning plagiarism.

Signed: _____

Date: _____

External Examiner

Prof. David Guéry-Odelin - University of Toulouse

Internal Examiner

Prof. Frank H. Peters - University College Cork

Abstract

Quantum waveguides are one of the key components in the developement of quantum technologies that experienced a new surge in popularity in recent years. In quantum computers, quantum particles have to be moved between different sites on a quantum chip through waveguides. The progressive miniaturization of quantum chips requires the waveguides to follow certain paths and so they need to be bent in order to be accomodated onto the chip. If the bending is too abrupt, instabilities are introduced in the system, possibly causing reflection and consequently data loss. This difficulty is usually overcome by adopting the adiabatic approach: the parameter representing the bending needs to vary gently along the waveguide, to prevent disruptive effects. This method, however, cannot be applied in many settings, in particular the ones that need a high degree of compactness. Thus, a new approach that would take into account all the different requirements is needed. "Shortcuts to Adiabaticity" (STA) offers the right platform to improve on adiabatic processes and in this thesis we will apply a protocol based on STA to maximize particle transmission fidelity in geometries where the adiabatic approach cannot be employed.

Aknowledgements

It has been a weird year and the list of people I have to thank is quite packed. I will roll them all in descending order of distance as I do not want to cross anybody. I will start with my family Maria, Maurizio, Gianluca, Andrea and granma Rosa (1484 km). I just miss you all immensely and hope we can rejoin soon. My friend Simone (1481 km), whose passion for good gin is only matched by his perseverance, our pointless discussions are - and always will be - cherished. Andreas, my supervisor (1140 km). Just thank you, the amount of time and effort you put to help me and your patience has been really inspiring. Thank to Anthony Kiely (207 km) who left us and is in a better place now (Dublin); your questions and suggestions have been always welcomed. Thank to Chris (88 km) and Tom (30 km) for the laughs. A special thank to Dave Rea (25 km), heart, soul and cultural guide of the Quantum Optics group that I proud myself to be part of. Thank to all my friends in the wonderful city of Cork, Annalisa, Oscar, Josè and Ransell (all approx 15 km), I cannot wait to have another inconsiderate, imprudent and extremely hilarious night out.

Finally, thanks to Claudia (0 km, in fact she is just dozing in the living room) who has been my anchor during many ups and downs but also my number one fan. I could not have made it without your support.

"*Il y aura, j'espére, des gens qui trouveront leur profit à déchiffrer tout ce gâchis*"

E. Galois

Contents

Declaration of Authorship i

Abstract ii

Aknowledgements iii

1 Introduction 1

2 Atomic Quantum Optics 9

2.1 Two level system 10

2.1.1 Bloch sphere 11

2.1.2 Two level Hydrogen atom 13

2.2 Coupling between two-level system and light 15

2.2.1 Exact Interaction Hamiltonian 15

2.2.2 Dipole approximation 16

2.2.3 Two level approximation 17

2.2.4 Rotating wave approximation 19

2.3 Atom in 2 dimensions 21

2.3.1 Rabi oscillation 21
2.3.2 Red and blue detuning 23
2.4 Optical Waveguides 25
2.4.1 Plane waves Optical Lattice 25
2.4.2 Painted potential 28

3 Shortcuts to Adiabaticity **33**
3.1 Adiabatic theorem 34
3.2 Inverse engineering 39
3.3 Counterdiabatic Driving 41
3.3.1 Application of the Counterdiabatic driving 44
3.4 Invariant-based engineering 46
3.4.1 Application of the invariant-based inverse engineering . . . 50

4 Bent Quantum waveguides **54**
4.1 Straight waveguides 55
4.2 Curved waveguides 57
4.2.1 Arc length parametrisation 58
4.2.2 Frenet-Serret Formulation 59
4.2.3 Hamiltonian in curvilinear coordinates 62

5 Semi-classical Design of Waveguide curvature **67**
5.1 Introduction 67
5.2 Circular bend and adiabatic approach 68
5.3 Classical-based inverse engineering 71

5.3.1 Newton's Equation in curved coordinates 72
5.3.2 Retrieving the curvature from particle trajectory 74
5.3.3 Results with Polynomial from [21] 77
5.4 Results with alternative Polynomials 79
5.4.1 Finding the polynomial 81
5.4.2 Calculation and Results 83
5.5 Robustness 84
5.5.1 Stability against initial displacement 84
5.5.2 Stability against dispersion of velocity 87

6 Quantum implementation of the bent waveguides 93
6.1 Introduction 93
6.2 Split operator method 95
6.3 Potential in Cartesian coordinates 97
6.3.1 Schrödinger equation in dimensionless units 98
6.3.2 Conversion from curvilinear to Cartesian 99
6.4 Fidelity 101
6.5 Results of numerical simulation 103
6.5.1 Circular bend 103
6.5.2 Optimized quantum waveguide 106

7 Summary and future prospects 111
7.1 Conclusion 111
7.2 Outlooks 113

Bibliography **121**

Chapter 1

Introduction

Quantum computing is a relatively novel approach that utilises quantum features, such as state entanglement and superposition, with the purpose of implementing a system able to outperform classical computers [1–4]. The importance of quantum computers resides on the fact that they can run algorithms capable of solving computational problems - deemed to be too time-demanding to be carried out by classical computers - in a reasonable time [5]. Consider for example the Shor algorithm [6], which has been demonstrated to exponentially speed up the factoring of an integer, compared to algorithms implemented on a classical computer.

The building block of quantum computing is the **qubit** [7, 8], the unit of information that can be considered as the quantum counterpart of the classical **bit**. In classical computing, a bit is a logical state that can assume one of only two

values. It is the smallest unit of information and it can be encoded in various physical systems that exist in either of two dinstinct states (for example two distinct voltage levels in an electrical circuit) and which are usually identified by 0 and 1. Furthermore, logic operations can be performed on a single bit as well as on several bits to execute calculations.

Correspondingly, a qubit is any state vector in a two-dimensional Hilbert space, hence we can write a general state as linear combination of two basis vectors. The basis is usually determined by the measurement process but usually the **computational basis** is used: the two basis vectors are denoted as $|0\rangle$ and $|1\rangle$.

A pure qubit is any coherent superposition of the two basis vectors and it is of the form $\alpha|0\rangle + \beta|1\rangle$ where α and β are two complex numbers such that $|\alpha|^2 + |\beta|^2 = 1$. A single qubit can be manipulated with **quantum gates**, mathematically identified by unitary operators that preserve the norm of the qubit and can be represented by 2×2 matrices. Take for example the NOT gate, the truth table for which is - in analogy with the classic logic gate - $|0\rangle \to |1\rangle$ and $|1\rangle \to |0\rangle$. So, for a general qubit

$$\alpha|0\rangle + \beta|1\rangle \xrightarrow{NOT} \alpha|1\rangle + \beta|0\rangle \tag{1.1}$$

and we can identify the NOT gate with a matrix X that acts on the vector's components according to

$$\mathrm{X}\begin{bmatrix}\alpha\\ \beta\end{bmatrix} = \begin{bmatrix}\beta\\ \alpha\end{bmatrix}. \tag{1.2}$$

So the matrix X can be written as

$$\mathrm{X} \equiv \begin{bmatrix} 0 & 1 \\ 1 & 0 \end{bmatrix}. \tag{1.3}$$

The unitarity property differentiates quantum gates from their classic counterparts as every unitary operator is by definition invertible, meaning every quantum gate is reversible by nature, in contrast with classic logic gates. This property is rooted in the fact that the physical realization of a gate is an experimental setup described by a Hamiltonian acting on a qubit for a specific amount of time. The Hamiltonian, according to the Schrödinger equation, generates the time evolution operator which is by definition unitary.

A class of important processes carried out on a single qubit is the **measurement**: considering a general normalized state $\alpha|0\rangle + \beta|1\rangle$, a measurement in the computational basis $\{|0\rangle, |1\rangle\}$ collapses the state yielding exclusively $|0\rangle$ or $|1\rangle$ as results, with probability $|\alpha|^2$ and $|\beta|^2$ respectively. More generally, we can choose any orthogonal basis $\{|v\rangle, |w\rangle\}$ and measure in that basis, by rewriting our state as $|\psi\rangle = \alpha'|v\rangle + \beta'|w\rangle$ and the outcome can be $|v\rangle$ or $|w\rangle$ with probability $|\alpha'|^2$ and $|\beta'|^2$ respectively.

It is also possible to combine multiple qubits to exploit a peculiar quantum trait, termed **entanglement**. Let us take, for simplicity, a state formed only by two qubits and we call the respective underlying Hilbert spaces $\mathcal{H}_A$ and $\mathcal{H}_B$ with $|i\rangle_A$, $|i\rangle_B$ with $i = 0, 1$ their respective computational bases. The combination

of the two qubits is a state vector in the tensor product space $\mathcal{H}_A \otimes \mathcal{H}_B$ and the usual choice for the basis is given by the collection of pure states of the form $|i\rangle_A \otimes |j\rangle_B$. We can use a more compact notation writing $|i\rangle_A \otimes |j\rangle_B$ as $|ij\rangle$ so, for example, the vector $|0\rangle_A \otimes |1\rangle_B$ is written as $|01\rangle$. These four basis states can be written as tensor product of the component system, in contrast with **entangled** states where the two qubits cannot be described independently from each other, and cannot be factored. Notable examples of entangled states are the so-called **Bell states**, defined as

$$\begin{aligned} |\Phi\rangle^{\pm} &= \frac{1}{2}(|00\rangle \pm |11\rangle) \\ |\Psi\rangle^{\pm} &= \frac{1}{2}(|01\rangle \pm |10\rangle). \end{aligned} \tag{1.4}$$

Entangled states are crucial in quantum computation as they make possible applications like quantum teleportation [9–11] and superdense coding [12–14]. These processes are impossible to realize with classical bits and they promise to dramatically improve comunication speed and security.

There are various physical implementations of quantum computers as the information carried by a qubit can be encoded in any two level system, be it photon polarization [15] or the spin of a particle [16], or indeed the internal state of a neutral atom [17].

For the remainder of this work we will focus on the latter. Similarly to classic computers, we would like to have a **central processing unit** (CPU) where operations are performed on a qubit, and a register to store the result of the

calculations. The transmission from the processing region to the memory is achieved by means of **waveguides** [18]: these are potential wells where the qubits are constrained to move along a preferred axis. The passage is of vital importance: it needs to leave the qubit unperturbed to avoid distortion of information but on the other hand, the passage has to be fast enough to minimize decoherence effects which otherwise would cause loss of information. Furthermore, we need just the right amount of flexibility, as the path between the CPU and the memory can be intricate.

To reach this goal, we need quantum techniques to control the system. These need to be stable against error propagation, but at the same time they need to be fast as we want to mitigate decoherence effects arising from the interaction between the state and the environment. Shortcuts to Adiabaticity (STA) [19, 20] meet all the aforementioned features. STA are a collection of protocols designed to drive a system via control of external parameters. In this thesis we want to employ Shortcuts to Adiabaticity to design waveguides capable of channeling particles in a stable and controllable fashion.

This work structure can be summarized as follows:

- chapter 2 will review the theoretical background required to model a qubit interacting with an electromagnetic field. We will start by giving a geometrical representation of the qubit via the Bloch sphere and proceed by describing the interaction Hamiltonian between light and a qubit. This will

lead to the definition of the Rabi frequency, as well as providing the tools to introduce optical lattices that can themselves be exploited to produce waveguides. The chapter is closed by the description of two experimental implementations of how quantum optical waveguides are obtained via the optical lattice approach.

- Chapter 3 will outline the Shortcuts to Adiabaticity technique. Firstly, the adiabatic theorem will be stated and demonstrated. Subsequently, Shortcuts to Adiabaticity will be introduced and we will describe the counter-diabatic and the invariant-based inverse engineering methods. Finally we will conclude by showing two applications of the aformentioned procedures to the same physical system.

- In chapter 4 we will turn our attention to quantum waveguides, starting from a straight waveguide in two dimensions and defining the associated free-particle Hamiltonian. We will then change the geometry of the system, effectively bending the waveguide, applying a smooth transformation that is nothing more than a change of coordinates. The change of coordinates will be reflected in the form assumed by the Hamiltonian that will transform accordingly and a curvature-induced effective potential will arise.

From chapter 5 onwards, we will make use of the concepts explained in previous chapters. In particular, we will apply the Shortcuts to Adiabaticity techniques to the tranformed Hamiltonian with the aim of optimizing the curvature to mini-

mize reflection, thus allowing the particle to be transmitted along the waveguides unperturbed. In particular the chapters will be structured as follows:

- in chapter 5 we will start with a review of the approach by F. Impens, R. Dubosq and D. Guèry-Odelin [21] where a classical mechanics inverse engineering method is used as a starting point to tailor an optimised curvature profile. We will then try to further extend this method and examine the robustness of the obtained curve.

- Chapter 6 will focus on the quantum aspect of this problem: we will employ the results obtained in chapter 5 to evaluate the fidelity of the shape of the waveguide when a quantum particle is involved in the process. In particlular we will outline the computational methods used to numerically solve the corresponding Schrödinger equation and assess the validity of the resulting profile of the waveguide.

- Finally, in chapter 7, we will provide a summary to this thesis and an outlook to future work.

A quick remark about the notation: we will use the caret superscript $\hat{}$ to identify both operators and normal unit vectors and its meaning will be evident from the context. The arrow superscript $\vec{}$ will be used to distinguish vector functions from operators with more than one component, but in both cases the boldface style will be used, to remark the fact that we are dealing with mathematical objects with more than one component. Finally, we will use the

Newton's notation when taking the derivative of a function with respect to the dependent variable. We will write $\dot{f}$ or $\ddot{f}$ for the first and second derivative respectively. In particular, the dependent variable would be either time (t) or the arc length (s), depending on the context.

Chapter 2

Atomic Quantum Optics

Many physical realizations of quantum computers rely on the manipulation of neutral atoms by laser light. In this implementation, qubit information is encoded into two internal electronic states and lasers with specific wavelength are employed to control them [22–24]. In the following sections we will review the underlying theory required to understand the interaction between an atom and light. In particular, we will focus on a two-level atomic quantum system and on how to give a geometric representation of every qubit as an unit vector on a Bloch sphere. We will then turn our attention and explain how an electromagnetic field interacts with a two-level system. This argument will be covered following the semi-classical approach given by Rabi in 1937 [25] which led to the discovery of the then so-called **Rabi Oscillation**. Finally, we will conclude with a review of optical lattices, how they have been implemented in experiments and how they can be used as quantum waveguides.

2.1 Two level system

Even the simplest atom - Hydrogen - has a complex electronic energy structure. In many physical processes, however, only some energy levels are involved, thus an approximation is often performed in order to make the whole framework easier to work with. An atomic state can be represented by a vector in a Hilbert space $\mathcal{H}$, the evolution of which is governed by the Hamiltonian $\hat{H}_A$ and its eigenvectors $\{|\psi_n\rangle\}$ form an orthonormal basis for $\mathcal{H}$. It follows that $\hat{H}_A$ can be rewritten as[1]

$$\hat{H}_A = \sum_n \hbar\omega_n |\psi_n\rangle \langle\psi_n| \tag{2.1}$$

where $\hbar\omega_n$ is the eigenvalue corresponding to the n^{th} eigenvector.

In many systems, only two levels play a significant role in the process. They are usually called the **ground** and the **excited** state and are generally labelled $|0\rangle$ and $|1\rangle$ respectively.

Let $\hbar\omega$ be the energy separation between the two states and suppose they are centered around some reference energy E_0, then we can write

$$\begin{aligned} \hat{H}_A |0\rangle &= (E_0 - \frac{1}{2}\hbar\omega) |0\rangle , \\ \hat{H}_A |1\rangle &= (E_0 + \frac{1}{2}\hbar\omega) |1\rangle . \end{aligned} \tag{2.2}$$

We would like to remark that this formalism can be employed for every system with two levels, wheter it is a $\frac{1}{2}$ spin particle or the electronic state of an atom.

[1] We assume discrete eigenvalues in order to simplify the notation

In the next sections we will give explicit expressions for $\hat{H}_A$, but first we need to rewrite the state and give it a more geometrical representation.

2.1.1 Bloch sphere

Every pure state is a unit vector and can hence be written as a combination of the two basis vectors as

$$|\psi\rangle = c_1 |0\rangle + c_2 |1\rangle , \tag{2.3}$$

where c_1, c_2 are complex numbers such that $|c_1|^2 + |c_2|^2 = 1$.
Since $c_1, c_2 \in \mathbb{C}$ we can write them using the Euler formalism

$$\begin{aligned} c_1 &= \rho_1 e^{i\phi_1}, \\ c_2 &= \rho_2 e^{i\phi_2}, \end{aligned} \tag{2.4}$$

where ϕ_1, ϕ_2, ρ_1, $\rho_2 \in \mathbb{R}$. So we can write

$$\begin{aligned} |\psi\rangle &= c_1 |0\rangle + c_2 |1\rangle \\ &= \rho_1 e^{i\phi_1} |0\rangle + \rho_2 e^{i\phi_2} |1\rangle \\ &= e^{i\phi_1} \left(\rho_1 |0\rangle + \rho_2 e^{i(\phi_2 - \phi_1)} |1\rangle\right). \end{aligned} \tag{2.5}$$

Two vectors in a Hilbert space are equivalent up to an overall phase that can be set freely i.e. $|\psi\rangle \sim |\psi\rangle\, e^{i\xi}$. So by setting $\xi = \phi_1$ we obtain

$$|\psi\rangle = \rho_1 |0\rangle + \rho_2 e^{i(\phi_2 - \phi_1)} |1\rangle . \tag{2.6}$$

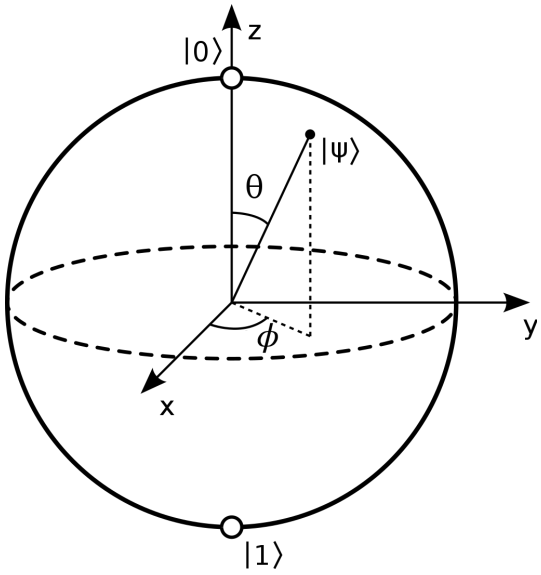


Figure 2.1: Bloch sphere showing a unit vector $|\psi\rangle$ and the two angles that identify it.

The quantity $\phi_2 - \phi_1$ is the relative phase between the two basis states. By naming $\phi = \phi_2 - \phi_1$, we can check that the normalization constrain is satisfied if we take an angle θ such that $\rho_1 = \cos(\theta/2)$ and $\rho_2 = \sin(\theta/2)$ and we can finally write the most general pure state as

$$|\psi\rangle = \cos(\theta/2)\,|0\rangle + e^{i\phi}\sin(\theta/2)\,|1\rangle\,. \tag{2.7}$$

The two variables (θ, ϕ) can be also interpreted as colatitude and longitude in spherical polar coordinates and they specify a point on the surface of the unit $\mathbb{R}^3$ ball as shown in figure 2.1. We can see how every pure state is uniquely identified by the couple (θ, ϕ), provided $\theta \in [0, \pi]$ and $\phi \in [0, 2\pi)$. In particular the two basis states are the two poles of the sphere. The evolution of a state

can then be visualized as a trajectory over the surface of the Bloch sphere. It is possible to extend this argument also to mixed states, which can be represented via density matrices. In this case, though, the state can be pictured as a point that is not bound to lie on the surface anymore, but it can be inside the sphere as well, i.e. it is part of the ball in $\mathbb{R}^3$.

2.1.2 Two level Hydrogen atom

We will now give more physical meaning to the two-level atom encountered earlier and we will show how to use the formalism in a real situation. Specifically, we will deal with a Hydrogen atom composed of an electron and a proton, where the time independent Hamiltonian can be written as

$$\hat{H}\left|\psi\right\rangle = \left[-\frac{\hat{\mathbf{p}}_p^2}{2m_p} - \frac{\hat{\mathbf{p}}_e^2}{2m_e} - \frac{e^2}{4\pi\epsilon_0}\frac{1}{|\vec{\mathbf{r}}_p - \vec{\mathbf{r}}_e|},\right]\left|\psi\right\rangle \tag{2.8}$$

where $\hat{\mathbf{p}}_p$, $\hat{\mathbf{p}}_e$ are the momentum operators - in position representation - for the proton and electron respectively, defined as $\hat{\mathbf{p}} := i\hbar\vec{\boldsymbol{\nabla}}$ with $\vec{\boldsymbol{\nabla}}$ gradient operator expressed in Cartesian coordinates. Moreover, m_p, m_e refer to proton and the eletcron masses, while $\vec{\mathbf{r}}_p, \vec{\mathbf{r}}_e$ are their position vectors and e is the elementary charge. Finally, ϵ_0 is the vacuum permittivity.

This problem has been extensively studied and solved exactly (see for example [26]) by moving to the centre of mass frame of reference. Defining the new

variables as

$$\begin{aligned} M &= m_p + m_e, & \mu &= \frac{m_p m_e}{m_p + m_e}, \\ \hat{\mathbf{P}} &= \hat{\mathbf{p}}_e + \hat{\mathbf{p}}_m, & \hat{\mathbf{p}} &= \frac{m_p}{M}\hat{\mathbf{p}}_e + \frac{m_e}{M}\hat{\mathbf{p}}_p, \\ \vec{\mathbf{R}} &= \frac{m_e\vec{\mathbf{r}}_e + m_p\vec{\mathbf{r}}_p}{m_e + m_p}, & \vec{\mathbf{r}} &= \vec{\mathbf{r}}_p - \vec{\mathbf{r}}_e, \end{aligned} \tag{2.9}$$

we obtain

$$\hat{H} = \frac{\hat{\mathbf{P}}^2}{2M} + \frac{\hat{\mathbf{p}}^2}{2\mu} - \frac{e}{4\pi\epsilon_0}\frac{1}{|\vec{\mathbf{r}}|} = \hat{H}_{CM} + \hat{H}_A, \tag{2.10}$$

with

$$\begin{aligned} \hat{H}_{CM} &= \frac{\hat{\mathbf{P}}^2}{2M}, \\ \hat{H}_A &= \frac{\hat{\mathbf{p}}^2}{2\mu} - \frac{e}{4\pi\epsilon_0}\frac{1}{|\vec{\mathbf{r}}|}. \end{aligned} \tag{2.11}$$

The corresponding time-independent Schrödinger equation $\hat{H}_A |\psi\rangle = E |\psi\rangle$ is solved by obtaining two separable partial differential equations, the solution of which is a combination of Leguerre polynomials and spherical harmonics. One can show that the eigenstates can be labelled by three quantum numbers and they satisfy the equation

$$\hat{H}_A |n, l, m\rangle = E_{n,l} |n, l, m\rangle . \tag{2.12}$$

Hence the Hamiltonian can be rewritten as $\hat{H}_A = \sum_{n,l,m} E_{n,l} |n, l, m\rangle \langle n, l, m|$. It is customary to employ the two-level approximation by considering only two eigenstates of the Hamiltonian and these will be referred to as $|0\rangle$ and $|1\rangle$.

2.2 Coupling between two-level system and light

The aim of this section is to investigate the behaviour of an atom when a beam of laser light is shone on it. In many experiments the wavelength of the laser is fine-tuned in such a way as to produce coupling between the ground and excited state. This is the rationale behind the two-level approximation as explained in the previous section.

2.2.1 Exact Interaction Hamiltonian

When taking into account the electromagnetic field, the effects of the **field vector** $\vec{\mathbf{A}}(\vec{\mathbf{r}}, t)$ and the **scalar potential** $\Phi(\vec{\mathbf{r}}, t)$ need to be included in the Hamiltonian driving the system. The Hamiltonian of two particles interacting with an electromagnetic field is well known in literature [26]: by applying the Coulomb gauge we can write the Hamiltonian for the system as follows

$$\begin{aligned}\hat{H} = &\frac{\hat{\mathbf{p}}_e}{2m_e} - \frac{e}{m_e}\vec{\mathbf{A}}(\vec{\mathbf{r}}_e, t)\hat{\mathbf{p}}_e + \frac{e^2}{2m_e}\vec{\mathbf{A}}^2(\vec{\mathbf{r}}_e, t) \\ &+ \frac{\hat{\mathbf{p}}_p}{2m_p} + \frac{e}{m_p}\vec{\mathbf{A}}(\vec{\mathbf{r}}_p, t)\hat{\mathbf{p}}_p + \frac{e^2}{2m_p}\vec{\mathbf{A}}^2(\vec{\mathbf{r}}_p, t) - \frac{1}{4\pi\epsilon_0}\frac{e^2}{|\vec{\mathbf{r}}_e - \vec{\mathbf{r}}_p|}.\end{aligned} \tag{2.13}$$

We can use the same change of variables (2.9) to obtain the Hamiltonian in the centre of mass frame of reference

$$\hat{H} = \frac{\hat{\mathbf{P}}^2}{2M} + \frac{\hat{\mathbf{p}}^2}{2\mu} - \frac{1}{4\pi\epsilon_0}\frac{e^2}{|\vec{\mathbf{r}}|} - \frac{e}{m_e}\vec{\mathbf{A}}\left(\vec{\mathbf{R}} + \frac{m_p}{M}\vec{\mathbf{r}}, t\right)\left(\frac{m_e}{M}\hat{\mathbf{P}} + \hat{\mathbf{p}}\right)$$
$$+ \frac{e^2}{2m_e}\vec{\mathbf{A}}^2\left(\vec{\mathbf{R}} + \frac{m_p}{M}\vec{\mathbf{r}}, t\right) + \frac{e}{m_p}\vec{\mathbf{A}}\left(\vec{\mathbf{R}} - \frac{m_e}{M}\vec{\mathbf{r}}, t\right)\left(\frac{m_p}{M}\hat{\mathbf{P}} + \hat{\mathbf{p}}\right) + \frac{e^2}{m_p}\vec{\mathbf{A}}^2\left(\vec{\mathbf{R}} - \frac{m_e}{M}\vec{\mathbf{r}}, t\right). \tag{2.14}$$

2.2.2 Dipole approximation

By assuming the dimensions of the atom are much less than the wavelength of the impinging laser (which is usually the case in experiments), we can apply the **dipole approximation**, by virtue of which we can rewrite

$$\vec{\mathbf{A}}\left(\vec{\mathbf{R}} + \frac{m_p}{M}\vec{\mathbf{r}}, t\right) \approx \vec{\mathbf{A}}\left(\vec{\mathbf{R}} - \frac{m_e}{M}\vec{\mathbf{r}}, t\right) \approx \vec{\mathbf{A}}(\vec{\mathbf{R}}, t) \tag{2.15}$$

and obtain the Hamiltonian of a Hydrogen atom coupled to an external electromagnetic field in the dipole approximation as

$$\begin{aligned}\hat{H}_{dip} &= \frac{\hat{\mathbf{P}}^2}{2M} + \frac{\hat{\mathbf{p}}^2}{2\mu} - \frac{1}{4\pi\epsilon_0}\frac{e^2}{|\vec{\mathbf{r}}|} - \frac{e}{\mu}\vec{\mathbf{A}}(\vec{\mathbf{R}}, t)\hat{\mathbf{p}} + \frac{e^2}{2\mu}\vec{\mathbf{A}}^2(\vec{\mathbf{R}}, t) \\ &= \frac{\hat{\mathbf{P}}^2}{2M} + \hat{H}_A - \frac{e}{\mu}\vec{\mathbf{A}}(\vec{\mathbf{R}}, t)\hat{\mathbf{p}} + \frac{e^2}{2\mu}\vec{\mathbf{A}}^2(\vec{\mathbf{R}}, t),\end{aligned} \tag{2.16}$$

where $\hat{H}_A$ is given by (2.11). By means of some mathematical manipulation, we finally obtain

$$\hat{H}_{dip} = \frac{\hat{\mathbf{P}}^2}{2M} + \hat{H}_A + (-e\vec{\mathbf{r}}) \cdot \vec{\mathbf{E}}(\vec{\mathbf{R}}, t) = \frac{\hat{\mathbf{P}}^2}{2M} + \hat{H}_A + \hat{H}_{int} \tag{2.17}$$

where $\hat{H}_{int} = (-e\vec{\mathbf{r}}) \cdot \vec{\mathbf{E}}(\vec{\mathbf{R}}, t)$ with $\vec{\mathbf{E}}(\vec{\mathbf{R}}, t)$ the electric field.

We now want to solve the Schrödinger equation relative to the Hamiltonian $\hat{H}_{dip}$. This corresponds to finding a function $|\psi(t, \vec{\mathbf{R}}, \vec{\mathbf{R}})\rangle$ that satisfies the Schrödinger equation

$$\hat{H}_{dip} \, |\psi(\vec{\mathbf{R}}, \vec{\mathbf{r}}, t)\rangle = i\hbar \frac{\partial}{\partial t} \, |\psi(\vec{\mathbf{R}}, \vec{\mathbf{r}}, t)\rangle \, . \tag{2.18}$$

The $\dfrac{\hat{\mathbf{P}}^2}{2M}$ term in 2.17 will be relevant in the following discussion as we will deal with an atom moving through a laser.

2.2.3 Two level approximation

So far, we have not made any assumption about the infinitely many eigenstates of the Hamiltonian. We want now to simplify the problem even further by considering only two levels of the Hydrogen spectrum, eigenfuctions of the form $\phi_n(\vec{\mathbf{r}})$ (note they depend only on the variable $\vec{\mathbf{r}}$) with $n = 0, 1$. The states are labelled accordingly $|0\rangle$ and $|1\rangle$. These two functions form an orthonormal basis for the respective Hilbert space, hence the identity matrix can be written as

$$\hat{\mathbb{1}} = \sum_{i=0}^{1} |i\rangle \langle i| = |0\rangle \langle 0| + |1\rangle \langle 1| \, . \tag{2.19}$$

Now the following chain of equalities holds.

$$\hat{H}_{int} = \hat{\mathbb{1}}\hat{H}_{int}\hat{\mathbb{1}} = \sum_{k,j} |j\rangle \langle j| (-e\vec{\mathbf{r}}) |k\rangle \langle k| \vec{\mathbf{E}}(\vec{\mathbf{R}}, t). \tag{2.20}$$

Let us focus on the $\langle j| (-e\vec{\mathbf{r}}) |k\rangle$ term, which is an integral of the form

$$\langle j| (-e\vec{\mathbf{r}}) |k\rangle = \int_{\mathbb{R}^3} d^3\vec{\mathbf{r}}\, \phi_j^*(\vec{\mathbf{r}})(-e\vec{\mathbf{r}})\phi_k(\vec{\mathbf{r}}). \tag{2.21}$$

We can clearly see that when j = k, the integral becomes

$$\int_{\mathbb{R}^3} d^3\vec{\mathbf{r}}\, |\phi_j(\vec{\mathbf{r}})|^2(-e\vec{\mathbf{r}}), \tag{2.22}$$

which is identically 0 as the function $|\phi_j(\vec{\mathbf{r}})|^2(-e\vec{\mathbf{r}})$ is a function with odd parity, hence the integral over $\mathbb{R}^3$ is zero. So the only remaining non-zero terms are the ones with j $\neq$ k and expanding (2.20) we obtain

$$\begin{aligned} \hat{H}_{int} &= [|0\rangle \langle 0| (-e\vec{\mathbf{r}}) |1\rangle \langle 1| + |1\rangle \langle 1| (-e\vec{\mathbf{r}}) |0\rangle \langle 0|] \vec{\mathbf{E}}(\vec{\mathbf{r}}, t) \\ &= [-\vec{\boldsymbol{\mu}}_{0,1} |0\rangle \langle 1| - \vec{\boldsymbol{\mu}}_{0,1} |1\rangle \langle 0|] \vec{\mathbf{E}}(\vec{\mathbf{r}}, t). \end{aligned} \tag{2.23}$$

In this case $\vec{\boldsymbol{\mu}}_{0,1} = \langle 0| e\vec{\mathbf{r}} |1\rangle$ is the element of the **dipole operator**, the matrix representation of which is

$$\hat{H}_{int} = \begin{bmatrix} 0 & -\vec{\boldsymbol{\mu}}_{0,1}\vec{\mathbf{E}}(\vec{\mathbf{R}}, t) \\ -\vec{\boldsymbol{\mu}}_{0,1}^*\vec{\mathbf{E}}(\vec{\mathbf{R}}, t) & 0 \end{bmatrix}. \tag{2.24}$$

2.2.4 Rotating wave approximation

We will now assume an incident monochromatic light of frequency ω_l hitting a two-level atom, where the energy gap between ground and excited state is $\hbar\omega$ and, for simplicity, we set the energy of the first level to 0. Thus, we can split the full Hamiltonian as $\hat{H}_{dip} = \hat{H}_0 + \hat{H}_1$ with

$$\hat{H}_0 = \hbar\omega_l \left|1\right\rangle \left\langle 1\right| \tag{2.25}$$

$$\hat{H}_1 = \frac{\hat{\mathbf{P}}^2}{2M} - \hbar(\omega_l - \omega) \left|1\right\rangle \left\langle 1\right| + \hat{H}_{int}, \tag{2.26}$$

We define $\Delta := \omega_l - \omega$ as the detuning frequency. The respective electric field function is

$$\vec{\mathbf{E}}(\vec{\mathbf{R}}, t) = \vec{\mathbf{E}}_0(\vec{\mathbf{R}}) e^{i(\vec{\mathbf{k}}\vec{\mathbf{R}} - \omega_l t)} + \vec{\mathbf{E}}_0(\vec{\mathbf{R}})^* e^{i(-\vec{\mathbf{k}}\vec{\mathbf{R}} + \omega_l t)} \tag{2.27}$$

and we can rewrite the interaction Hamiltonian (2.24) as

$$\begin{aligned}
\hat{H}_{int} &= -\vec{\boldsymbol{\mu}}_{0,1} \left(\vec{\mathbf{E}}_0(\vec{\mathbf{R}}) e^{i(\vec{\mathbf{k}}\vec{\mathbf{R}} - \omega_l t)} + \vec{\mathbf{E}}_0(\vec{\mathbf{R}})^* e^{i(-\vec{\mathbf{k}}\vec{\mathbf{R}} + \omega_l t)} \right) \left|1\right\rangle \left\langle 0\right| \\
&- \vec{\boldsymbol{\mu}}^*_{0,1} \left(\vec{\mathbf{E}}_0(\vec{\mathbf{R}}) e^{i(\vec{\mathbf{k}}\vec{\mathbf{R}} - \omega_l t)} + \vec{\mathbf{E}}_0(\vec{\mathbf{R}})^* e^{i(-\vec{\mathbf{k}}\vec{\mathbf{R}} + \omega_l t)} \right) \left|0\right\rangle \left\langle 1\right| \\
&= -\hbar \left(\Omega(\vec{\mathbf{R}}) e^{-i\omega_l t} + \widetilde{\Omega}(\vec{\mathbf{R}}) e^{i\omega_l t} \right) \left|1\right\rangle \left\langle 0\right| - \hbar \left(\widetilde{\Omega}(\vec{\mathbf{R}})^* e^{-i\omega_l t} + \Omega(\vec{\mathbf{R}})^* e^{i\omega_l t} \right) \left|0\right\rangle \left\langle 1\right|,
\end{aligned} \tag{2.28}$$

where we defined the so called **Rabi frequencies** as follows:

$$\Omega(\vec{\mathbf{R}}) := \frac{\vec{\boldsymbol{\mu}}_{0,1} \cdot \vec{\mathbf{E}}_0(\vec{\mathbf{R}}) e^{i\vec{\mathbf{k}}\vec{\mathbf{R}}}}{\hbar}, \qquad \widetilde{\Omega}(\vec{\mathbf{R}}) := \frac{\vec{\boldsymbol{\mu}}_{0,1} \cdot \vec{\mathbf{E}}_0(\vec{\mathbf{R}})^* e^{-i\vec{\mathbf{k}}\vec{\mathbf{R}}}}{\hbar}. \tag{2.29}$$

We need now to move to the interaction picture via an unitary transformation

$$\hat{H}_{1,I} = \hat{U}_t \, \hat{H}_{int} \, \hat{U}_t^\dagger, \tag{2.30}$$

where the unitary operator $\hat{U}_t$ is of the form

$$\hat{U}_t = e^{i\hat{H}_0 t/\hbar}, \tag{2.31}$$

recalling that $\hat{H}_0$ is time-independent. The Hamiltonian $\hat{H}_1$ expressed in the interaction picture becomes then

$$\begin{aligned} \hat{H}_{1,I} = \frac{\hat{\mathbf{P}}^2}{2M} - \hbar\Delta \left|1\right\rangle \left\langle 1\right| - \hbar \left(\Omega(\vec{\mathbf{R}}) + \widetilde{\Omega}(\vec{\mathbf{R}}) e^{i2\omega_l t}\right) \left|1\right\rangle \left\langle 0\right| \\ - \hbar \left(\widetilde{\Omega}^*(\vec{\mathbf{R}}) e^{-i2\omega_l t} + \Omega^*(\vec{\mathbf{R}})\right) \left|0\right\rangle \left\langle 1\right|. \end{aligned} \tag{2.32}$$

Assuming the frequency of the electric field is close to the transition frequency ω (usually the case in experiments), we have $\Delta \ll \omega_l + \omega$. This implies we can neglect the $e^{\pm i2\omega_l t}$ term as it oscillates much faster than the other term, averaging to zero on any appreciable time scale. So the Hamiltonian with the rotating wave approximation becomes then

$$\hat{H}_{1,I} = \frac{\hat{\mathbf{P}}^2}{2M} - \hbar\Delta \left|1\right\rangle \left\langle 1\right| - \hbar\Omega(\vec{\mathbf{R}}) \left|1\right\rangle \left\langle 0\right| - \hbar\Omega^*(\vec{\mathbf{R}}) \left|0\right\rangle \left\langle 1\right| \equiv \frac{\hat{\mathbf{P}}^2}{2M} - \frac{\hbar}{2} \begin{bmatrix} 0 & \Omega(\vec{\mathbf{R}}) \\ \Omega^*(\vec{\mathbf{R}}) & 2\Delta \end{bmatrix}. \tag{2.33}$$

We have finally found the Hamiltonian of a two-level system interacting with a fast oscillating laser (rotating wave approximation) and with wavelength much

bigger than the size of the atom (dipole approximation).

2.3 Atom in 2 dimensions

Lasers have been used extensively to produce optical waveguides by tuning the intensity and the frequency of the beam that in turn will result in different Hamiltonians (2.33). We will be dealing with planar waveguides in the next chapters, so it is natural to study the behaviour of an atom moving through a 2D region where laser light is shone. We will see in particular how the intensity of the laser can give rise to peculiar effects.

2.3.1 Rabi oscillation

We will start with a laser shining perpendicularly on a plane with constant intensity throughout the region. These two conditions cause the Rabi frequencies to become space independent:

- the perpendicularity feature means $\vec{\mathbf{k}} \cdot \vec{\mathbf{R}} = 0$,
- constant intensity implies $\vec{\mathbf{E}}_0(\vec{\mathbf{R}}) = \vec{\mathbf{E}}_0$.

The Hamiltonian of the system then becomes

$$\hat{H}_{1,I} = -\frac{\hbar^2}{2M}\frac{\partial^2}{\partial x^2} - \frac{\hbar^2}{2M}\frac{\partial^2}{\partial y^2} - \frac{\hbar}{2}\begin{bmatrix} 0 & \Omega \\ \Omega^* & 2\Delta \end{bmatrix}. \tag{2.34}$$

To solve this problem, we need to find a vector that satisties

$$i\hbar\frac{\partial}{\partial t}\begin{pmatrix}\psi_0(x,y,t)\\ \psi_1(x,y,t)\end{pmatrix} = \hat{H}_{1,I}\begin{pmatrix}\psi_0(x,y,t)\\ \psi_1(x,y,t)\end{pmatrix}. \tag{2.35}$$

Since the laser intensity is constant all over the space, we can use an ansatz of the form

$$\begin{pmatrix}\psi_0\\ \psi_1\end{pmatrix} = f(x,y,t)\begin{pmatrix}\chi_0(t)\\ \chi_1(t)\end{pmatrix} \tag{2.36}$$

and inserting it back into (2.35) we obtain two conditions

$$i\hbar\frac{\partial f}{\partial t} = -\frac{\hbar^2}{2M}\frac{\partial^2 f}{\partial x^2} - \frac{\hbar^2}{2M}\frac{\partial^2 f}{\partial y^2}, \tag{2.37}$$

$$i\hbar\frac{\partial}{\partial t}\begin{pmatrix}\chi_0\\ \chi_1\end{pmatrix} = -\frac{\hbar}{2}\begin{bmatrix}0 & \Omega\\ \Omega^* & 2\Delta\end{bmatrix}\begin{pmatrix}\chi_0\\ \chi_1\end{pmatrix}. \tag{2.38}$$

Focusing only on the second equation and recalling that

$$\begin{pmatrix}\chi_0\\ \chi_1\end{pmatrix} = \chi_0(t)\,|0\rangle + \chi_1(t)\,|1\rangle\,, \tag{2.39}$$

we can see how $|\chi_0(t)|^2$ is the probabilty to find the atom in state $|0\rangle$ at time t. And similarly for $|\chi_1(t)|^2$, giving the pobability of finding the atom in quantum state $|1\rangle$.

The solution of equation (2.38) for $\Delta \in \mathbb{R}$, assuming the system starts in the

ground state for $t = 0$ i.e. $\chi_1(0) = 0$, is given by

$$\chi_0(t) = e^{i\Delta t/2}\left[\cos\left(\frac{\Omega_R}{2}t\right) - i\frac{\Delta}{\Omega_R}\sin\left(\frac{\Omega_R}{2}t\right)\right], \tag{2.40}$$

$$\chi_1(t) = e^{i\Delta t/2}\, i\frac{\Omega^*}{\Omega_R}\,\sin\left(\frac{\Omega_R}{2}t\right) \tag{2.41}$$

where

$$\Omega_R = \sqrt{|\Omega|^2 + \Delta^2}. \tag{2.42}$$

So the respective probabilties are

$$|\chi_0(t)|^2 = \cos^2\left(\frac{\Omega_R}{2}t\right) + \frac{\Delta^2}{\Omega_R^2}\sin^2\left(\frac{\Omega_R}{2}t\right), \tag{2.43}$$

$$|\chi_1(t)|^2 = \frac{|\Omega|^2}{\Omega_R^2}\sin^2\left(\frac{\Omega_R}{2}t\right). \tag{2.44}$$

We can also check that if we shine a laser with frequency equal to the energy gap of the two states ($\Delta = 0$), the system will show an oscillatory behaviour. On the other hand, if $\Delta \gg |\Omega|$ equation (2.43) is identically equal to 1, meaning the system will remain in the ground state unperturbed.

2.3.2 Red and blue detuning

In the next example, we will consider a laser arriving perpendicularly onto the xy plane and the intensity of which changes along the plane. For these conditions, the Rabi frequencies change accordingly and we have

$$\Omega(x, y) := \frac{\vec{\boldsymbol{\mu}}_{0,1} \cdot \vec{\mathbf{E}}_0(x, y)}{\hbar}. \tag{2.45}$$

The Schrödinger equation then becomes

$$i\hbar\frac{\partial}{\partial t}\begin{pmatrix}\psi_0(x,y,t)\\ \psi_1(x,y,t)\end{pmatrix} = \left\{-\frac{\hbar^2}{2M}\frac{\partial^2 f}{\partial x^2} - \frac{\hbar^2}{2M}\frac{\partial^2 f}{\partial y^2} - \frac{\hbar}{2}\begin{bmatrix}0 & \Omega(x,y)\\ \Omega^*(x,y) & 2\Delta\end{bmatrix}\right\}\begin{pmatrix}\psi_0(x,y,t)\\ \psi_1(x,y,t)\end{pmatrix}. \tag{2.46}$$

This equation can be rewritten in its component form

$$i\hbar\frac{\partial}{\partial t}\psi_0 = -\frac{\hbar}{2M}\frac{\partial^2\psi_0}{\partial x^2} - \frac{\hbar}{2M}\frac{\partial^2\psi_0}{\partial y^2} - \frac{\hbar}{2}\Omega(x,y)\psi_1, \tag{2.47}$$

$$i\hbar\frac{\partial}{\partial t}\psi_1 = -\frac{\hbar}{2M}\frac{\partial^2\psi_1}{\partial x^2} - \frac{\hbar}{2M}\frac{\partial^2\psi_1}{\partial y^2} - \frac{\hbar}{2}\Omega^*(x,y)\psi_0 - \hbar\Delta\psi_1. \tag{2.48}$$

Assuming now $|\Delta| \gg 1$, equation (2.48) simplifies, giving us the following relation

$$\psi_1 \approx -\frac{1}{2\Delta}\Omega^*(x,y)\psi_0 \tag{2.49}$$

and inserting this result into equation (2.47) we obtain

$$i\hbar\frac{\partial\psi_0}{\partial t} \approx -\frac{\hbar}{2M}\frac{\partial^2\psi_0}{\partial x^2} - \frac{\hbar}{2M}\frac{\partial^2\psi_0}{\partial y^2} + \frac{\hbar}{4\Delta}|\Omega(x,y)|^2\psi_1 = \frac{P^2}{2M} + V(x,y)\psi_1 \tag{2.50}$$

where

$$V(x,y) = \frac{\hbar|\Omega(x,y)|^2}{4\Delta} \tag{2.51}$$

and is called the **effective potential**. We can see that $V(x,y)$ has only a mechanical effect on the system i.e. it will not enable any state transition. In fact, following relation (2.49), it is clear how the excited state has almost zero probability of being populated.

Moreover, from (2.51), we have three different possibile outcomes depending on the detuning frequency

- $\omega_l > \omega \implies V(x,y) > 0$ the potential is repulsive, termed **blue detuning**,
- $\omega_l < \omega \implies V(x,y) < 0$ the potential is attractive, giving **red detuning**,
- $\omega_l \lll \omega$ or $\omega_l \ggg \omega \implies V(x,y) \approx 0$ the laser has no effect on the system.

2.4 Optical Waveguides

2.4.1 Plane waves Optical Lattice

We have already shown how a laser can be employed to create both an attractive or a repulsive potential in section 2.3.2. By overlapping two counter-propagating laser beams we can then produce a standing wave, where an atom can be trapped: take for example two plane waves of the form (we assume constant intensity and polarization for simplicity)

$$\vec{\mathbf{E}}(x,t) = \frac{\vec{\mathbf{E}}_0}{2} e^{\pm ikx - i\omega_l t}. \tag{2.52}$$

The superposition effect of the two interferring waves produces a total electric field, the amplitude of which can be expressed as

$$\vec{\mathbf{E}}_T(x,t) = \cos(kx)\mathrm{Re}\{\vec{\mathbf{E}}_0 e^{-i\omega_l t}\}. \tag{2.53}$$

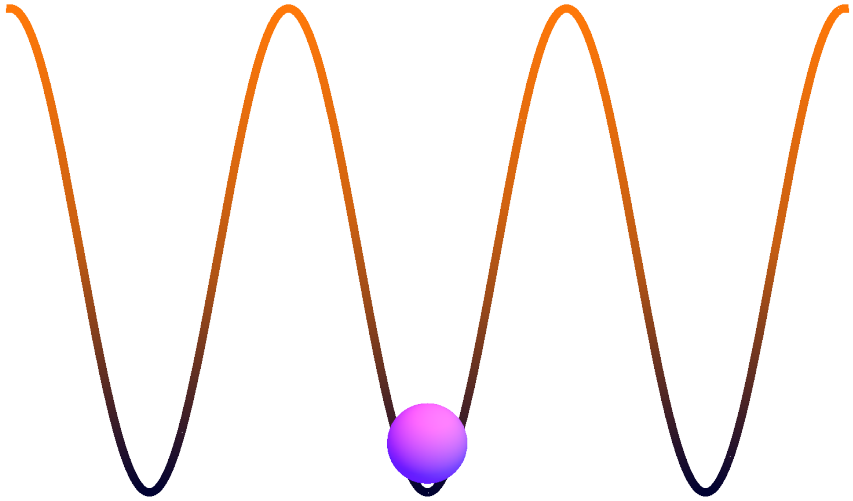


Figure 2.2: Sketch of the optical 1D lattice produced by two identical counter-propagating lasers. The purple sphere represents the particle that can be trapped in every potential minimum.

As previously discussed, if the laser frequency ω_l greatly differs from the transition frequency of the two-state atom ω, i.e. if $|\omega - \omega_l| = |\Delta| \gg 1$, we get an effective potential

$$V(x) = \frac{\hbar|\Omega_0|^2}{4\Delta}\cos^2(kx) \tag{2.54}$$

with $\Omega_0 = \frac{\vec{\mu}\cdot\vec{\mathbf{E}}_0^*}{\hbar}$. The potential (2.54) is periodic and each minimum is effectively a trap. Figure 2.2 shows how a neutral atom can be stored in the evenly spaced traps generated by the overlapping lasers.

We will now extend our argument to examine the effects of lasers in two dimensions. Let us consider four lasers shining perpendicularly to each other as shown in figure 2.3(a). They are two pairs of counter-propagating lasers and for simplicity we assume they lie on the xy plane and they are perpendicular to

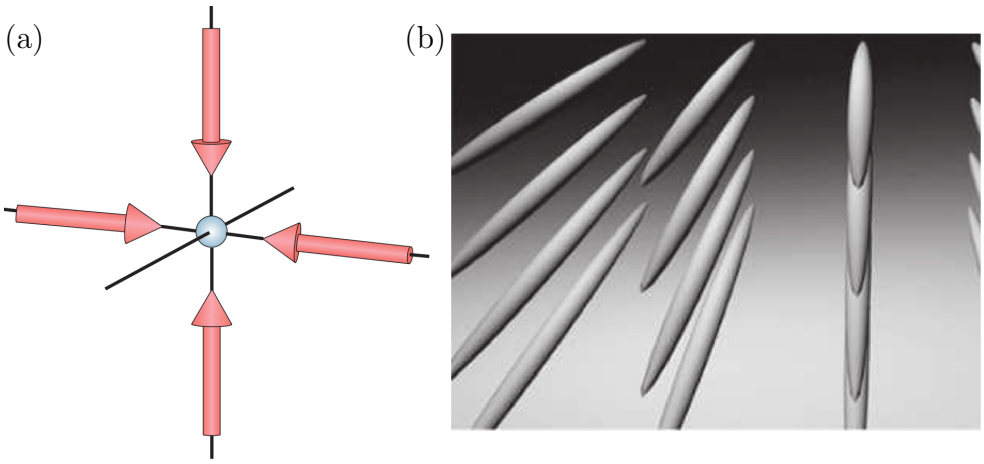


Figure 2.3: Optical lattice formed by superimposing lasers. In figure (a) the diagram of the incoming lasers while figure (b) is a sketch of the resulting lattice of straight tubes. Figures are from [27].

each other. We can see that the in this situation the particle possesses only one spacial degree of freedom, being forced to move linearly along one direction and it is clear how this condition is equivalent to a linear waveguide.

Supposing the relative phase between the lasers on the x direction and the ones along y is ϕ, we can describe the model by means of the following equations (again assuming same intensity and wavevector)

$$\vec{\mathbf{E}}_x(x,t) = \frac{\vec{\mathbf{E}}_0}{2} e^{\pm ikx - i\omega_l t}, \tag{2.55}$$

$$\vec{\mathbf{E}}_y(y,t) = e^{i\phi}\frac{\vec{\mathbf{E}}_0}{2} e^{\pm iky - i\omega_l t} \tag{2.56}$$

and - similarly to (2.53) - the total electric field is

$$\vec{\mathbf{E}}_T(x,y,t) = \Re\{\vec{\mathbf{E}}_0 e^{-i\omega_l t}[\cos(kx) + e^{i\phi}\cos(ky)]\}. \tag{2.57}$$

Finally the optical potential can be written as

$$\begin{aligned} V(x,y,t) &= \frac{1}{4\Delta\hbar}\left(\vec{\boldsymbol{\mu}}_{1,2}\vec{\mathbf{E}}_T(x,y,t)\right)\left(\vec{\boldsymbol{\mu}}_{1,2}\vec{\mathbf{E}}_T(x,y,t)\right)^* \\ &= \frac{1}{4\Delta\hbar}|\vec{\boldsymbol{\mu}}_{1,2}\vec{\mathbf{E}}_0|^2\left(\cos^2(kx)+\cos^2(ky)+e^{i\phi}\cos(ky)+e^{-i\phi}\cos(ky)\right) \\ &= \frac{\hbar}{4\Delta}|\Omega_0|^2\left(\cos^2(kx)+\cos^2(ky)+2\cos(\phi)\cos(ky)\right). \end{aligned} \tag{2.58}$$

An interference factor $2\cos(\phi)\cos(ky)$ arises, depending on the relative phase between the two fields and so the choice of ϕ is crucial in order to obtain different optical lattices, as shown in figure 2.4. From (2.58) we can see that the interference factor $2\cos(\phi)\cos(ky)$ is equal to zero for $\phi = \mathrm{n}\pi/2\,, \mathrm{n} \in \mathbb{Z}$ corresponding to a lattice that shows the same periodicity in both directions.

The mathematical approach to three dimensions is basically an extension of the argument as presented earlier in this section, with the notable difference that, in this case, the particle is confined to one point. This setting corresponds to a crystal lattice and it can be used to simulate real crystal properties by employing only laser light.

2.4.2 Painted potential

The previous section gave a simple - yet useful - description on the approach adopted to generate an optical potential using plane waves with constant intensity over a certain region. While the lattice generated is regular and can be fine-tuned, it does not allow the flexibility required to obtain waveguides of

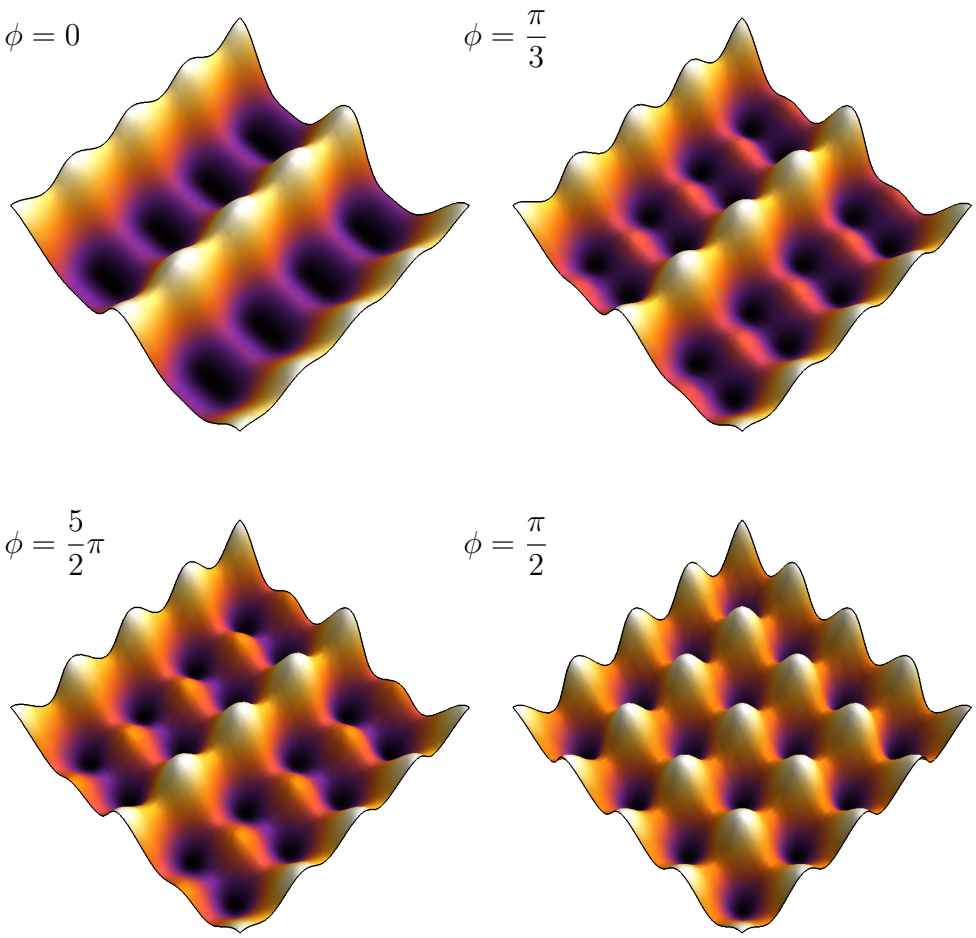


Figure 2.4: Effects on the potential for different relative phase ϕ between the two couples of incoming lasers. It is important to remark that for $\phi = \pi/2$ the lattice is periodic in both x and y direction with the same periodicity.

a particular shape. It is possible, however, to utilize lasers of various shapes, directions and intensities to produce the desired waveguide.

Recently, **painted potentials** have been adopted in many experimental setups [28–31], to give more freedom and new options to design ad hoc potentials. We

will give an overview of two different systems to produce the painted potential. In the first one, a single optical tweezer is moved rapidly to generate a time-avereged potential, while in the second, a Digital Mirror Device (DMD) is used to produce an array of optical tweezers to form an array of traps.

Time averaged optical potential

Optical tweezers are tightly focused laser beams used to trap and move atoms by exerting a net force on their electric dipole - similar to what have been explained in section 2.4.1 - thus enabling one to manipulate particles. In [32], rapidly moving optical tweezers have been used to form waveguides. In these experiment, ^{87}Rb atoms are released in a sheet of light that inhibits movement in one direction. Subsequently, optical tweezers are driven at a frequency greater than the response frequency of the atoms so that the effective trap is stationary with respect to the characteristic timescale of their evolution (see figure 2.5). The motion of the optical tweezers paints a time-averaged potential and the trajectory can be designed in order to obtain the desired waveguide geometry. Figure 2.5 shows how the tweezers are moved in order to force particles to move along a waveguide.

DMD-controlled optical tweezers

A different approach to optical tweezers can be found in [33]. The key component in this experimental approach is the digital mirror device (DMD), an instrument consisting of an array of thousands of micromechanical mirrors (MM). Each MM

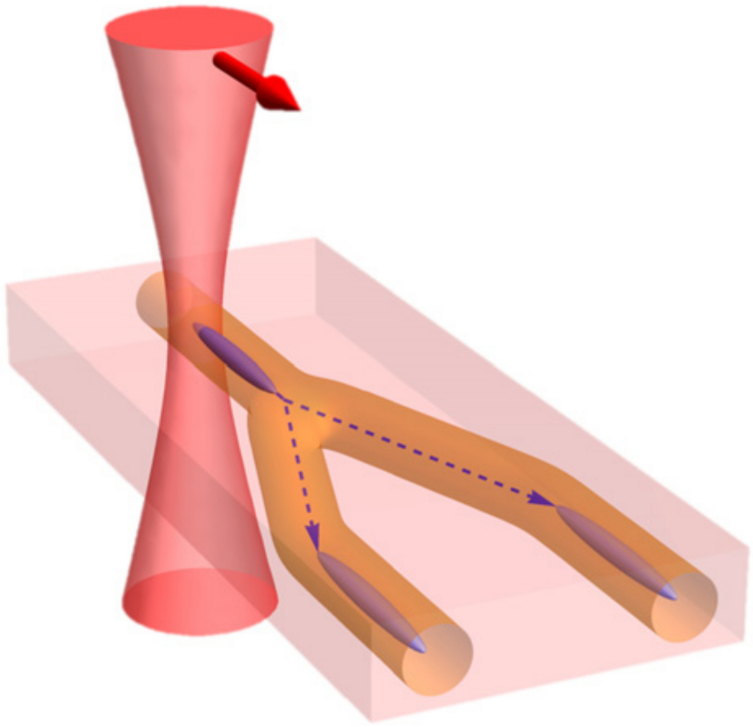


Figure 2.5: Depiction of the tightly focused optical tweezers acting on the sheet of light to produce a time-averaged optical dipole potential with waveguide shape. Figure from [32].

can be independently switched between two angles: when light impinges on a MM it can be reflected in two different directions, depending on the MM angle. Every MM can thus be considered as an on-off switch and collectively the DMD can be set up in order to produce a so-called **holographic mask**. Interposing the DMD between the trapping beam and the target particle generates an array of traps, the position of which on the plane depends on the chosen holographic mask, as in figure 2.6. This technique shows a great amount of freedom and flexibility in relation to the geomerty of the trapping array and it can clearly be

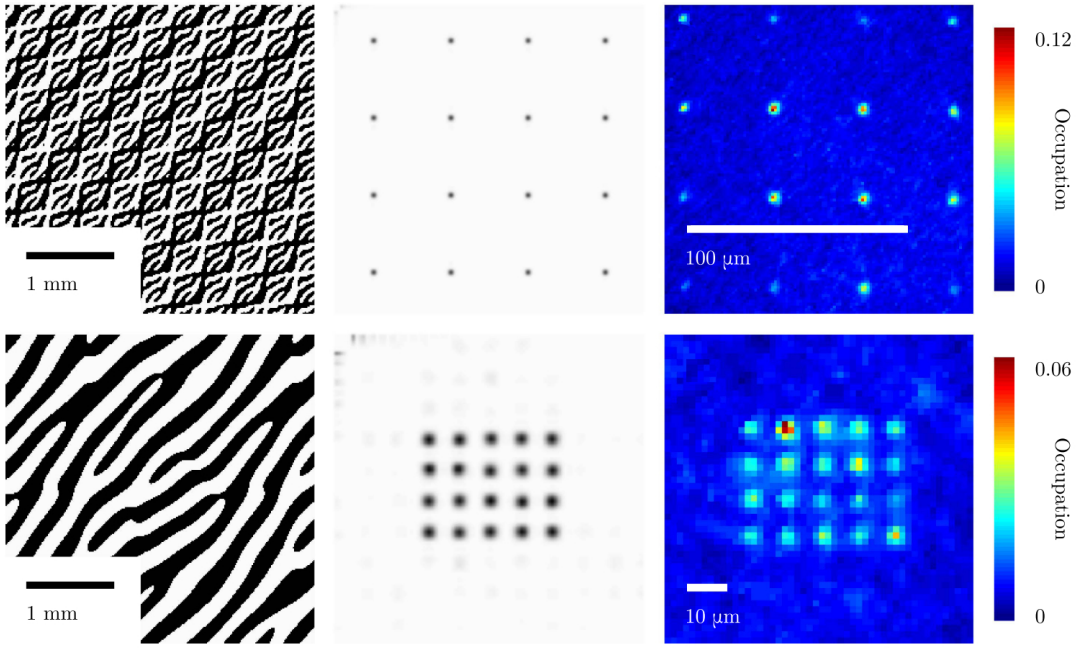


Figure 2.6: Collection of trapping arrays. For each case the holographic masks produced by the DMD, the simulated trapping potentials and fluorescence images of the trapped atoms are shown. Figure extracted from [33].

customised to produce waveguides.

Having reviewed all the relevant properties of qubits and the methods of manipulating them, we will focus our attention next on the theoretical approaches that will exploit the Shortcuts to Adiabaticity (STA) protocols, in order to optimize quantum waveguides. In the next chapter we will give an overview of the STA approach and then apply it to quantum waveguides.

Chapter 3

Shortcuts to Adiabaticity

Shortcuts To Adiabaticity (STA)[19, 20, 34] is a novel blend of different techniques aiming to control the dynamics of a quantum system without relying on the adiabatic approximation. Adiabatic processes require that the time-dependent driving varies slowly with respect to the intrinsic response of the system. STAs want to achieve the same outcomes reached with adiabatic protocols but in a shorter time and with greater robustness, so as to minimize the negative effects of the interaction between the system and the environment (namely decoherence and error accumulation). Some of the STA techniques rely on specific theoretical tools and will be presented later. Still, the common denominator involves finding tunable parameters that can be adjusted to produce the desired final state.

In the next sections two of the most prominent STA protocols will be presented

and covered in some detail, as well as presenting some examples of their application. First,though, we need to prove the **Adiabatic theorem**.

3.1 Adiabatic theorem

The adiabatic theorem was proven by Max Born and Vladimir Fock in 1928 [35] and describes how a system evolves under the action of a slowly varying time-dependent Hamiltonian. In its original version, it was stated as:

"*A physical system remains in its instantaneous eigenstate if a given perturbation is acting on it slowly enough and if there is a gap between the eigenvalue and the rest of the Hamiltonian's spectrum.*"

We assume no degeneracy in the Hamiltonian spectrum, i.e. for every time, there exists a unique eigenvector for a given eigenvalue:

$$\begin{aligned} &\text{If } \exists \left|n(t)\right\rangle, \left|m(t)\right\rangle : \hat{H}(t)\left|n(t)\right\rangle = E(t)\left|n(t)\right\rangle \\ &\text{and } \hat{H}(t)\left|m(t)\right\rangle = E(t)\left|m(t)\right\rangle \forall\, t \implies \left|n(t)\right\rangle = \left|m(t)\right\rangle . \end{aligned} \tag{3.1}$$

In addition, we assume that the set $\{|n(t)\rangle\}$ forms a basis for the underlying Hilbert space at every time. Given these prescriptions, we can write the eigenvalue equation as

$$\hat{H}(t)\left|n(t)\right\rangle = E_n(t)\left|n(t)\right\rangle , \tag{3.2}$$

and the Schrödinger equation is thus given by

$$i\hbar\frac{\partial}{\partial t}\left|\psi(t)\right\rangle = \hat{H}(t)\left|\psi(t)\right\rangle. \tag{3.3}$$

For a constant Hamiltonian, the eigenstates would have acquired a phase of the form $e^{iE_nt/\hbar}$. In this case, however, we have $E_n(t)$ and we need to introduce the **dynamic phase**:

$$e^{i\theta_n(t)}, \text{ where } \theta_n(t) = -\frac{1}{\hbar}\int_0^t d\tau E_n(\tau). \tag{3.4}$$

We can now write the general state as

$$\left|\psi(t)\right\rangle = \sum_n c_n(t)e^{i\theta_n(t)}\left|n(t)\right\rangle \tag{3.5}$$

and substituting it into (3.3) we get

$$\begin{aligned}
i\hbar\frac{\partial}{\partial t}\left|\psi(t)\right\rangle &= i\hbar\frac{\partial}{\partial t}\left(\sum_n c_n(t)e^{i\theta_n(t)}\left|n(t)\right\rangle\right) \\
&= i\hbar\left(\sum_n \dot{c}_n(t)e^{i\theta_n(t)}\left|n(t)\right\rangle - c_n(t)\frac{i}{\hbar}E_n(t)e^{i\theta_n(t)}\left|n(t)\right\rangle c_n(t)e^{i\theta_n(t)}\frac{\partial}{\partial t}\left|n(t)\right\rangle\right) \\
&= \sum_n i\hbar\dot{c}_n(t)e^{i\theta_n(t)}\left|n(t)\right\rangle + c_n(t)e^{i\theta_n(t)}E_n(t)\left|n(t)\right\rangle + i\hbar c_n(t)e^{i\theta_n(t)}\frac{\partial}{\partial t}\left|n(t)\right\rangle,
\end{aligned} \tag{3.6}$$

and

$$\hat{H}(t)\left|\psi(t)\right\rangle = \hat{H}(t)\left(\sum_n c_n(t)e^{i\theta_n(t)}\left|n(t)\right\rangle\right) = \sum_n c_n(t)e^{i\theta_n(t)}E_n(t)\left|n(t)\right\rangle. \quad (3.7)$$

So, combining equations (3.6) and (3.7), we obtain:

$$\begin{aligned}&\sum_n i\hbar\dot{c}_n(t)e^{i\theta_n(t)}\left|n(t)\right\rangle + \cancel{c_n(t)e^{i\theta_n(t)}E_n(t)\left|n(t)\right\rangle} + i\hbar c_n(t)e^{i\theta_n(t)}\frac{\partial}{\partial t}\left|n(t)\right\rangle \\ &= \cancel{\sum_n c_n(t)e^{i\theta_n(t)}E_n(t)\left|n(t)\right\rangle},\end{aligned} \quad (3.8)$$

and we are left with:

$$\begin{aligned}&\sum_n \cancel{i\hbar}\dot{c}_n(t)e^{i\theta_n(t)}\left|n(t)\right\rangle + \cancel{i\hbar}c_n(t)e^{i\theta_n(t)}\frac{\partial}{\partial t}\left|n(t)\right\rangle \\ &= \sum_n e^{i\theta_n(t)}\dot{c}_n(t)\left|n(t)\right\rangle + e^{i\theta_n(t)}c_n(t)\frac{\partial}{\partial t}\left|n(t)\right\rangle = 0.\end{aligned} \quad (3.9)$$

We can now take the inner product between (3.9) and $\langle m(t)|$ and exploit the orthonormality to obtain:

$$\begin{aligned}0 &= \sum_n e^{i\theta_n(t)}\dot{c}_n(t)\left\langle m(t)|n(t)\right\rangle + e^{i\theta_n(t)}c_n(t)\left\langle m(t)\right|\left[\frac{\partial}{\partial t}\left|n(t)\right\rangle\right] \\ &= \sum_n e^{i\theta_n(t)}\dot{c}_n(t)\delta_{m,n} + e^{i\theta_n(t)}c_n(t)\left\langle m(t)\right|\frac{\partial}{\partial t}n(t)\rangle \\ &= e^{i\theta_m(t)}\dot{c}_m(t) + \sum_n e^{i\theta_n(t)}c_n(t)\left\langle m(t)\right|\frac{\partial}{\partial t}n(t)\rangle.\end{aligned} \quad (3.10)$$

This allows us to write a differential equation for $c_m(t)$:

$$\dot{c}_m(t) = -\sum_n e^{i(\theta_n(t)-\theta_n(t))} c_n(t) \langle m(t)| \frac{\partial}{\partial t} n(t)\rangle \,. \tag{3.11}$$

We need now to understand what $\langle m(t)| \frac{\partial}{\partial t} n(t)\rangle$ is. Taking a derivative with respect of time in (3.2) on both sides, we have

$$\begin{aligned} \frac{\mathrm{d}}{\mathrm{d}t}\left(\hat{H}(t)\,|n(t)\rangle\right) &= \frac{\mathrm{d}}{\mathrm{d}t}\left(E(t)\,|n(t)\rangle\right) \\ \dot{\hat{H}}\,|n(t)\rangle + \hat{H}\frac{\partial}{\partial t}\,|n(t)\rangle &= \dot{E}_n(t)\,|n(t)\rangle + E_n(t)\frac{\partial}{\partial t}\,|n(t)\rangle \,. \end{aligned} \tag{3.12}$$

And projecting onto $\langle m(t)|$, with $m \neq n$

$$\begin{aligned} \langle m(t)|\,\dot{\hat{H}}\,|n(t)\rangle + \langle m(t)|\,\hat{H}\frac{\partial}{\partial t}\,|n(t)\rangle &= \dot{E}_n(t)\,\langle m(t)|n(t)\rangle + E_n(t)\,\langle m(t)|\frac{\partial}{\partial t} n(t)\rangle \\ \langle m(t)|\,\dot{\hat{H}}\,|n(t)\rangle + E_m(t)\,\langle m(t)|\frac{\partial}{\partial t} n(t)\rangle &= 0 + E_n(t)\,\langle m(t)|\frac{\partial}{\partial t} n(t)\rangle \,. \end{aligned} \tag{3.13}$$

We can finally rearrange (3.13) and get:

$$\langle m(t)|\frac{\partial}{\partial t} n(t)\rangle = \frac{\langle m(t)|\,\dot{\hat{H}}\,|n(t)\rangle}{E_n(t) - E_m(t)}. \tag{3.14}$$

Now by substituting this result into (3.11), we are left with

$$\dot{c}_m(t) = -c_m(t)\,\langle m(t)|\frac{\partial}{\partial t} m(t)\rangle - \sum_{m\neq n} e^{i(\theta_n(t)-\theta_n(t))} c_n(t) \frac{\langle m(t)|\,\dot{\hat{H}}\,|n(t)\rangle}{E_n(t) - E_m(t)}. \tag{3.15}$$

This is the exact solution of the problem and we can see that there is a non-zero

probability of transition, by virtue of the second term of (3.15).

The adiabatic approximation amounts to neglecting the second part of (3.15) and it can be applied when

$$\frac{\langle m(t)|\,\dot{\hat{H}}\,|n(t)\rangle}{E_n(t)-E_m(t)} \lll \langle m(t)|\frac{\partial}{\partial t}m(t)\rangle \sim \frac{E_m}{\hbar}. \tag{3.16}$$

From a physical standpoint, this requirement translates to the fact that the frequency of variation of the Hamiltonian is negligible when compared to the intrinsic timescale of the whole system. Imposing this approximation on (3.15) we obtain

$$\dot{c}_m(t) = -c_m(t)\,\langle m(t)|\frac{\partial}{\partial t}m(t)\rangle \implies c_m(t) = e^{i\gamma_m(t)}c_m(0) \tag{3.17}$$

$$\text{where } \gamma_m(t) = i\int_0^t d\tau\,\langle m(\tau)|\frac{\partial}{\partial \tau}m(\tau)\rangle\,. \tag{3.18}$$

We can finally prove the claim as expressed at the beginning of the chapter if we can show that in fact γ_m is real, thus conferring an overall phase to the initial state, hence forbidding transitions to different states. We can easily highlight this fact recalling that for every t the state is normalized. Hence the time derivative

has to be zero:

$$
\begin{aligned}
0 = \frac{\partial}{\partial t}\langle n(t)|n(t)\rangle &= \left[\frac{\partial}{\partial t}\langle n(t)|\right]|n(t)\rangle + \langle n(t)|\left[\frac{\partial}{\partial t}|n(t)\rangle\right] \\
&= \left(\langle n(t)|\left[\frac{\partial}{\partial t}|n(t)\rangle\right]\right)^{*} + \langle n(t)|\left[\frac{\partial}{\partial t}|n(t)\rangle\right] \\
&\implies \left(\langle n(t)|\left[\frac{\partial}{\partial t}|n(t)\rangle\right]\right)^{*} = -\langle n(t)|\left[\frac{\partial}{\partial t}|n(t)\rangle\right],
\end{aligned}
\tag{3.19}
$$

meaning γ_m is real.

3.2 Inverse engineering

The term **inverse engineering** refers to an approach geared toward designing a Hamiltonian that will meet certain requirements regarding the dynamics of the system under consideration. Let us focus on closed linear quantum systems of which we need to describe their evolution in time. Recalling the Schrödinger equation, every state $|\psi\rangle$ needs to obey the relation

$$
i\hbar\frac{\partial}{\partial t}|\psi(t)\rangle = \hat{H}|\psi(t)\rangle\,\forall t. \tag{3.20}
$$

Now, we can employ the Schrödinger picture and write every state at a certain time t as a time evolution of the initial state $|\psi(0)\rangle$ in the following way

$$
|\psi(t)\rangle = \hat{U}(t)|\psi(0)\rangle\,. \tag{3.21}
$$

Here $\hat{U}(t)$ is a unitary operator i.e. $\hat{U}(t)\hat{U}^{\dagger}(t) = \hat{U}^{\dagger}(t)\hat{U}(t) = \hat{\mathbb{1}}$ and we can subsitute it back in (3.20), obtaining

$$i\hbar\frac{\partial}{\partial t}\hat{U}(t)\left|\psi(0)\right\rangle = \hat{H}\hat{U}(t)\left|\psi(0)\right\rangle. \tag{3.22}$$

Since $|\psi(0)\rangle$ is a constant state and the above equation has to hold for every state, (3.22) can be rewritten in term of the time evolution operator as

$$i\hbar\frac{\partial}{\partial t}\hat{U}(t) = \hat{H}\hat{U}(t) \longrightarrow i\hbar\dot{\hat{U}}(t) = \hat{H}\hat{U}(t). \tag{3.23}$$

By applying $\hat{U}^{\dagger}(t)$ on both sides of (3.23) and recalling the unitarity of $\hat{U}(t)$, we have

$$\begin{aligned} i\hbar\dot{\hat{U}}(t) &= \hat{H}\hat{U}(t) \\ i\hbar\dot{\hat{U}}(t)\hat{U}^{\dagger}(t) &= \hat{H}\hat{U}(t)\hat{U}^{\dagger}(t) \\ i\hbar\dot{\hat{U}}(t)\hat{U}^{\dagger}(t) &= \hat{H}\,\hat{\mathbb{1}} \\ i\hbar\dot{\hat{U}}(t)\hat{U}^{\dagger}(t) &= \hat{H}. \end{aligned} \tag{3.24}$$

So in the end we have a time-dependent Hamiltonian of the form

$$\hat{H}(t) = i\hbar\dot{\hat{U}}\hat{U}^{\dagger}. \tag{3.25}$$

Our goal is now to design a unitary time evolution operator $\hat{U}(t)$ of the form

$$\hat{U}(t) = \sum_{n} |n(t)\rangle\langle n(0)| \tag{3.26}$$

where the states $|n(t)\rangle$ form a complete basis that need to satisfy a time-dependent Schrödinger equation driven by the Hamiltonian (3.25). In the common framework the Hamiltonian is set at initial and final time: this imposes some boundary conditions that fix $|n(t)\rangle$ at the beginning and at the end of the process. On the other hand, there is still freedom to choose the states that will evolve between the states at initial and final time. Different techniques have been developed according to the choice of set of some instantaneous eigenstates. In particular

- in the **counterdiabatic driving** approach the quantum states $|n(t)\rangle$ are instantaneous eigenstates of a reference Hamiltonian $\hat{H}_0(t)$,
- in **invariant-based engineering**, $|n(t)\rangle$ are eigenstates of the invariant of an assumed Hamiltonian form.

In the following sections those two methods will be covered in detail.

3.3 Counterdiabatic Driving

The counterdiabatic paradigm [36–39] aims to design an inverse-engineered Hamiltonian $\hat{H}(t)$, starting from a reference Hamiltonian $\hat{H}_0(t)$ so that the final dynamics follows exactly the instantaneous eigenstates of $\hat{H}_0(t)$. We will follow Berry's [39] approach to explain the procedure. Recalling section 3.1, if a Hamiltonian

$\hat{H}_0(t)$ that can be written as

$$\hat{H}_0(t) = \sum_n E_n(t) \left|n(t)\right\rangle \left\langle n(t)\right| , \tag{3.27}$$

varies "slowly" in time, we can apply the adiabatic approximation and claim that every state, starting from an eigenstate $|n(0)\rangle$, will remain the same n^{th} eigenstate of $\hat{H}_0$ at every time t and it will acquire an extra time-dependent phase and can hence be written as

$$\left|\psi_n(t)\right\rangle = e^{i\zeta_n(t)} \left|n(t)\right\rangle , \tag{3.28}$$

where

$$\zeta_n(t) = -\frac{1}{\hbar}\int_0^t d\tau E_n(\tau) + i\int_0^t d\tau \left\langle n(\tau)\right| \frac{\partial}{\partial\tau} n(\tau)\rangle . \tag{3.29}$$

We would like to highlight that these states are approximate solutions of an approximate problem. What we would like to find is a Hamiltonian $\hat{H}(t)$ for which the states $|\psi_n(t)\rangle$ are **exact** solutions for $\hat{H}(t)$

$$i\hbar\frac{\partial}{\partial t}\left|\psi_n(t)\right\rangle = \hat{H}(t)\left|\psi_n(t)\right\rangle . \tag{3.30}$$

We need to define a time evolution operator $\hat{U}(t)$ such that the relation (3.25) is satisfied. A clever choice is to set

$$\hat{U}(t) = \sum_n e^{i\zeta_n(t)} \left|n(t)\right\rangle \left\langle n(0)\right| , \tag{3.31}$$

and we are now in a position to calculate $i\hbar\dot{\hat{U}}\hat{U}^\dagger$. We will split the calculation into several parts

$$\begin{aligned} i\hbar\dot{\hat{U}}(t) &= i\hbar\frac{\partial}{\partial t}\sum_n e^{i\zeta_n(t)}\left|n(t)\right\rangle\left\langle n(0)\right| \\ &= i\hbar\sum_n i\dot{\zeta}_n(t)e^{i\zeta_n(t)}\left|n(t)\right\rangle\left\langle n(0)\right| + e^{i\zeta_n(t)}\left|\frac{\partial}{\partial t}n(t)\right\rangle\left\langle n(0)\right|. \end{aligned} \tag{3.32}$$

We need to evaluate $\dot{\zeta}_n(t)$, by differentiating (3.29) (it is just the application of the fundamental theorem of calculus)

$$\dot{\zeta}_n(t) = -\frac{1}{\hbar}E_n(t) + i\left\langle n(t)\right|\frac{\partial}{\partial t}n(t)\rangle\,, \tag{3.33}$$

and by substituting it in (3.32), we get

$$\sum_n e^{i\zeta_n(t)}\left[\left|n(t)\right\rangle E_n(t)\left\langle n(0)\right| - i\hbar\left\langle n(t)\right|\frac{\partial}{\partial t}n(t)\rangle\left|n(t)\right\rangle\left\langle n(0)\right| + i\hbar\left|\frac{\partial}{\partial t}n(t)\right\rangle\left\langle n(0)\right|\right]. \tag{3.34}$$

Now, the only term left to calculate is the adjoint of $\hat{U}(t)$

$$\begin{aligned} &\hat{U}^\dagger(t) = \sum_n e^{(i\zeta_n(t))^*}(\left|n(t)\right\rangle\left\langle n(0)\right|)^\dagger = \sum_n e^{-i\zeta_n^*(t)}\left|n(0)\right\rangle\left\langle n(t)\right| = \\ &\sum_n e^{-i\zeta_n(t)}\left|n(0)\right\rangle\left\langle n(t)\right|. \end{aligned} \tag{3.35}$$

It is easy to check that $\zeta_n^*(t) = \zeta_n(t)$. The first integrand is real by definition, while we have already proved in (3.19) that $\left\langle n(t)\right|\frac{\partial}{\partial t}n(t)\rangle \in \mathbb{R}\ \forall\ \left|n(t)\right\rangle$.

Combining (3.32) and (3.3), we finally obtain

$$\begin{aligned}
&\sum_n e^{i\zeta_n(t)} e^{-i\zeta_n(t)} \Big[|n(t)\rangle E_n(t) \langle n(0)| - i\hbar \langle n(t)| \frac{\partial}{\partial t} n(t)\rangle |n(t)\rangle \langle n(0)| \\
&+ i\hbar |\frac{\partial}{\partial t} n(t)\rangle \langle n(0)| \Big] \cdot \Big[|n(0)\rangle \langle n(t)| \Big] \\
&= \sum_n |n(t)\rangle E_n(t) \langle n(t)| + i\hbar \left[|\frac{\partial}{\partial t} n(t)\rangle \langle n(t)| - \langle n(t)| \frac{\partial}{\partial t} n(t)\rangle |n(t)\rangle \langle n(t)| \right],
\end{aligned} \tag{3.36}$$

where in the second step we used the fact that the states are normalized for every t ($t = 0$ in this case). By comparison, we can rewrite (3.36) as

$$\hat{H}(t) = \hat{H}_0(t) + \hat{H}_{CD}(t), \tag{3.37}$$

where

$$\hat{H}_{CD}(t) = i\hbar \left[|\frac{\partial}{\partial t} n(t)\rangle \langle n(t)| - \langle n(t)| \frac{\partial}{\partial t} n(t)\rangle |n(t)\rangle \langle n(t)| \right] \tag{3.38}$$

is the counterdiabatic Hamiltonian which was being sought.

3.3.1 Application of the Counterdiabatic driving

We will now give an example of the application of the counterdiabatic approach. In particular we will show how to retrieve a counterdiabatic Hamiltonian in a two level system. We will follow the arguments as outlined in [40].

The most general operator in a system with two levels can be written, in matrix

form, as follows

$$\hat{H}_0(t) = \frac{\hbar}{2}\begin{bmatrix} -\Delta(t) & |\Omega(t)|e^{i\alpha(t)} \\ |\Omega(t)|e^{-i\alpha(t)} & \Delta(t) \end{bmatrix}. \tag{3.39}$$

$\hat{H}_0(t)$ can describe a variety of different settings, be it the coupling between two atomic states with a laser or be it a particle with spin 1/2 in a magnetic field. Regardless of the underlying physical system, we can diagonalize (3.39) and recover the two eigenvalues relative to the eigenstates $|\lambda_\pm\rangle$

$$\hat{H}_0(t)\,|\lambda_\pm\rangle = \pm\hbar\frac{\tilde{\Omega}}{2}\,|\lambda_\pm\rangle \quad \text{where } \tilde{\Omega} = \sqrt{\Delta^2 + |\Omega|^2}. \tag{3.40}$$

The instantaneous eigenstates have the form

$$\begin{aligned} |\lambda_-(t)\rangle &= -\sin\left(\frac{\theta(t)}{2}\right)e^{i\alpha(t)/2}\,|0\rangle + \cos\left(\frac{\theta(t)}{2}\right)e^{-i\alpha(t)/2}\,|1\rangle\,, \\ |\lambda_+(t)\rangle &= \cos\left(\frac{\theta(t)}{2}\right)e^{i\alpha(t)/2}\,|0\rangle + \sin\left(\frac{\theta(t)}{2}\right)e^{-i\alpha(t)/2}\,|1\rangle\,, \end{aligned} \tag{3.41}$$

where

- $\theta(t) \equiv \arccos\left(-\dfrac{\Delta(t)}{\tilde{\Omega}}\right)$,
- $|0\rangle\,, |1\rangle$ are the canonical basis vector $\begin{pmatrix} 1 \\ 0 \end{pmatrix}$ and $\begin{pmatrix} 0 \\ 1 \end{pmatrix}$.

Following (3.37) we can write $\hat{H}_{CD}(t) = \hat{H}^{(1)}_{CD}(t) + \hat{H}^{(2)}_{CD}(t)$ with

$$\hat{H}^{(1)}_{CD}(t) = i\hbar \sum_n |\dot{n}\rangle \langle n| \equiv \frac{\hbar}{2} \begin{bmatrix} -\dot{\alpha} & -ie^{i\alpha}\dot{\theta} \\ ie^{-i\alpha(t)}\dot{\theta} & \dot{\alpha} \end{bmatrix},$$

$$\hat{H}^{(2)}_{CD}(t) = -i\hbar \sum_n \langle n(t)|\dot{n}(t)\rangle |n(t)\rangle \langle n(t)| \equiv \frac{\hbar}{2} \cos[\theta]\dot{\alpha} \begin{bmatrix} cos[\theta] & e^{i\alpha}sin[\theta] \\ e^{-i\alpha}sin[\theta] & -cos[\theta] \end{bmatrix}. \tag{3.42}$$

3.4 Invariant-based engineering

The dynamical invariants approach [34, 41–43] is inspired by the work published by Lewis and Riesenfeld [44], where for a time-dependent Hamiltonian $\hat{H}(t)$, an **invariant** is a self-adjoint operator $\hat{I}(t)$ which satisfies

$$\frac{\mathrm{d}\hat{I}}{\mathrm{d}t} = \frac{\partial \hat{I}}{\partial t} + \frac{1}{i\hbar}[\hat{I}, \hat{H}] = 0. \tag{3.43}$$

We can work up the eigenstates for the Hamiltonian starting from the eigenstates of $\hat{I}(t)$. Suppose $\{|n(t)\rangle\}$ is a set of non-degenerate eigenstates for $\hat{I}(t)$ such that

$$\hat{I}(t) |n(t)\rangle = \epsilon_n(t) |n(t)\rangle , \tag{3.44}$$

we can show that the eigenvalues $\{\epsilon_n(t)\}$ are time-independent by differentiating (3.44) (the time dependence is omitted)

$$\frac{\partial \hat{I}}{\partial t} |n\rangle + \hat{I} \frac{\partial}{\partial t} |n\rangle = \frac{\partial \epsilon_n}{\partial t} |n\rangle + \epsilon_n \frac{\partial}{\partial t} |n\rangle . \tag{3.45}$$

Applying (3.43) to $|n\rangle$, we get

$$0 = i\hbar \left[\frac{\partial \hat{I}}{\partial t} + [\hat{I}, \hat{H}] \right] |n\rangle = \frac{\partial \hat{I}}{\partial t} |n\rangle + \hat{I}\hat{H} |n\rangle - \epsilon_n \hat{H} |n\rangle , \tag{3.46}$$

and taking the scalar product with a state $\langle m|$ yields

$$0 = i\hbar \langle m| \frac{\partial \hat{I}}{\partial t} |n\rangle + \langle m| \hat{I}\hat{H} |n\rangle - \langle m| \epsilon_n \hat{H} |n\rangle = i\hbar \langle m| \frac{\partial \hat{I}}{\partial t} |n\rangle + (\epsilon_m - \epsilon_n) \langle m| \hat{H} |n\rangle . \tag{3.47}$$

If $m = n$ we have

$$\langle m| \frac{\partial \hat{I}}{\partial t} |n\rangle = 0. \tag{3.48}$$

Now taking the scalar product of (3.45) with $|n\rangle$, we obtain

$$\begin{aligned} \langle n| \frac{\partial \hat{I}}{\partial t} |n\rangle + \langle n| \hat{I} \frac{\partial}{\partial t} |n\rangle &= \langle n| \frac{\partial \epsilon_n}{\partial t} |n\rangle + \epsilon_n \langle n| \frac{\partial}{\partial t} n\rangle \\ \langle n| \frac{\partial \hat{I}}{\partial t} |n\rangle + \cancel{\epsilon_n \langle n| \frac{\partial}{\partial t} |n\rangle} &= \frac{\partial \epsilon_n}{\partial t} \langle n|n\rangle + \cancel{\epsilon_n \langle n| \frac{\partial}{\partial t} |n\rangle} \\ \langle n| \frac{\partial \hat{I}}{\partial t} |n\rangle &= \frac{\partial \epsilon_n}{\partial t} \\ \implies \frac{\partial \epsilon_n}{\partial t} &= 0. \end{aligned} \tag{3.49}$$

We want now to find a connection between the solutions of the invariant $\hat{I}$ and those of the Hamiltonian $\hat{H}$. To achieve this goal, we will rewrite equation (3.45) with the condition (3.49)

$$(\epsilon_n - \hat{I}) \frac{\partial}{\partial t} |n\rangle = \frac{\partial \hat{I}}{\partial t} |n\rangle . \tag{3.50}$$

The scalar product with $|m\rangle$ gives

$$\begin{aligned} \langle m|(\epsilon_n - \hat{I})|\frac{\partial}{\partial t}n\rangle &= \langle m|\frac{\partial \hat{I}}{\partial t}|n\rangle \\ (\epsilon_n - \epsilon_m)\,\langle m|\frac{\partial}{\partial t}n\rangle &= \langle m|\frac{\partial \hat{I}}{\partial t}|n\rangle\,. \end{aligned} \tag{3.51}$$

We can rewrite the second term of the previous relation using (3.47) to see that

$$\begin{aligned} i\hbar\,\langle m|\,\frac{\partial \hat{I}}{\partial t}\,|n\rangle &= -(\epsilon_m - \epsilon_n)\,\langle m|\hat{H}|n\rangle \\ \langle m|\,\frac{\partial \hat{I}}{\partial t}\,|n\rangle &= \frac{1}{i\hbar}(\epsilon_n - \epsilon_m)\,\langle m|\hat{H}|n\rangle\,. \end{aligned} \tag{3.52}$$

Finally we can subsitute (3.52) into (3.51) obtaining

$$i\hbar(\epsilon_n - \epsilon_m)\,\langle m|\frac{\partial}{\partial t}n\rangle = (\epsilon_n - \epsilon_m)\,\langle m|\hat{H}|n\rangle\,. \tag{3.53}$$

If $m \neq n$ it is clear to see that

$$i\hbar\,\langle m|\frac{\partial}{\partial t}n\rangle = \langle m|\hat{H}|n\rangle\,, \tag{3.54}$$

but we cannot make the same statement if $m = n$ because if $i\hbar\,\langle n|\,\frac{\partial}{\partial t}\,|n\rangle = \langle n|\hat{H}|n\rangle$ would hold, we can deduce that the state $|n\rangle$ is a solution of the Schrödinger equation $i\hbar\frac{\partial}{\partial t}\,|n\rangle = \hat{H}(t)\,|n\rangle$. However, we are still free to choose an overall phase $\alpha_n(t)$ arbitrarily, and define a new set of states

$$|n_\alpha\rangle = e^{i\alpha_n(t)}\,|n\rangle\,. \tag{3.55}$$

These new states will still be eigenstate for $\hat{I}(t)$ but at the same time they will make the relation (3.52) true for every n. We will show that this requirement corresponds to solving a first-order differential equation where $\alpha_n(t)$ is the unkown variable, by examining the following relation

$$\begin{aligned} i\hbar \langle n_\alpha | \frac{\partial}{\partial t} n_\alpha \rangle &= \langle n_\alpha | \hat{H} | n_\alpha \rangle \\ i\hbar \langle e^{-i\alpha_n(t)} n | \frac{\partial}{\partial t} e^{i\alpha_n(t)} n \rangle &= \langle e^{-i\alpha_n(t)} n | \hat{H} | e^{i\alpha_n(t)} n \rangle \\ i\hbar e^{i\alpha_n(t)} \langle n | e^{i\alpha_n(t)} \left[i\frac{\mathrm{d}\alpha_n}{\mathrm{d}t} + \frac{\partial}{\partial t} \right] | n \rangle &= e^{2i\alpha_n(t)} \langle n | \hat{H} | n \rangle \\ \cancel{i\hbar e^{2i\alpha_n(t)}} \left(\langle n | \frac{\mathrm{d}i\alpha_n}{\mathrm{d}t} | n \rangle + \langle n | \frac{\partial}{\partial t} n \rangle \right) &= \cancel{e^{2i\alpha_n(t)}} \langle n | \hat{H} | n \rangle . \end{aligned} \tag{3.56}$$

Rearranging the terms, we finally obtain a first-order differential equation

$$\hbar \frac{\mathrm{d}\alpha_n}{\mathrm{d}t} = \langle n | i\hbar \frac{\partial}{\partial t} - \hat{H} | n \rangle , \tag{3.57}$$

and the integral form for the phase is given by

$$\alpha_n(t) = \frac{1}{\hbar} \int_0^t d\tau \, \langle n | i\hbar \frac{\partial}{\partial \tau} - \hat{H} | n \rangle . \tag{3.58}$$

The overall phase $\alpha_n(t)$ acquired from the state is often called **Lewis-Riesenfeld phase**.

A general solution for the Schrödinger equation can finally be expressed as

$$\psi(t) = \sum_n c_n \left| n \right\rangle_\alpha = \sum_n c_n e^{i\alpha_n(t)} \left| n \right\rangle , \tag{3.59}$$

where the coefficients c_n are time-independent. This approach has been used in its early days to solve the system for a known Hamiltonian. STA try to reverse this idea by designing the Hamiltonian starting from a prescribed state evolution.

3.4.1 Application of the invariant-based inverse engineering

We will apply the invariant engineering protocol to the two level system, as in [42], described by the same Hamiltonian (3.39), albeit written in terms of its real and complex part as follows

$$\hat{H}_0(t) = \frac{\hbar}{2}\begin{bmatrix} -\Delta(t) & \Omega_R(t) - i\Omega_I(t) \\ \Omega_R(t) + i\Omega_I(t) & \Delta(t) \end{bmatrix} \tag{3.60}$$

and the invariant operator can be set as given by

$$\hat{I}(t) = \frac{\hbar}{2}\begin{bmatrix} \cos(\theta(t)) & \sin(\theta(t))e^{-i\alpha(t)} \\ \sin(\theta(t))e^{i\alpha(t)} & -\cos(\theta(t)) \end{bmatrix}. \tag{3.61}$$

The operator can be diagonalized, obtaining two eigenvectors $|\phi_+(t)\rangle$ and $|\phi_-(t)\rangle$ with respective eigenvalues $\pm\frac{\hbar}{2}$ such that

$$|\phi_+(t)\rangle = \begin{pmatrix} \cos(\theta/2)e^{-i\alpha/2} \\ \sin(\theta/2)e^{i\alpha/2} \end{pmatrix}, \tag{3.62}$$

$$|\phi_-(t)\rangle = \begin{pmatrix} \sin(\theta/2)e^{-i\alpha/2} \\ -\cos(\theta/2)e^{i\alpha/2} \end{pmatrix} \tag{3.63}$$

In order to fulfill relation (3.43), the variables θ and α have to satisfy

$$\dot{\theta} = \Omega_I \cos(\alpha) - \Omega_R \sin(\alpha), \tag{3.64}$$

$$\dot{\alpha} = -\Delta - \cot(\theta)\big(\Omega_R \cos(\alpha) + \Omega_I \sin(\alpha)\big). \tag{3.65}$$

As explained in section 3.4, we can write a general solution for the Hamiltonian applying (3.59)

$$|\Psi(t)\rangle = c_+ e^{i\kappa_+(t)} |\phi_+\rangle + c_- e^{i\kappa_-(t)} |\phi_-\rangle , \tag{3.66}$$

where $c_\pm$ are constant complex coefficients and $\kappa_\pm$ are the Lewis-Riesenfeld phases, satisfying (3.58)

$$\dot{\kappa}_\pm = \frac{1}{\hbar} \langle \phi_\pm | i\hbar \frac{\partial}{\partial t} - \hat{H}_0 | \phi_\pm \rangle . \tag{3.67}$$

In particualar, we can set a pure state of the form

$$|\psi(t)\rangle = |\phi_+(t)\rangle \, e^{-i\gamma(t)/2} \text{ where } \gamma(t) = -2\kappa_+ = 2\kappa_-, \tag{3.68}$$

and we can see that

$$\dot{\gamma} = \frac{1}{\sin(\theta)}(\cos(\alpha)\Omega_R + \sin(\alpha)\Omega_I). \tag{3.69}$$

We will employ the settings described up to this point to inverse engineer the Hamiltonian in order to achieve a population inversion, i.e. we want to start in a state

$$|\psi(0)\rangle = \begin{pmatrix} e^{-i\alpha(0)/2} \\ 0 \end{pmatrix} e^{-i\gamma(0)/2}, \tag{3.70}$$

and end up in a state

$$|\psi(T)\rangle = \begin{pmatrix} 0 \\ e^{i\alpha/2} \end{pmatrix} e^{-i\gamma(T)/2}, \tag{3.71}$$

at the end of the process.

Assuming $\theta(t)$, $\alpha(t)$ and $\gamma(t)$ are given and have to fulfill some boundary conditions, we can invert (3.64) and (3.65), obtaining

$$\Omega_R = \cos(\alpha)\sin(\theta)\dot{\gamma} - \sin(\alpha)\dot{\theta}, \tag{3.72}$$

$$\Omega_I = \sin(\alpha)\sin(\theta)\dot{\gamma} + \cos(\alpha)\dot{\theta}, \tag{3.73}$$

$$\Delta = -\cos(\theta)\dot{\gamma} - \dot{\alpha}. \tag{3.74}$$

We hence have found a way to tune the real and imaginary part of the Raby frequency Ω_R, Ω_I respectively, and the detuning frequency Δ to achieve the

desired transition.

This concludes our review of different STA techniques, in the next section we will discuss how to mathematically define waveguides and how the free-particle Hamiltonian changes according to the geometry of the system under consideration.

Chapter 4

Bent Quantum waveguides

Having described the STA techniques we want now to apply them to waveguides. The aim of this chapter is to give a mathematical description of waveguides in order to obtain the Hamiltonian of the system. The Hamiltonian will be the reference upon which Shortcuts to Adiabaticity are based. In the remainder of the work, we will restrict our attention to curved waveguides in two dimensions, starting considering a straight patch and then introducing bending and calculating the effects of the curvature on the free-particle Hamiltonian. We assume a harmonic transverse confinement with constant trapping frequency all along the waveguide. Moreover, all the waveguides in this work will have two external leads that need to be joined by a general curved patch as shown in figure 4.1. In the next sections we will give a geometric characterization of waveguides, showing how they can be described in terms of differentiable curves. We will then perform a change of coordinates moving from Cartesian to curvilinear co-

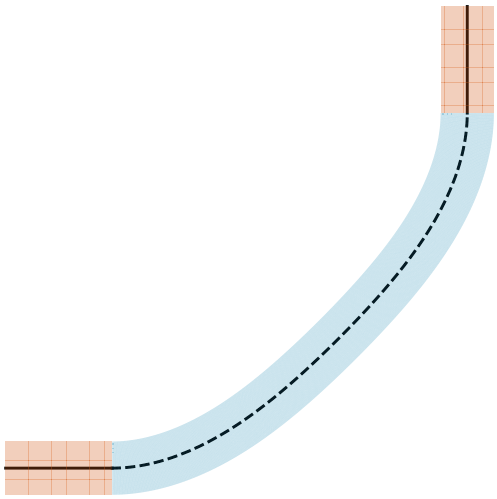


Figure 4.1: Sketch of the prototype of waveguides we will encounter in this work: two straight ends need to be connected by a curved section. Our aim is to design the curve in order to meet all the constraints.

ordinates and finally we will calculate how this transformation is reflected in the Hamiltonian of the system.

4.1 Straight waveguides

As prevously stated, the waveguides considered in this work are formed by two external leads connected by a patch of general shape. Solving the Hamiltonian in the straight regime will give solutions that can be used a reference upon which base further calculations and also will provide boundary conditions the wave functions inside the curved section needs to meet. Let us first consider a straight 2-D waveguide in cartesian coordinates (x, y) with transverse trapping of the form $V(y) = \frac{1}{2}m\omega^2 y^2$, with ω constant along the curve.

The Schrödinger equation of the confined particle is:

$$i\hbar\frac{\partial}{\partial t}\Psi(x,y,t) = \hat{H}\Psi(x,y,t) = \left[-\frac{\hbar^2}{2m}\frac{\partial^2}{\partial x^2} - \frac{\hbar^2}{2m}\frac{\partial^2}{\partial y^2} + \frac{1}{2}m\omega^2 y^2\right]\Psi(x,y,t). \tag{4.1}$$

Since the potential is time-independent, we can separate the wave function into a product of two functions, looking for solutions of the form $\Psi(x,y,t) = \Phi(t)\psi(x,y)$. Hence we are interested in solving the time-independent Schrödinger equation

$$\left[-\frac{\hbar^2}{2m}\frac{\partial^2}{\partial x^2} - \frac{\hbar^2}{2m}\frac{\partial^2}{\partial y^2} + \frac{1}{2}m\omega^2 y^2\right]\psi(x,y) = E\psi(x,y). \tag{4.2}$$

In equation (4.2), x and y are called **longitudinal** and **transverse** coordinates and we can see that it is clearly separable with the solution being a product of travelling waves with longitudinal wavenumber α_n and normalized transverse wave functions $\phi_n(y)$, which are solutions of the one-dimensional harmonic oscillator, with energy ϵ_n

$$\psi_n(x,y) = e^{i\pm\alpha_n x}\phi_n(y), \tag{4.3}$$

$$\phi_n(y) = \left(\frac{m\omega}{\pi\hbar}\right)^{1/4}\frac{1}{\sqrt{2^n n!}}H_n(y)e^{-y^2/2}, \tag{4.4}$$

$$\epsilon_n = \left(n+\frac{1}{2}\right)\hbar\omega, \qquad \alpha_n = \sqrt{k^2-\epsilon_n}, \tag{4.5}$$

where $H_n(y)$ is the Hermite polynomial of order n and $k^2 = 2E/\hbar\omega$. We can see from (4.5) that α_n has to be a real number, otherwise the exponential function in (4.3) will diverge. This condition is met only for $k > \epsilon_n$ for a certain n.

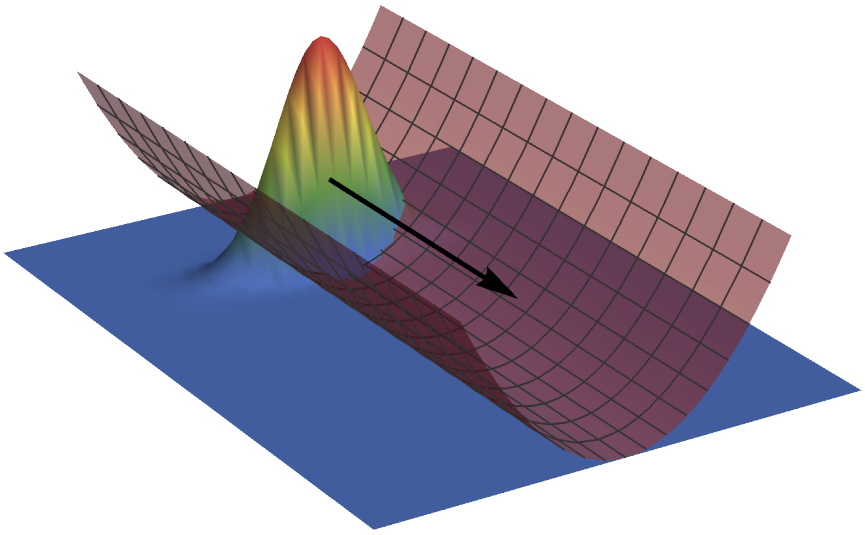


Figure 4.2: Depiction of the potential of a straight 2-D waveguide and the relative wave functionfor $n = 0$.

The situation is summarized in figure 4.2: we now have additional boundary conditions the wave function needs to satisfy when entering and leaving the curved section. In the next section we will build the mathematical framework that will help us in rewriting the Hamiltonian of a bent waveguide.

4.2 Curved waveguides

A curved waveguide can be thought as a trap extending along a curve, with the centre of the trap following its center. In this section we will start by exploring all the relevant features of this curve, starting from different ways of parametrising it and explaining how to define a new set of coordinates that define the curve.

This will help us giving a coordinate transformation that will, in turn, transform the Hamiltonian (4.2) producing an extra attractive potential term.

4.2.1 Arc length parametrisation

A curve in $\mathbb{R}^2$ can be defined parametrically in Cartesian coordinates, as a vector function

$$\vec{\mathbf{\Gamma}} : [a, b] \to \mathbb{R}^2 \qquad \vec{\mathbf{\Gamma}} : t \mapsto \begin{pmatrix} \xi(t) \\ \eta(t) \end{pmatrix} = \xi(t)\hat{\mathbf{x}} + \eta(t)\hat{\mathbf{y}} \tag{4.6}$$

where $[a, b]$ is an interval in $\mathbb{R}$ and $\hat{\mathbf{x}}$, $\hat{\mathbf{y}}$ are the standard unit vectors in the xy directions of the two-dimensional Cartesian plane. For the remainder of the work we will assume that ξ and η are continuosly differentiable functions and that the curve is not self-intersecting. The definition (4.6) is the most general parametrisation of a curve but the most useful one in this case is the **arc length parametrisation**. The arc length is defined as follows:

$$s(t) := \int_0^t d\tau \left|\left|\dot{\vec{\mathbf{\Gamma}}}(\tau)\right|\right| = \int_0^t d\tau \sqrt{\dot{\xi}(\tau)^2 + \dot{\eta}(\tau)^2} \tag{4.7}$$

and we can invert this function to reparameterize the curve $\vec{\mathbf{\Gamma}}(t) \to \vec{\mathbf{\Gamma}}(s)$. Even if this parametrisation seems counterproductive, adding more complexity, we will show that $\left|\left|\dot{\vec{\mathbf{\Gamma}}}(s)\right|\right| = 1$.

From equation (4.7) is clear that:

$$s(a) = 0$$
$$\dot{s}(t) = \left|\left|\dot{\vec{\mathbf{\Gamma}}}(t)\right|\right| > 0 \text{ from the fundamental theorem of calculus.}$$

If we set $L = s(b)$, $s(t)$ is a continuous increasing function, which means it admits an inverse $s^{-1}(t) : [0, L] \to [a, b]$ and the arc length parametrisation is given by $\left(\vec{\mathbf{\Gamma}} \circ s^{-1}\right)(t)$.

We can now evaluate the derivative exploiting the inverse calculus theorem:

$$\frac{\mathrm{d}}{\mathrm{d}t}\left(\vec{\mathbf{\Gamma}} \circ s^{-1}\right)(t) = \dot{\vec{\mathbf{\Gamma}}}(s^{-1}(t))\frac{\mathrm{d}}{\mathrm{d}t}(s^{-1}(t)) = \frac{\dot{\vec{\mathbf{\Gamma}}}(s^{-1}(t))}{\dot{s}(s^{-1}(t))} = \frac{\dot{\vec{\mathbf{\Gamma}}}(s^{-1}(t))}{\left|\left|\dot{\vec{\mathbf{\Gamma}}}(s^{-1}(t))\right|\right|}. \tag{4.8}$$

This will make the calculation easier when moving to the Frenet frame.

4.2.2 Frenet-Serret Formulation

Having a curve $\vec{\mathbf{\Gamma}}(t)$, we can build a curvilinear frame $(\hat{\mathbf{t}}, \hat{\mathbf{n}})$ by taking $\hat{\mathbf{t}}$ to be the unit vector tangent to the curve and subsequently defining $\hat{\mathbf{n}}$ as the unit vector perpendicular to $\hat{\mathbf{t}}$ such that the couple $(\hat{\mathbf{t}}, \hat{\mathbf{n}})$ forms a orthonormal right-handed oriented coordinate system. The tangent unit vector can be easily found to be:

$$\hat{\mathbf{t}}(t) = \frac{\dot{\vec{\mathbf{\Gamma}}}(t)}{\left|\left|\dot{\vec{\mathbf{\Gamma}}}(t)\right|\right|} = \frac{1}{\sqrt{\dot{\xi}(t)^2 + \dot{\eta}(t)^2}}\begin{pmatrix}\dot{\xi}(t)\\ \dot{\eta}(t)\end{pmatrix}. \tag{4.9}$$

To find the vector perpendicular to $\hat{\mathbf{t}}$, we need to find a vector $\hat{\mathbf{n}}$ such that $\hat{\mathbf{t}} \cdot \hat{\mathbf{n}} = 0$ and impose the normalization. It is straightforward to take a vector of the form:

$$\begin{pmatrix} -\dot{\eta}(t) \\ \dot{\xi}(t) \end{pmatrix}, \tag{4.10}$$

so that the normalized vector is

$$\hat{\mathbf{n}}(t) = \frac{1}{\sqrt{\dot{\xi}(t)^2 + \dot{\eta}(t)^2}} \begin{pmatrix} -\dot{\eta}(t) \\ \dot{\xi}(t) \end{pmatrix}. \tag{4.11}$$

As we saw in the previous section, the arc length parametrisation implies $\left|\left|\dot{\vec{\mathbf{\Gamma}}}(s)\right|\right| = 1$, so we can simplify the expression of the coordinate frame axis as:

$$\hat{\mathbf{t}}(s) = \begin{pmatrix} \dot{\xi}(s) \\ \dot{\eta}(s) \end{pmatrix}, \qquad \hat{\mathbf{n}}(s) = \begin{pmatrix} -\dot{\eta}(s) \\ \dot{\xi}(s) \end{pmatrix}. \tag{4.12}$$

Moreover, we can see that the three vectors $\vec{\mathbf{\Gamma}}$, $\hat{\mathbf{t}}$ and $\hat{\mathbf{n}}$ have to obey to three differential equations, the so called Frenet-Serret equations

$$\frac{\mathrm{d}\vec{\mathbf{\Gamma}}(s)}{\mathrm{d}s} = \hat{\boldsymbol{t}}(s), \qquad \frac{\mathrm{d}\hat{\boldsymbol{t}}(s)}{\mathrm{d}s} = \gamma(s)\hat{\boldsymbol{n}}(s), \qquad \frac{\mathrm{d}\hat{\boldsymbol{n}}(s)}{\mathrm{d}s} = -\gamma(s)\hat{\boldsymbol{t}}(s). \tag{4.13}$$

The first one is trivial and it has already been proven. To obtain the remaining two equations, we need to evaluate the derivatives of $\hat{\mathbf{t}}$ and $\hat{\mathbf{n}}$ with respect of the s variable and recall that a vector resulting from the differentiation of another vector is always perpendicular to the initial one. So for example, the derivation

of $\hat{\mathbf{t}}$ yields:

$$\frac{\mathrm{d}}{\mathrm{d}s}\begin{pmatrix}\dot{\xi}(s)\\ \dot{\eta}(s)\end{pmatrix} = \begin{pmatrix}\ddot{\xi}(s)\\ \ddot{\eta}(s)\end{pmatrix}. \tag{4.14}$$

The vector $\dfrac{\mathrm{d}\hat{\mathbf{t}}}{\mathrm{d}s}$ is perpendicular to $\hat{\mathbf{t}}$, therefore parallel to $\hat{\mathbf{n}}$ and can thus be written as

$$\begin{aligned}\left(\frac{\mathrm{d}\hat{\mathbf{t}}(s)}{\mathrm{d}s}\cdot\hat{\mathbf{n}}(s)\right)\hat{\mathbf{n}}(s) &= \begin{pmatrix}\ddot{\xi}(s)\\ \ddot{\eta}(s)\end{pmatrix}^{\top}\cdot\begin{pmatrix}-\dot{\eta}(s)\\ \dot{\xi}(s)\end{pmatrix}\hat{\mathbf{n}}(s) = \\ \left[\dot{\xi}(s)\ddot{\eta}(s)-\ddot{\xi}(s)\dot{\eta}(s)\right]\hat{\mathbf{n}}(s).&\end{aligned} \tag{4.15}$$

Finally, we can retrieve the second equation of (4.13) by setting

$$\gamma(s) := \dot{\xi}(s)\ddot{\eta}(s) - \ddot{\xi}(s)\dot{\eta}(s), \tag{4.16}$$

where $\gamma(s)$ is called **signed curvature** of $\vec{\mathbf{\Gamma}}(s)$. We can obtain similarly the third Frenet-Serret equation by using the same argument for the derivative of $\hat{\mathbf{n}}$.

Every point $\vec{\mathbf{P}} = (X, Y)$ in $\mathbb{R}^2$ can now be described in terms of the new coordinates (s, u) via the following coordinate trasformation:

$$\vec{\mathbf{P}}(s,u) = \vec{\mathbf{\Gamma}}(s) + u\hat{\mathbf{n}}(s), \qquad \begin{pmatrix}X(s,u)\\ Y(s,u)\end{pmatrix} = \begin{pmatrix}\xi(s)-\dot{\eta}(s)u\\ \eta(s)+\dot{\xi}(s)u\end{pmatrix}. \tag{4.17}$$

Having shown how to express the coordinate transformation from Cartesian to curvilinear frame of reference, we are now ready to evaluate how this change of

coordinates affects the Hamiltonian (4.2), in particular the kinetic energy terms $\frac{\partial^2}{\partial x^2}$ and $\frac{\partial^2}{\partial y^2}$.

4.2.3 Hamiltonian in curvilinear coordinates

A waveguide that extends along a curve is conveniently described by means of its axis. This induces the coordinate transformation (4.17) that modifies the geometry of the system and consequently modifies the form of the Hamiltonian (4.2). The trapping potential in curvilinear coordinates can be easily rewritten as a quadratic function of the transverse coordinate u, while more calculation needs to be undertaken in order to exprees the kinetic operator

$$\hat{T} := -\frac{\hbar^2}{2m}\left(-\frac{\partial^2}{\partial x^2} - \frac{\partial^2}{\partial y^2}\right) = -\frac{\hbar^2}{2m}\Delta \tag{4.18}$$

in the new frame of reference.

To evaluate how a differential operator acts in different coordinates, we need to obtain the metric tensor $\mathbf{G}$ for the new system, which encapsulates the geometry in this new frame of reference. In this case $\mathbf{G}$ assumes the form of a 2×2 matrix with elements g_{ij} $i, j = 1, 2$ and it can be connected with the metric tensor $\mathbf{E}$ of the system expressed in Cartesian coordinates via the following relation

$$\mathbf{G} = \mathbf{J}^\top \mathbf{E}\, \mathbf{J}, \tag{4.19}$$

where $\mathbf{J}$ is the Jacobian of the transformation, defined as:

$$\mathbf{J} = \begin{bmatrix} \dfrac{\partial X}{\partial s} & \dfrac{\partial X}{\partial u} \\ \dfrac{\partial Y}{\partial s} & \dfrac{\partial Y}{\partial u} \end{bmatrix} = \begin{bmatrix} \dot{\xi} - \ddot{\eta}u & -\dot{\eta} \\ \dot{\eta} + \ddot{\xi}u & +\dot{\xi} \end{bmatrix}. \tag{4.20}$$

In this case also, the metric tensor $\mathbf{E}$ is nothing more that the identiy matrix $\mathbb{1}_2$, hence the new metric tensor can be easily calculated

$$\mathbf{G} = \mathbf{J}^\top \mathbf{J} = \begin{bmatrix} (1-u\gamma)^2 & 0 \\ 0 & 1 \end{bmatrix}. \tag{4.21}$$

The metric tensor $\mathbf{G}$ is diagonal as expected, considering that the Frenet-Serret system is othonormal. Furthermore, it simplifies the calculation of the Laplacian operator Δ that can be expressed in the new coordinates using the following relation

$$\Delta = \frac{1}{\sqrt{g}} \sum_i \frac{\partial}{\partial x_i} \left(\frac{\sqrt{g}}{g_{ii}} \frac{\partial}{\partial x_i} \right) = \frac{1}{\sqrt{g}} \left[\frac{\partial}{\partial s} \left(\frac{\sqrt{g}}{g_{11}} \frac{\partial}{\partial s} \right) + \frac{\partial}{\partial u} \left(\frac{\sqrt{g}}{g_{22}} \frac{\partial}{\partial u} \right) \right], \tag{4.22}$$

where g is the determinant of $\mathbf{G}$, easily found to be $(1-u\gamma)^2$.

We are finally ready to write the Laplacian operator in curvilinear coordinates as:

$$\Delta = \frac{1}{1-u\gamma} \left[-\frac{\partial}{\partial s} \left(\frac{1}{1-u\gamma} \frac{\partial}{\partial s} \right) - \frac{\partial}{\partial u} \left((1-u\gamma) \frac{\partial}{\partial u} \right) \right]. \tag{4.23}$$

The change of coordinates affects also the way integrals are evaluated. In par-

ticular, having a normalized wave function $\psi(x, y)$:

$$\int dxdy \, ||\psi(x,y)||^2 = \int \mathrm{Det}(\mathbf{J}) dsdu \, ||\psi(s,u)||^2 = \int dsdu(1-\gamma u) \, ||\psi(s,u)||^2 \,, \tag{4.24}$$

and we can see that it is convenient to use $\psi(s,u) = \dfrac{\phi(s,u)}{\sqrt{1-u\gamma}}$.

Using the prescriptions mentioned above, we can now evaluate how the Hamiltonian changes. The calculations will be carried out with respect to each variable.

Dependence on u

Taking into account only the part of the Hamiltonian dependent o u, we obtain:

$$\begin{aligned}
&\frac{1}{1-u\gamma}\frac{\partial}{\partial u}(1-u\gamma)\frac{\partial}{\partial u}\frac{\phi}{\sqrt{1-u\gamma}} \\
&= \frac{1}{1-u\gamma}\frac{\partial}{\partial u}(1-u\gamma)\left(\frac{\gamma\phi}{2(1-u\gamma)^{3/2}} + \frac{1}{\sqrt{1-u\gamma}}\frac{\partial\phi}{\partial u}\right) \\
&= \frac{1}{1-u\gamma}\frac{\partial}{\partial u}\left(\frac{-\gamma\phi}{2\sqrt{1-u\gamma}} + \sqrt{1-u\gamma}\frac{\partial\phi}{\partial u}\right) \\
&= \frac{1}{1-u\gamma}\left(\frac{\gamma^2\phi}{4(1-u\gamma)^{3/2}} + \cancel{\frac{\gamma}{2\sqrt{1-u\gamma}}\frac{\partial\phi}{\partial u}} - \cancel{\frac{\gamma}{2\sqrt{1-u\gamma}}\frac{\partial\phi}{\partial u}} + \sqrt{1-u\gamma}\frac{\partial^2\phi}{\partial u^2}\right) \\
&= \frac{\gamma^2}{4(1-u\gamma)^2}\frac{\phi}{\sqrt{1-u\gamma}} + \frac{1}{\sqrt{1-u\gamma}}\frac{\partial^2\phi}{\partial u^2}.
\end{aligned} \tag{4.25}$$

Dependence on s

We need to evaluate only the part dependent on the s variable:

$$\begin{aligned}
&\frac{1}{1-u\gamma}\frac{\partial}{\partial s}\left(\frac{1}{1-u\gamma}\right)\frac{\partial}{\partial s}\frac{\phi}{\sqrt{1-u\gamma}} \\
&= \frac{1}{1-u\gamma}\frac{\partial}{\partial s}\left(\frac{1}{1-u\gamma}\right)\left(\frac{u\dot{\gamma}\phi}{2(1-u\gamma)^{3/2}} + \frac{1}{\sqrt{1-u\gamma}}\frac{\partial\phi}{\partial s}\right) \\
&= \frac{1}{1-u\gamma}\frac{\partial}{\partial s}\left(\frac{u\dot{\gamma}\phi}{2(1-u\gamma)^{5/2}} + \frac{1}{(1-u\gamma)^{3/2}}\frac{\partial\phi}{\partial s}\right) \\
&= \frac{1}{1-u\gamma}\left(\frac{5}{4}\frac{u^2\dot{\gamma}^2\phi}{(1-u\gamma)^{7/2}} + \frac{u\ddot{\gamma}\phi}{2(1-u\gamma)^{5/2}} + \frac{2u\dot{\gamma}}{(1-u\gamma)^{5/2}}\frac{\partial\phi}{\partial s} + \frac{1}{(1-u\gamma)^{3/2}}\frac{\partial^2\phi}{\partial s^2}\right) \\
&= \left(\frac{5}{4}\frac{u^2\dot{\gamma}^2}{(1-u\gamma)^4} + \frac{u\ddot{\gamma}}{2(1-u\gamma)^3}\right)\frac{\phi}{\sqrt{1-u\gamma}} + \frac{1}{\sqrt{1-u\gamma}}\left(\frac{2u\dot{\gamma}}{(1-u\gamma)^3}\frac{\partial\phi}{\partial s} + \frac{1}{(1-u\gamma)^2}\frac{\partial^2\phi}{\partial s^2}\right) \\
&= \left(\frac{5}{4}\frac{u^2\dot{\gamma}^2}{(1-u\gamma)^4} + \frac{u\ddot{\gamma}}{2(1-u\gamma)^3}\right)\frac{\phi}{\sqrt{1-u\gamma}} + \frac{1}{\sqrt{1-u\gamma}}\left(\frac{\partial}{\partial s}\frac{1}{(1-u\gamma)^2}\frac{\partial\phi}{\partial s}\right).
\end{aligned} \tag{4.26}$$

Eventually, by joining equations (4.25) and (4.26) we obtain:

$$\begin{aligned}
&\Delta\left(\frac{1}{\sqrt{1-u\gamma}}\phi(s,u)\right) \\
&= \frac{1}{\sqrt{1-u\gamma}}\left[-\frac{\partial}{\partial s}\frac{1}{(1-u\gamma)^2}\frac{\partial}{\partial s} - \frac{\partial^2}{\partial u^2} + V(s,u)\right]\phi(s,u) &(4.27)\\
&= \frac{1}{\sqrt{1-u\gamma}}E\phi(s,u), &(4.28)
\end{aligned}$$

and we can see how the $\dfrac{1}{\sqrt{1-u\gamma}}$ term can be cancelled out from equation (4.27) and (4.28). Furthermore, $V(s,u)$ is called **induced potential** given by:

$$V(s,u) := -\frac{\gamma^2}{4(1-u\gamma)^2} - \frac{u\ddot{\gamma}}{2(1-u\gamma)^3} - \frac{5}{4}\frac{u^2\dot{\gamma}^2}{(1-u\gamma)^4}. \tag{4.29}$$

To summarize: beginning with the time-independent Schrödinger equation in

Cartesian coordinates (4.1), we moved to a different frame of reference, the origin of which lies on a curve and obtained the Hamiltonian $\hat{H}_{curv}$ in curved coordinates

$$\hat{H}_{curv} := \frac{\hbar^2}{2m}\left[-\frac{\partial}{\partial s}\frac{1}{(1-u\gamma)^2}\frac{\partial}{\partial s} - \frac{\partial^2}{\partial u^2} + V(s,u)\right] + \frac{1}{2}m\omega^2 u^2. \tag{4.30}$$

A new attractive potential $V(s,u)$ appears due to the change of geometry but the form of the harmonic trapping is maintained as we can see from the last term in (4.30).

Having shown how the geometry of the system is reflected in the Hamiltonian and we are now ready to apply the STA approach in this particular setting.

Chapter 5

Semi-classical Design of Waveguide curvature

5.1 Introduction

In the previous chapters we gave an overview of quantum waveguides and characterized the mathematical framework needed to describe the behaviour of a particle in curved geometry.

In this chapter we will be presented with the following problem: two straight ends separated by an angle α and our goal is to connect the two parts to enable transmission, minimizing the transverse excitation of the outcoming particle.

The natural choice would be to have the two parts connected by an arc of a circle, but we will show that a constant radius generates instabilities in the

particle. To overcome this effects we will reverse engineer the curvature of the bent section using a semi-classical approach introduced by Impens, Dubosq and Guéry-Odelin in [21]. We will then try to expand this method even further in order to optimize the performances of the waveguide.

In the next section, we will look at the reference case of a circular bend connecting two straight ends.

5.2 Circular bend and adiabatic approach

As stated earlier, the simplest candidate to connect two straight sections forming an angle α is a portion of a circle of radius R. We can set $\alpha = \pi/2$, corresponding to the situation depicted in figure 5.1. Recalling (4.30), we need a function of the curvature $\gamma_c(s)$ with respect of the arc length. The curvature is defined as the inverse of the radius of the osculating circle at every point: $\gamma_c(s) = 1/R(s)$. In this case, the radius is constant, so the curvature is a step function of the form

$$\gamma_c(s) = \begin{cases} 1/R & \text{if } s \in [0, R\alpha] \\ 0 & \text{otherwise} \end{cases} , \tag{5.1}$$

and the external potential is a sum of the trapping potential $V_\perp(u)$ and the induced potential $V(s,u)$ (4.29) that change accordingly, becoming

$$V_\perp(u) + V(s,u) = \frac{1}{2}m\omega^2 u^2 - \frac{(\gamma_c)^2}{4(1-u\gamma_c)^2} - \cancel{\frac{u\ddot{\gamma}_c}{2(1-u\gamma_c)^3}} - \frac{5}{4}\cancel{\frac{u^2\dot{\gamma}_c^{\,2}}{(1-u\gamma_c)^4}} \tag{5.2}$$

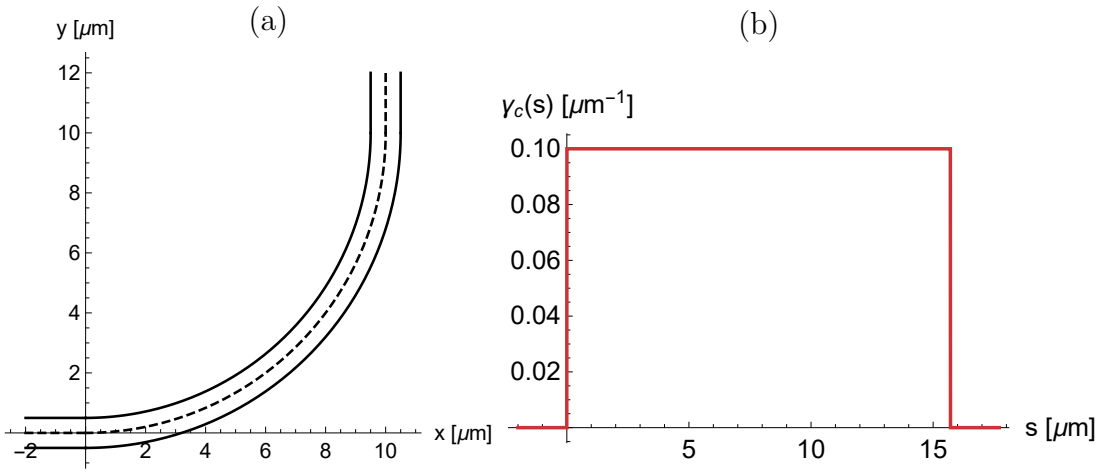


Figure 5.1: Schematic picture of the straight ends connected by circular bend of length $R\,\pi/2$ (a) with $R = 10\,\mu\text{m}$ and the relative curvature function in red (b).

Thus the whole Hamiltonian simplifies, yielding the following time-independent Schrödinger equation:

$$\left[-\frac{1}{(1-u\gamma_c)^2}\frac{\partial^2}{\partial s^2} - \frac{\partial^2}{\partial u^2} - \frac{\gamma^2}{4(1-u\gamma_c)^2} + V_\perp(u)\right]\psi(s,u) = k^2\,|\psi(s,u)\rangle\,. \quad (5.3)$$

We want to note that this equation can be exactly solved if the harmonic trapping is replaced by a well with hard walls. This approximation can be performed assuming the trapping potential is sufficiently strong, effectively producing a waveguide with hard walls, where $V_\perp(u)$ is zero inside the walls and infinite outside. We can then apply the change of variable $r \equiv 1 - \gamma_c u$ so that (5.3) becomes

$$\begin{aligned} &\left[\frac{1}{r^2}\frac{\partial^2}{\partial s^2} + \gamma_c^2\frac{\partial^2}{\partial r^2} + \frac{\gamma_c^2}{4r^2}\right]\psi(s,r) = -k^2\psi(s,r) \\ &\frac{\partial^2}{\partial s^2}\psi(s,r) + \left[r^2\gamma_c^2\frac{\partial^2}{\partial r^2} + \cancel{r^2}\frac{\gamma_c^2}{4\cancel{r^2}} - r^2k^2\right]\psi(s,r) = 0 \end{aligned} \quad (5.4)$$

and we can separate the variables noting that the radial equation corresponds to a Bessel equation and can be solved exactly with solutions of the form

$$\psi_l(s,r) = \frac{1}{\sqrt{r}} S_l(s) \Upsilon_l(r) \tag{5.5}$$

where $S_l(s)$ is a periodic function and $\Upsilon_l(r)$ is a combination of Bessel and Neumann functions. These functions need to meet boundary conditions, i.e. they need to be continuously differentiable in the whole waveguide and in particular at the junction between the straight and curved section. It has been shown by Lin and Jaffe in [45] that for big curvatures, it is not possible to match the internal solutions of the Schrödinger equation in the curved sections with the corresponding solutions in the straight ends. On the other hand, it has been proved that the system is solvable for small curvatures.

This results paved the way for a series of studies focusing on waveguides within the small curvature approximation [46–48]: in these settings, the curvature function varies slowly and continuosly along the curve and its magnitude never increases up to a critical level. This regime can be thought as an adiabatic approximation, with the arc length s acting as the time parameter and the whole Hamiltonian changing as s progresses.

Having a wave packet of dispersion σ, the adiabatic conditions can be summarized by:

$$\sigma \left|\gamma\right| \ll 1, \quad \sigma \left|\frac{\mathrm{d}\gamma}{\mathrm{d}s}\right| \ll 1, \quad \sigma \left|\frac{\mathrm{d}\gamma}{\mathrm{d}s^2}\right| \ll 1. \tag{5.6}$$

Now let us go back to the harmonic trapping. Within these limits, the effective potential $V(s,u)$ becomes dominated by the first term and loses the dependency from u, thus the total external potential becomes

$$V_\perp(u) + V(s,u) \approx V_\perp(u) + V(s) = \frac{1}{2}m\omega^2 u^2 - \frac{\gamma(s)^2}{4}. \tag{5.7}$$

These constraints are very strict and cannot be applied in many experimental setups. In the following sections we will try to overcome this limitations by inverse engineering the shape of the waveguide: the curvature function will be obtained by means of a classical argument and will be then used to solve the Schrödinger equation.

We will start by reviewing the paper by Impens et al. [21] that sparked this research.

5.3 Classical-based inverse engineering

We have already explained the effects caused by the discontinuity of the curvature function: the discontinuity generates transverse excitation that, in turn, will produce mixing between the transverse and longitudinal modes of the wave function, hence reducing the fidelity of the whole process.

In the paper [21] of Impens, Dubosq and Guéry-Odelin, the key idea is to solve the Newton's equations in curved 2D geometry to explicitely find the expression of the curvature in terms of the trajectory of the particle. The trajectory can then

be freely chosen in order to meet the required boundary conditions. In particular, these constraints are defined with the aim of minimizing the transverse excitation at the end of the curve.

First, we will show how the Newton's equations are affected by the change in geometry.

5.3.1 Newton's Equation in curved coordinates

As explained in chapter 4, given a curve $\vec{\mathbf{\Gamma}}(s)$ we can define the curvilinear coordinates $\hat{\boldsymbol{t}}(s)$ and $\hat{\boldsymbol{n}}(s)$ which obey the Frenet-Serret equations (4.13).

Every point in $\mathbb{R}^2$ can now be identified by a vector $\vec{\boldsymbol{r}}(s,u) = \vec{\mathbf{\Gamma}}(s) + u\hat{\boldsymbol{n}}(s)$. In this case, however, we also need to include the dependence of the curvilinear coordinates s and u from the time variable t that will tacitly be assumed for the remainder of the chapter. With this in mind, the equations of motion in curvilinear coordinates are now derived in the usual way.

Let us start with:

$$m\frac{\mathrm{d}^2\vec{\boldsymbol{r}}(s,u)}{\mathrm{d}t^2} = -\nabla V_{\perp}(s,u).$$

where $V_{\perp}$ is a general confining external potential (for the moment we are not assuming harmonic trapping) and ∇ is the divergence operator expressed in

curvilinear coordinates :

$$\nabla := \begin{pmatrix} \frac{1}{1-u\gamma}\frac{\partial}{\partial s} \\ \frac{\partial}{\partial u} \end{pmatrix} \implies \nabla V_\perp(s,u) = \frac{1}{1-u\gamma}\frac{\partial V_\perp(s,u)}{\partial s}\hat{\boldsymbol{t}}(s) + \frac{\partial V_\perp(s,u)}{\partial u}\hat{\boldsymbol{n}}(s). \tag{5.8}$$

We need now to evaluate the derivative of the position vector with respect of time t as follows (the explicit dependence from s is omitted for clarity):

$$\begin{aligned} &\frac{\mathrm{d}\vec{\boldsymbol{r}}(s,u)}{\mathrm{d}t} = \frac{\mathrm{d}}{\mathrm{d}t}(\vec{\boldsymbol{\Gamma}} + u\hat{\boldsymbol{n}}) = \frac{\mathrm{d}\vec{\boldsymbol{\Gamma}}}{\mathrm{d}s}\dot{s} + \dot{u}\hat{\boldsymbol{n}} + u\frac{\mathrm{d}\hat{\boldsymbol{n}}}{\mathrm{d}s}\dot{s} = \hat{\boldsymbol{t}}\dot{s} + \dot{u}\hat{\boldsymbol{n}} - u\gamma\hat{\boldsymbol{t}}\dot{s} \\ &= \dot{s}\,(1-u\gamma)\,\hat{\boldsymbol{t}} + \dot{u}\hat{\boldsymbol{n}}. \end{aligned} \tag{5.9}$$

where $\dot{s}$ and $\dot{u}$ are the total time derivative of the respective coordinate. Continuing with the second derivative, we get:

$$\begin{aligned} &\frac{\mathrm{d}^2\vec{\boldsymbol{r}}(s,u)}{\mathrm{d}t^2} = \frac{\mathrm{d}}{\mathrm{d}t}\left(\dot{s}\,(1-u\gamma)\,\hat{\boldsymbol{t}} + \dot{u}\hat{\boldsymbol{n}}\right) \\ &= \ddot{s}\,(1-u\gamma)\,\hat{\boldsymbol{t}} + \dot{s}\left(-\dot{u}\gamma - u\frac{\mathrm{d}\gamma}{\mathrm{d}s}\dot{s}\right)\hat{\boldsymbol{t}} + \dot{s}\,(1-u\gamma)\,\frac{\mathrm{d}\hat{\boldsymbol{t}}}{\mathrm{d}s}\dot{s} + \ddot{u}\hat{\boldsymbol{n}} + \dot{u}\frac{\mathrm{d}\hat{\boldsymbol{n}}}{\mathrm{d}s}\dot{s} \\ &= \ddot{s}\,(1-u\gamma)\,\hat{\boldsymbol{t}} - \dot{s}\left(\dot{u}\gamma + u\frac{\mathrm{d}\gamma}{\mathrm{d}s}\dot{s}\right)\hat{\boldsymbol{t}} + \dot{s}\,(1-u\gamma)\,\gamma\hat{\boldsymbol{n}}\dot{s} + \ddot{u}\hat{\boldsymbol{n}} - \dot{u}\gamma\hat{\boldsymbol{t}}\dot{s} \\ &= \left[\ddot{s}(1-u\gamma) - \dot{s}(\dot{\gamma}u + 2\gamma\dot{u})\right]\hat{\boldsymbol{t}} + \left[\ddot{u} + \dot{s}^2\gamma(1-u\gamma)\right]\hat{\boldsymbol{n}}. \end{aligned} \tag{5.10}$$

We can finally write the two differential equations of motion by projecting (5.8) and (5.10) i.e. we will separate the parts along the $\hat{\mathbf{t}}$ axis from the ones along

the $\hat{\mathbf{n}}$ axis:

$$\ddot{s}(1-u\gamma) - \dot{s}(\dot{\gamma}u + 2\gamma\dot{u}) + \frac{\partial V_\perp}{\partial s} = 0, \tag{5.11}$$

$$\ddot{u} + \dot{s}^2\gamma(1-u\gamma) + \frac{\partial V_\perp}{\partial u} = 0 \tag{5.12}$$

with $\gamma = \gamma(s(t))$. Moreover we are dealing with a conservative potential (depending only from the position coordinates), hence from (5.9) we can retrieve the equation describing the conservation of energy:

$$\begin{aligned} E &= m\left|\left|\frac{\mathrm{d}\vec{\boldsymbol{r}}(s,u)}{\mathrm{d}t}\right|\right|^2 + V_\perp(s,u) = m\left(\dot{u}^2 + \dot{s}^2(1-u\gamma)^2\right) + V_\perp(s,u) \\ &\implies \dot{u}^2 + \dot{s}^2(1-u\gamma)^2 + \frac{2V_\perp(s,u)}{m} = \frac{2E}{m}. \end{aligned} \tag{5.13}$$

5.3.2 Retrieving the curvature from particle trajectory

We are now ready to solve the problem of obtaining the curvature γ as a function of s as in [21]. In the following, we assume a harmonic transverse trapping potential with constant frequency, of the form $V_\perp(u) = \frac{1}{2}m\omega^2u^2$ and we set the angle $\alpha = \pi/2$. In this case, the equations of motion become:

$$\ddot{s}(1-u\gamma) - \dot{s}(\dot{\gamma}u + 2\gamma\dot{u}) = 0, \tag{5.14}$$

$$\ddot{u} + \dot{s}^2\gamma(1-u\gamma) + \omega^2u = 0, \tag{5.15}$$

$$\dot{u}^2 + \dot{s}^2(1-u\gamma)^2 + \omega^2u^2 = \frac{2E}{m}. \tag{5.16}$$

From equation (5.16) we can set $v_k = \dot{s}(1 - u\gamma)$ and check that $\dot{v_k} = \dot{s}\gamma\dot{u}$ from equation (5.14). In this way, (5.16) becomes:

$$\dot{u}^2 + v_k + \omega^2 u^2 = \frac{2E}{m}. \tag{5.17}$$

We can now obtain v_k by imposing the desired smooth transverse particle trajectory $u(t)$ and subsequently get $\dot{s}$ and γ. In particular:

$$\dot{s} = v_k + \frac{\dot{v_k} u}{\dot{u}} \tag{5.18}$$

$$\gamma(t) = \frac{\dot{v}_k}{\dot{s}\dot{u}}. \tag{5.19}$$

The curvature γ in (5.19) is a function of the time parameter: to obtain the parametrisation of γ as a function of the arc length we need to exploit the relation (5.18) that can be numerically integrated to obtain the function $s(t)$. This function can be therefore inverted to obtain the desired reparametrisation.

The actual curve can be retrieved from the curvature $\gamma(s)$ by solving the differential equations (4.13) and obtaining the three vectors $\vec{\mathbf{\Gamma}}$, $\hat{\boldsymbol{t}}$, $\hat{\boldsymbol{n}}$, given the initial conditions

$$\vec{\mathbf{\Gamma}}(s(0)) = \begin{bmatrix} 0 \\ 0 \end{bmatrix}, \quad \hat{\boldsymbol{t}}(s(0)) = \begin{bmatrix} 1 \\ 0 \end{bmatrix}, \quad \hat{\boldsymbol{n}}(s(0)) = \begin{bmatrix} 0 \\ 1 \end{bmatrix} \tag{5.20}$$

so the curve is represented by the resulting vector function $\vec{\mathbf{\Gamma}}(s(t))$ and the

condition

$$\vec{\mathbf{\Gamma}}(s(2T)) = (R, R) \tag{5.21}$$

needs to hold in order to ensure the continuity of the curve, where $2T$ is the total time required by the particle to complete the curved segment. To design the transverse particle trajectory $u(t)$ the symmetry of the system is exploited, i.e. the path is split into two halves with the whole process taking a total time $2T$. The transvere trajectory needs to obey the following prescriptions:

- $u_{sta}(0) = \dot{u}_{sta}(0) = \ddot{u}_{sta}(0) = 0$,
- $u_{sta}(T) = \Delta u$,
- $\dot{u}_{sta}(T) = \ddot{u}_{sta}(T) = 0$,
- $u_{sta}(2T) = \dot{u}_{sta}(2T) = \ddot{u}_{sta}(2T) = 0$,

with Δu the maximum deviation from a circular trajectory, allowed in the middle of the curve. These constraints can be motivated by the fact that we want to avoid any kind of excitation both at the entrance and at the end of the bent section. Moreover, the condition set in the middle ($t = T$) is needed to ensure robustness against velocity and position dispersion.

Within the class of functions that satisfy these prescriptions, in [21] the following polynomial has been chosen

$$u_{sta}(t) = \Delta u \, P\left(\frac{t}{T}\right) = \Delta u \left(10\left(\frac{t}{T}\right)^3 - 15\left(\frac{t}{T}\right)^4 + 6\left(\frac{t}{T}\right)^5\right) \tag{5.22}$$

and it will be used for the first half of the path i.e. in the interval $[0, T]$. For the second half, the symmetry of the problem imposes the usage of $P\left(\frac{2T-t}{T}\right)$. The parameter Δu is connected with the maximum curvature γ_m reached at $t = T$ by the following relation:

$$\Delta u = -\frac{1}{4\gamma_m}\left(\sqrt{1 + \frac{8\dot{s}(0)^2\gamma_m^2}{\omega^2}} - 1\right) \tag{5.23}$$

with $\dot{s}(0)$ initial velocity of the incoming particle. The total time T and the value Δu cannot be choosen at will becuase the resulting curve obtained from the process explained earlier does not always fullfill the condition (5.21). Hence, we need to solve the whole problem self-consistently for different Δu and T until the final curve ends in the point (R, R) with some preset accuracy.

We have therefore shown how the curvature $\gamma(s)$ can be evaluated solely by imposing the desired particle trajectory $u_{sta}(t)$ and some initial conditions and we are now ready to perform some calculations.

5.3.3 Results with Polynomial from [21]

We need to set up the initial parameters, so to obtain the final curvature:

- $\omega = 2\pi \times 1705$ Hz,
- $s_0 = 20$ mm/s,

this leads us to get $\Delta u \approx -0.61$ µm and $2T \approx 0.88$ ms.

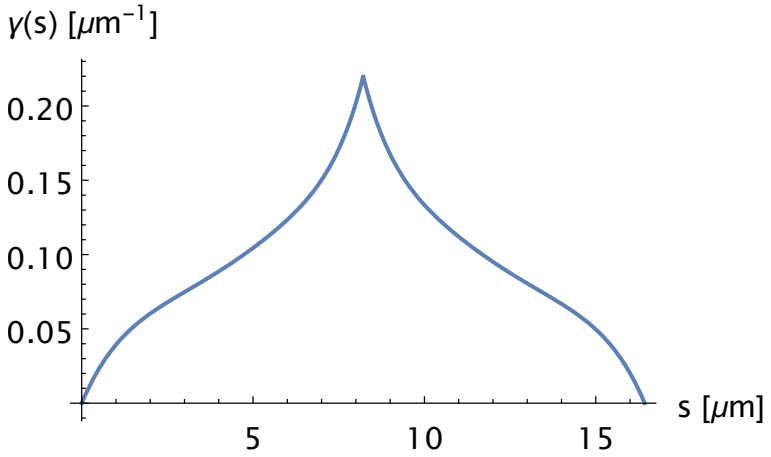


Figure 5.2: Curvature $\gamma(s)$ as a function of the arc length, based on the particle trajectory 5.22 .

We now have both $\dot{s}(t)$ and $\gamma(s(t))$. By integrating $\dot{s}(t)$ we can obtain the curvature as a function of the arc length as shown in figure 5.2. The curve is finally obtained following the prescriptions explained in section 5.3.2 and the final solution is shown in figure 5.3.

The curvature is a continous function with no discontinuity but it presenents a cusp in the middle of the curve. This may cause singularity problems and numerical instabilities and therefor we presume that having the trajectory $u(t)$ characterized by a smooth polynomial defined all over the interval $[0, 2T]$ - as opposed to two polynomials each defined over the half interval - would produce a continuously differentiable curvature, hence a curve more robust against variation of initial conditions.

In the next section we will use different polynomials with the aim of obtaining

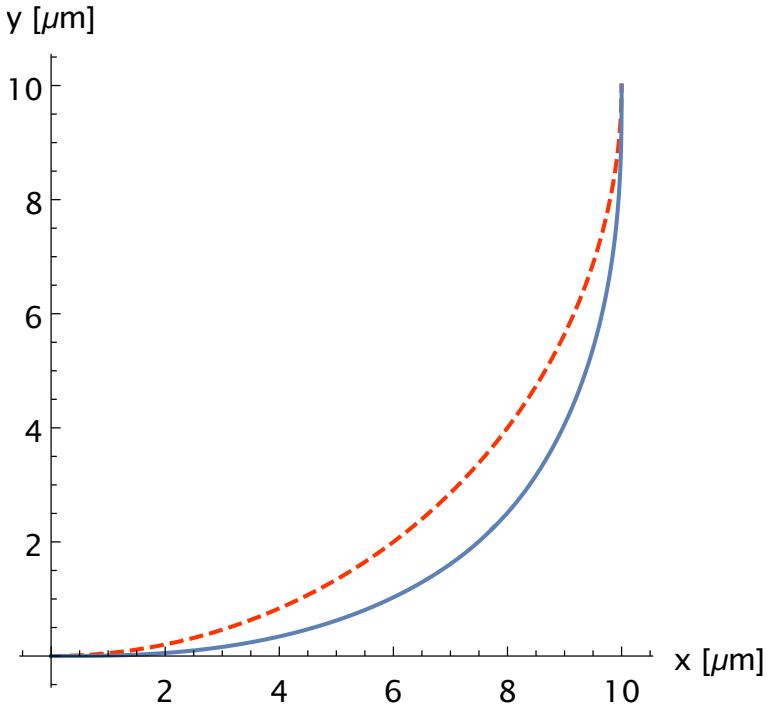


Figure 5.3: View from the top of the curve $\vec{\mathbf{\Gamma}}$ obtained by integration of the curvature function γ, based on the particle trajectory 5.22 . The dashed curve is the corresponding circular bending for reference, see section 5.2.

a smoother function for the curvature.

5.4 Results with alternative Polynomials

The non differentiable point of the curve in section 5.3.3 is the result of the polynomial (5.22) being a combination of two different polynomials. We want to use new transverse trajectories for the particle, and we will refer to them by using the capital letter $U(t)$, with the purpose of producing a smooth trajectory from start to finish, i.e. in the whole time interval $[0, 2T]$. The conditions the

trajectory of the particle have to meet are the same as expressed in (5.3.2), except for the fact that we impose the derivative be 0 up to the n^{th} order and so they can be rewitten as

- $U^{(i)}(0) = 0 \quad \text{for} \quad i = 0, ..., n,$
- $U^{(0)}(T) = \Delta U,$
- $U^{(i)}(T) = 0 \quad \text{for} \quad i = 1, ..., n,$
- $U^{(i)}(2T) = 0 \quad \text{for} \quad i = 0, ..., n.$

We would like to remark that for each different n we have to evaluate the corresponding maximum displacement ΔU_n and the time T_n required by the particle to reach the middle of the curve. So we we will write every particle trajectory as

$$U_n(t) = \Delta U_n \, P_n(t/T_n) \tag{5.24}$$

where P_n is a polynomial the coefficients of which change according to n.

In the remainder we will identify every particle trajectory by the number n, and to keep the notation consistent, U_1 will refer to the particle trajectory $u_{sta}(t)$ used in the previous section and the same notation will be used for the polynomial P_1 that will replace $P(t)$ of 5.22. We will employ the same notation for the curvature and we will write γ_n to specify the curvature obtained by the polynomial P_n, as opposed to γ_1 and γ_c that will refer to curvature calculated in section 5.3.2 and the curvature of the circular waveguide respectively and will be used as a

reference. Similarly, $\vec{\mathbf{\Gamma}}_n$ will identify the curve obtained by the corresponding curvature γ_n, and $\vec{\mathbf{\Gamma}}_1$ while $\vec{\mathbf{\Gamma}}_c$ will refer to the curve retrieved from γ_1 and to the arc of a circle respectively.

In the next section we will give an example of the procedure used to obtain the desired polynomial.

5.4.1 Finding the polynomial

To illustrate the procedure, we will use a polynomial with $n = 2$ for which the constraints are the same as 5.3.2. The polynomial is of the form:

$$P_2\left(\frac{t}{T_2}\right) = \sum_{m=0}^{\infty} a_m \left(\frac{t}{T_2}\right)^m. \tag{5.25}$$

We need to calculate the derivatives of (5.25) with respect of t

$$\dot{P}_2(t/T_2) = \frac{\mathrm{d}P_2(t/T_2)}{\mathrm{d}t} = \sum_{m=0}^{\infty} \frac{\mathrm{d}}{\mathrm{d}t}\left(a_m t^m\right) = \sum_{m=1} n a_m t^{m-1} = \sum_{m=0}^{\infty} (n+1) a_{n+1} t^m \tag{5.26}$$

$$\begin{aligned}\ddot{P}_2(t/T_2) &= \frac{\mathrm{d}\dot{P}_2(t/T_2)}{\mathrm{d}t} = \sum_{m=0}^{\infty} \frac{\mathrm{d}}{\mathrm{d}t}\left[(n+1) a_{n+1} t^m\right] \\ &= \sum_{m=1}^{\infty} n(n+1) a_{n+1} t^{m-1} = \sum_{m=0}^{\infty} (n+1)(n+2) a_{n+2} t^m.\end{aligned} \tag{5.27}$$

Every time we evaluate the two relations at a certain time, we are left with two linear equations where the unknown variables are the coefficients a_m. For

example, the request $\dot{U}_2(T) = 0$ corresponds to the following linear equation

$$0 = \dot{U}_2(T_2) = \Delta U \dot{P}_2(1) = \sum_{m=0}^{\infty}(m+1)a_{m+1} = a_1 + 2a_2 + 3a_3 + ... \tag{5.28}$$

We have a total of nine constraints, that can be thought as the solution vector of dimension 9 for the linear system. This also means that the minimum requirement to have a single unique solution for the system, is to have 9 equations. This indicates that the polynomial has to be of order 8 and we can rewrite the system in matrix form as M. The rank of M is equal to the dimension of the linear system, then the system allows a single unique solution that can be found to be

$$P_2(t/T_2) = 32\left(\frac{t}{T_2}\right)^3 - 96\left(\frac{t}{T_2}\right)^4 + 120\left(\frac{t}{T_2}\right)^5 - 76\left(\frac{t}{T_2}\right)^6 + 24\left(\frac{t}{T_2}\right)^7 - 3\left(\frac{t}{T_2}\right)^8 \tag{5.29}$$

and finally the particle trajectory for $n = 2$ can be written as

$$U_2(t) = \Delta U_2 \, P_2(t/T_2). \tag{5.30}$$

Increasing the order of the polynomial will only result in a bigger matrix, having to accomodate more constraints.

In this work we test polynomial up to $n = 6$ and the corresponding polynomials $P_n(\tau)$ are shown in figure 5.4.

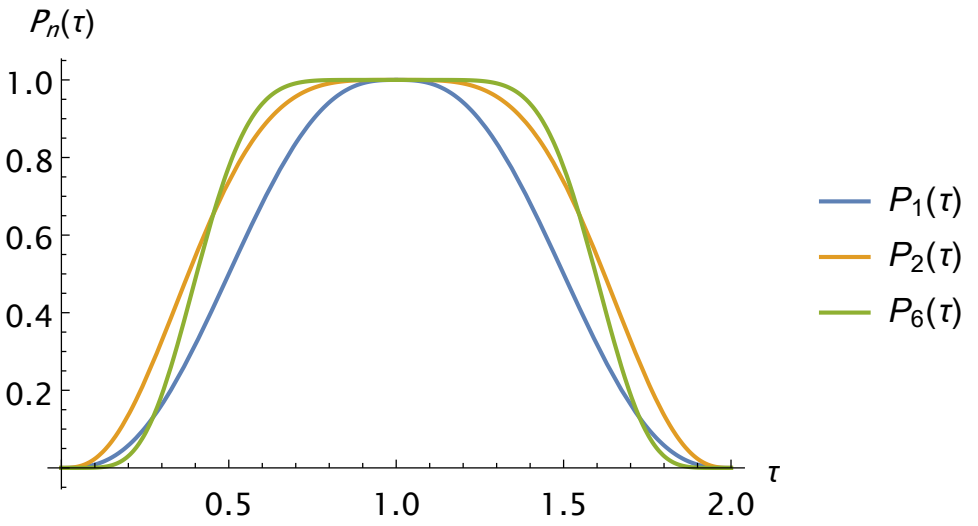


Figure 5.4: Comparison between different test trajectories in dimensionless units for $\tau = t/T_n$.

5.4.2 Calculation and Results

Mirroring the same argument of section 5.3.2, we obtain new curvature profiles as shown in figure 5.5 for $n = 2$ and $n = 6$, where we can see that the cusp in the middle of the curvature has vanished. Increasing the order of the polynomial will lead to a flatter curvature around the centre of the curve but steeper variation at the beginning and at the end of the curved section. We can then retrieve the curve $\vec{\mathbf{\Gamma}}_n$ in the same fashion as in section 5.3.2, to obtain the shape shown in figure 5.6.

We will now proceed comparing the stability of these new curves against initial errors.

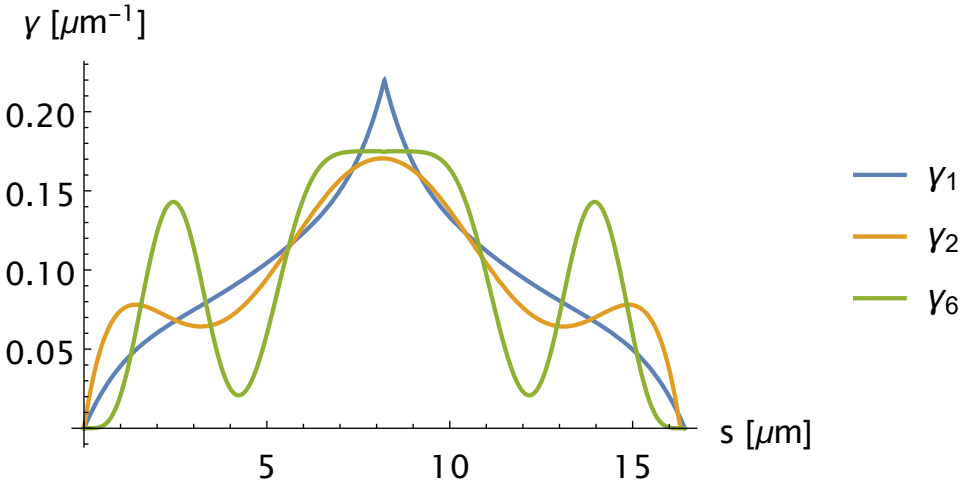


Figure 5.5: Curvature $\gamma_n(s)$ as a function of the arc length for different n compared with the curvature γ_1 .

5.5 Robustness

Having obtained the shape of the waveguides for different desired trajectories, we now want to test the robustness of the curvatures against initial displacement and dispersion of initial velocity.

We will substitute the expression of the curvature previously obtained for polynomials $P_n(t)$ of different n to solve the Newton's differential equations (5.14) and (5.15) with different initial conditions, to evaluate new transverse trajectories $U_\delta(t)$.

5.5.1 Stability against initial displacement

In this case the velocity of the incoming particle will be kept constant, with $s_0 = 20\,\text{mm/s}$, but we will impose an initial displacement from the center of the

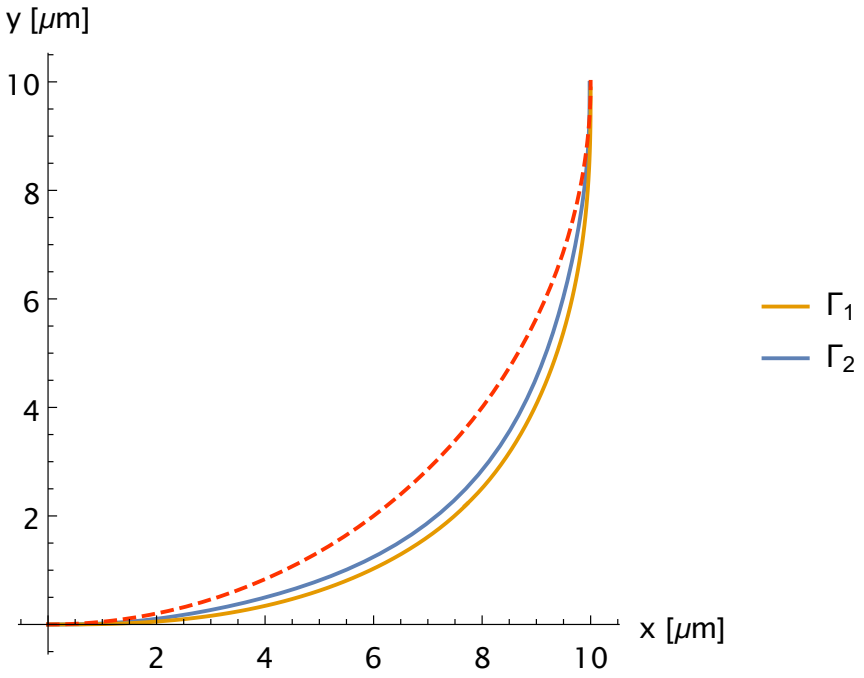


Figure 5.6: Profile of the curve $\vec{\mathbf{\Gamma}}_2$ evaluated from the curvature γ_2 compared with the one obtained from γ_1. Again, the red dashed line represents the arc of a circle.

trap. This condition can be written as :

$$U_\delta(0) = \delta U. \tag{5.31}$$

In the following, δU will range in the interval $[-0.1, 0.1]$ µm. The displacement will cause turbulence in the system and this will eventually lead to oscillation at the end of the curved section as in figure 5.7. We call the final amplitude of the oscillation Y_f. We changed the initial displacement δU linearly, evaluated the corresponding maximum oscillation amplitude Y_f and compared the performances of each curve $\vec{\mathbf{\Gamma}}_n$ with different n. In figure 5.8 the results for the curve

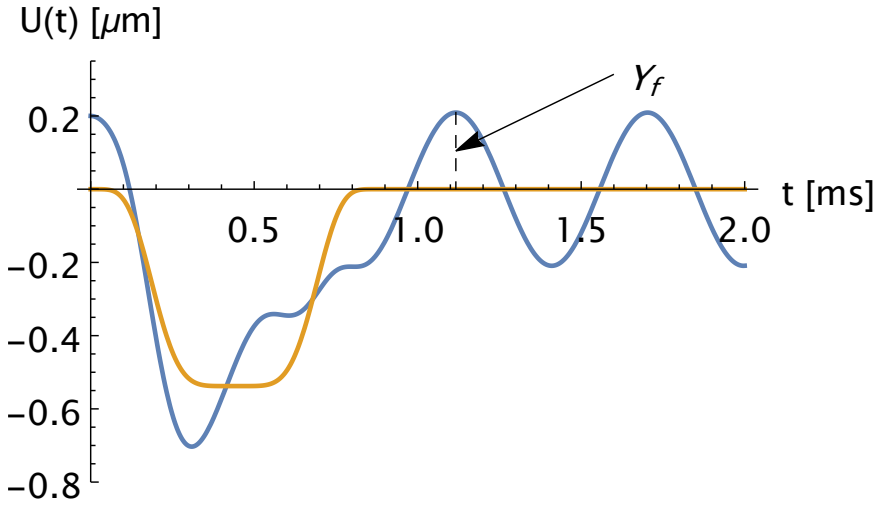


Figure 5.7: Example of how the initial displacement affects the final oscillation of the particle, in yellow the transverse trajectory for no initial displacement, in blue the trajectory with $\delta U = 0.2$ µm. The particle trajectory is obtained from the curve $\vec{\mathbf{\Gamma}}_5$.

$\vec{\mathbf{\Gamma}}_4$ are summarized.

Different curves show similar behaviour, namely the final amplitude oscillation Y_f grows linearly according to the initial displacement δU. To compare the robustness of different curves we make a linear fit for the two different branches and then averaged the absolute values of the obtained linear coefficients and we call it **sensitivity**. We use ρ_p to identify the sensitivity against the variation of initial position. Then we plot the values for the different curves in figure 5.9. The most robust curve is the one with the lowest ρ_p as it means that given the same initial displacement, the one with the lowest ρ_p ensures the highest suppression of final oscillation amplitude compared to the other curves.

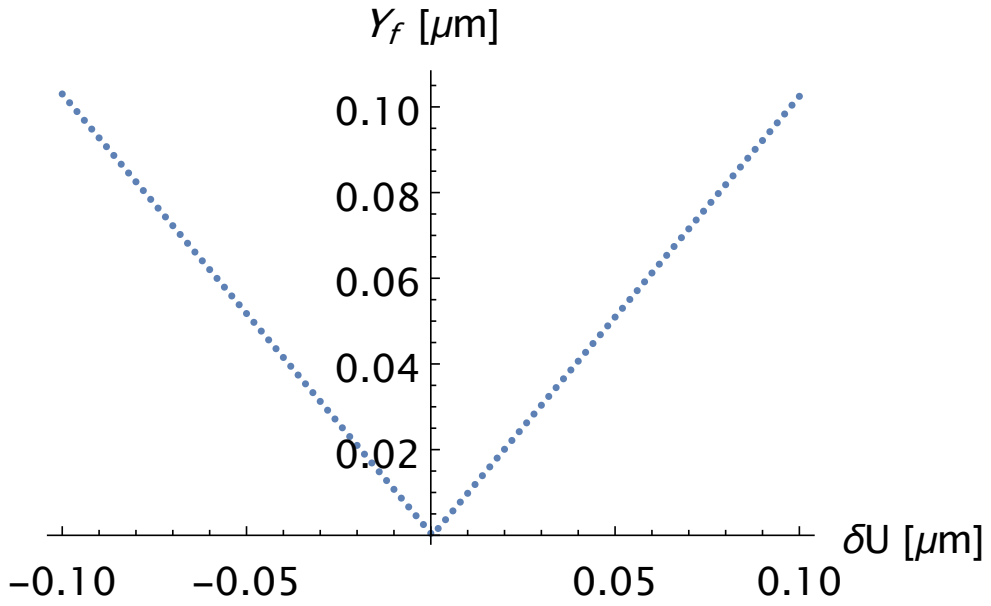


Figure 5.8: Final amplitude Y_f versus initial displacement δU for the curve $\vec{\mathbf{\Gamma}}_4$.

Figure 5.9 shows that the highest robustness is achieved by the curvature obtained from the polynomial P_2 even by a small margin.

5.5.2 Stability against dispersion of velocity

Now the particle will start travelling from the middle of the waveguide and we will only change its initial velocity that will be of the form:

$$\dot{s}(0) = s_0 + \delta s_0 \equiv S_0. \tag{5.32}$$

The approach is similar to the one used to check the robustness of the curve against initial displacement: we will have a particle starting in the middle of the trap i.e. $U_\delta(0) = 0$, but in this case we will assume that the particle has

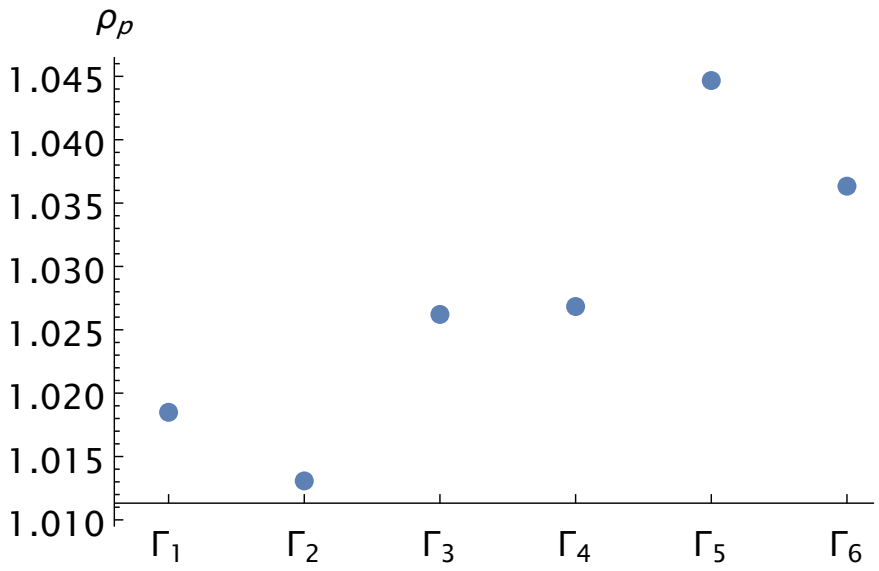


Figure 5.9: Sensitivity ρ_p of different curves $\vec{\mathbf{\Gamma}}_n$ against initial displacement. For every curve we calculated the slope of the resulting linear fit, see text for details.

an initial tangential velocity S_0. As an example, figure 5.10 shows the effects that the initial velocity has on the transverse particle trajectory for the curve $\vec{\mathbf{\Gamma}}_3$. Again, a transverse excitation is retained by the particle after the curved segment, resulting in an oscillatory behaviour that can be quantified - similarly to what we have done in the previous section - by the oscillation amplitude Y_f

We will evaluate the maximum amplitude of the oscillation as we vary the initial velocity in the interval $[-0.1s_0, 0.1s_0]$ and repeat this calculation for different curves $\vec{\mathbf{\Gamma}}_n$ with $n = 1, 2, ..., 6$.

The results are summarized in figure 5.11 and figure 5.12 where we can clearly see that for every curve there is a particular velocity, the value of which is less

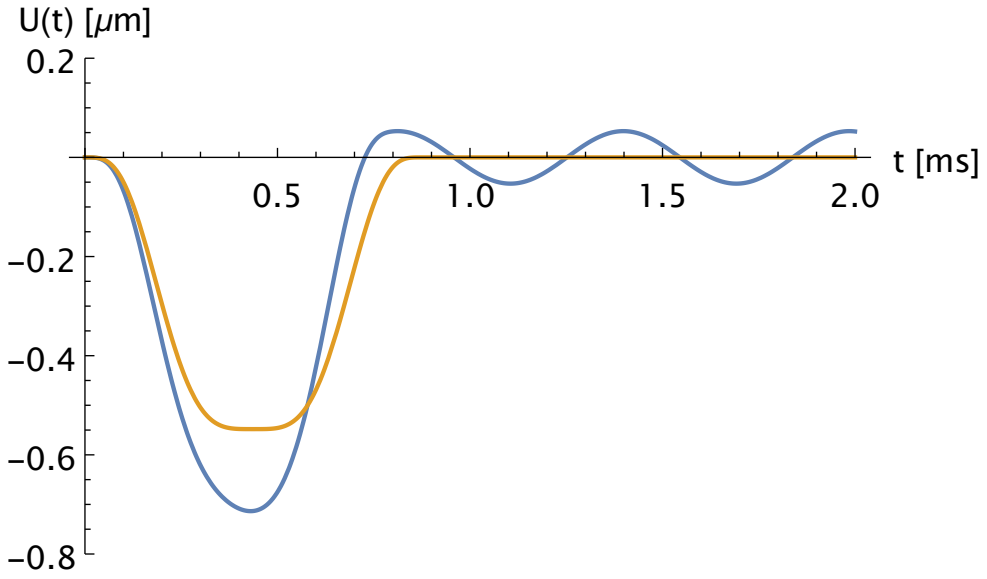


Figure 5.10: Effects of the initial velocity on the final excitation of the particle. In blue the transverse trajectory with initial velocity set to 22 mm/s, relative to the curve $\vec{\mathbf{\Gamma}}_3$. The yellow line is the trajectory of the particle for $s_0 = 20$ mm/s included for reference.

than s_0, that yields no final oscillation Y_f. In particular, for $\vec{\mathbf{\Gamma}}_2$, this value is very close to s_0, dramatically increasing the robustness of this curve against the dispersion of initial velocity.

Unlike the case of section 5.5.1, where the relation between initial displacement and final amplitude was clearly nearly linear and symmetric in the shown parameters range, in this case, defining and evaluating the sensitivity of the waveguide is not as straightforward.

We wanted to quantify the value of this important feature for the waveguide and we have consequently decided to concentrate our attention closer to the central

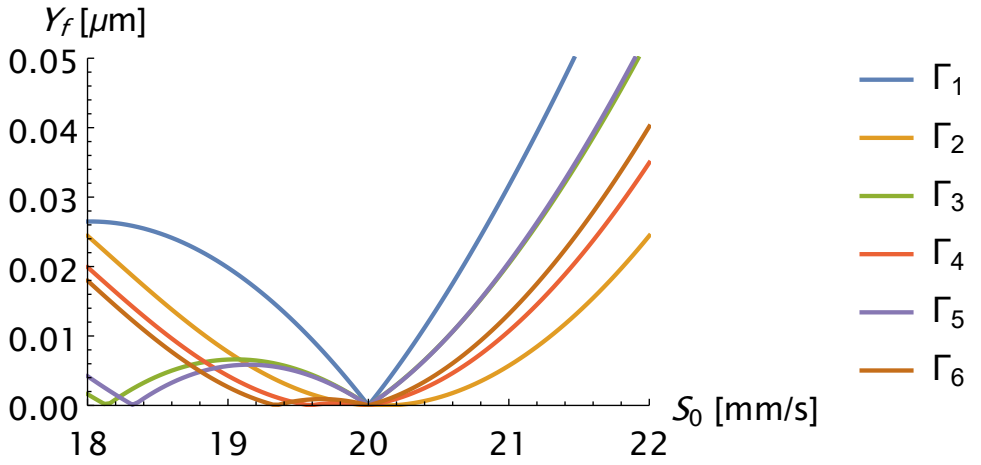


Figure 5.11: Effects of the dispersion of initial velocity S_0 on the maximum final oscillation amplitude Y_f.

value s_0 where a linear approximation can be performed as in figure 5.12. The inhibiting effects are even more striking in this graph as we can see that $\vec{\mathbf{\Gamma}}_2$ effectively suppresses any final oscillation for $S_0 \geq s_0$.

The actual value of the sensitivity of the waveguide against initial velocity is then obtained adopting the same approach we used in section 5.5.1. Two different interpolations have been made, one for $S_0 \leq s_0$ and the other for $S_0 \geq s_0$ and averaged the resulting linear coefficients that we call it ρ_v. We have repeated this calculation for $n = 1, ..., 6$ and the results are finally shown in figure 5.13.

Again, the most stable curve is the one for which ρ_v has the lowest value, as it ensures the highest stability against a spectrum of velocities centered around s_0. From figure 5.13, we can see that the curve with the lowest sensitivity, hence the most robust, is $\vec{\mathbf{\Gamma}}_2$.

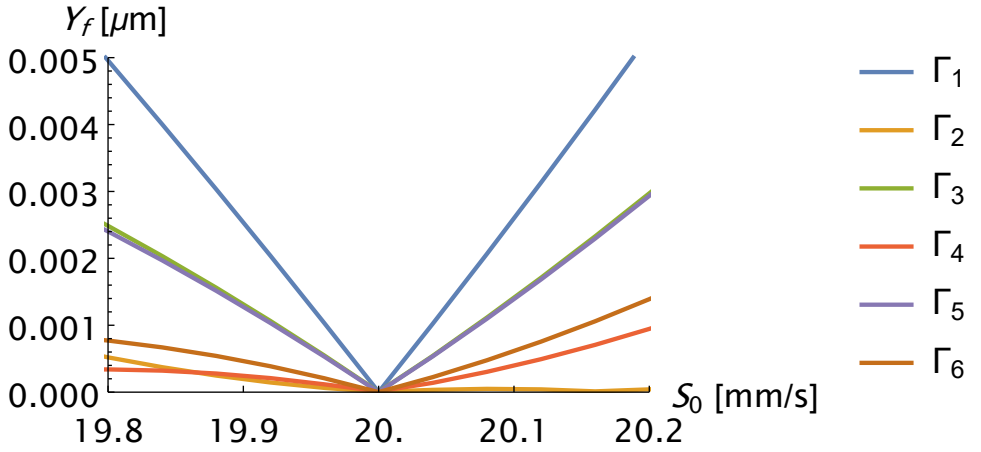


Figure 5.12: Inset of figure 5.11 in a smaller interval centerd around s_0.

This result and the one obtained in 5.5.1 have shown that the curve with the best features is $\vec{\mathbf{\Gamma}}_2$ as it ensures the lowest sensitivity against both the initial displacement and dispersion of initial velocity.

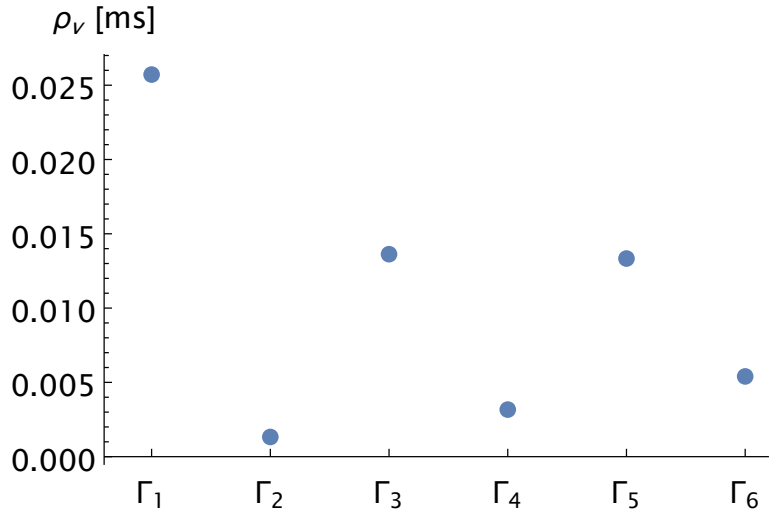


Figure 5.13: Sensitivity ρ_v against initial velocity for different curves $\vec{\mathbf{\Gamma}}_n$ resulting from the calculation of the linear fit around s_0, see text for details.

We are now ready to turn our attention to the quantum realm: having obtained the curvatures and verified their robustness in classical settings, in the next chapter we will test their efficiency solving the time-dependent Schrödinger equation by means of numerical algorithms. In particular we will use the the split operator method, firstly described by Fleck et al in [49]. We will then define and evaluate the fidelity for the different curves in quantum settings.

Chapter 6

Quantum implementation of the bent waveguides

6.1 Introduction

In chapter 5 we have used an approach inspired by Shortcuts to Adiabaticity to inverse engineer the shape of a curved waveguide to improve the robustness with respect to the circular shape and we have also confirmed their effectiveness by means of classical arguments. In particular, we have shown that the most stable and robust curve is the one obtained from the curvature γ_2.

However, our aim is to employ waveguides in quantum computing, hence we need to test the strength of this shape in a quantum environment. To reach this

goal we need to solve the time-dependent Schrödinger equation:

$$i\hbar\frac{\partial}{\partial t}\left|\psi(t)\right\rangle = \hat{H}\left|\psi(t)\right\rangle \tag{6.1}$$

where the Hamiltonian operator has the form

$$-\frac{\hbar^2}{2m}\left[\frac{\partial}{\partial s}\frac{1}{(1-u\gamma)^2}\frac{\partial}{\partial s}+\frac{\partial^2}{\partial u^2}+\frac{\gamma^2}{4(1-u\gamma)^2}+\frac{u\ddot{\gamma}}{2(1-u\gamma)^3}-\frac{5}{4}\frac{u^2\dot{\gamma}^2}{(1-u\gamma)^4}\right]+\frac{1}{2}m\omega^2u^2. \tag{6.2}$$

In this case γ is the curvature obtained from the semiclassical calculation of chapter 5. This equation cannot be solved analytically, so we need to use numerical methods.

In this chapter we will start by reviewing the split-operator method [49] that will be used to evolve the wave function. First the wave function will evolve in a circular waveguide that will serve as a reference, then we will change the shape of the waveguide so that the bottom of the harmonic trap follows the curve that has been inverse engineered with the semiclassical STA approach of chapter 5.

Finally, we will compare the results obtained in these different settings by evaluating the fidelity in each process.

6.2 Split operator method

Let the Schrödinger equation with a standard time-independent Hamiltonian be given as:

$$i\hbar\frac{\partial}{\partial t}\left|\psi(t)\right\rangle = \hat{H}\left|\psi(t)\right\rangle = \left(\hat{T}+\hat{V}\right)\left|\psi(t)\right\rangle \tag{6.3}$$

where $\hat{T}$ and $\hat{V}$ are the kinetic energy and potential operator respectively.

The split operator method relies heavily on the Fourier transform as we will show later in the section and we found it more convenient to express the Hamiltonian in Cartesian coordinates. So, in this case and in the following simulations, the Hamiltonian will be of the form

$$\hat{H} = -\frac{\hbar^2}{2m}\left[\frac{\partial^2}{\partial x^2}+\frac{\partial^2}{\partial y^2}\right] + V_\perp(x,y) \tag{6.4}$$

where $V_\perp(x,y)$ is the harmonic trapping in Cartesian coordinates. Altough this choice will simplify the following calculations, we will need to also convert the transverse potential $V_\perp$ from curvilinear to Cartesian coordinates and this process will be explained in section 6.3.

Having an initial state $|\psi(t_0)\rangle$ at time t_0, the state at time $t = t_0 + \Delta t$ can be evaluated via the time evolution operator

$$\left|\psi(t)\right\rangle = \left|\psi(t_0+\Delta t)\right\rangle = \exp\left\{-\frac{i\hat{H}}{\hbar}\Delta t\right\}\left|\psi(t_0)\right\rangle. \tag{6.5}$$

This operator exponential can be expressed in terms of the series expansion

$e^{\hat{X}} = \sum_{n=0}^{m} \frac{1}{n!} \hat{X}^n$ and for $\Delta T \ll 1$ we can truncate the series to the second order:

$$\exp\left\{-\frac{i\hat{H}}{\hbar}\Delta t\right\} = \mathbb{1} - \frac{i\Delta t}{\hbar}\left(\hat{T}+\hat{V}\right)\Delta t - \frac{\Delta t^2}{2\hbar^2}\left(\hat{T}+\hat{V}\right)^2 + \mathcal{O}(\Delta t)^3. \tag{6.6}$$

Expanding the right hand side of (6.6), we obtain

$$\begin{aligned}&\mathbb{1} + 2\left(-i\frac{\Delta t}{2\hbar}\hat{V} - \frac{\Delta t^2}{4\hbar^2}\hat{V}^2\right) + \left(-i\frac{\Delta t}{\hbar}\hat{T} - \frac{\Delta t^2}{2\hbar^2}\hat{T}^2\right) - \frac{\Delta t^2}{2\hbar^2}\left(\hat{T}\hat{V}+\hat{V}\hat{T}\right) + \mathcal{O}(\Delta t^3)\\ &= \exp\left\{-\frac{i\hat{V}}{2\hbar}\Delta t\right\}\exp\left\{-\frac{i\hat{T}}{\hbar}\Delta t\right\}\exp\left\{-\frac{i\hat{V}}{2\hbar}\Delta t\right\} + \mathcal{O}(\Delta t^3).\end{aligned} \tag{6.7}$$

As already stated, this expression has an error of Δt^3 but this splitting becomes very useful from a numerical standpoint as the two operators $\hat{T}$ and $\hat{V}$ are diagonal in their own respective basis, hence making it easier to perform the exponential in this particular form. The change of representation corresponds to a change of basis and can be performed via the Fourier transform $\mathcal{F}[\cdot]$ from position to momentum space, while the inverse $\mathcal{F}^{-1}[\cdot]$ corresponds to a change of basis from momentum to position space.

In two dimensions, the Fourier transform is given by

$$\mathcal{F}\left[\langle\hat{\mathbf{r}}|\psi(t)\rangle\right](\vec{\mathbf{p}}) = \frac{1}{2\pi\hbar}\int_{\mathbb{R}^2} d^2\vec{\mathbf{r}}\, e^{-i\vec{\mathbf{p}}\vec{\mathbf{r}}/\hbar}\,\langle\hat{\mathbf{r}}|\psi(t)\rangle\,. \tag{6.8}$$

Finally, we can express the evolution of the state as follows

$$\begin{aligned}&\langle\hat{\mathbf{r}}|\psi(t_0+\Delta t)\rangle = \\ &\exp\left\{-\frac{i\hat{V}}{2\hbar}\Delta t\right\}\mathcal{F}^{-1}\left[\exp\left\{-\frac{i\hat{T}}{\hbar}\Delta t\right\}\mathcal{F}\left[\exp\left\{-\frac{i\hat{V}}{2\hbar}\Delta t\right\}\langle\hat{\mathbf{r}}|\psi(t_0)\rangle\right]\right].\end{aligned} \tag{6.9}$$

Clearly, this calculation is computationally demanding as the Fourier transform has to be performed many times, but the Fast Fourier Transform (FFT) algorithm [50] provides an efficient solution and dramatically increases the speed of the simulation. Furthermore, the algorithm can be easily parallelized on specific Graphic Processing Units (GPU), to improve the velocity of this method even further.

In the next section we will describe the method we employed to obtain the Cartesian trapping potential $V_\perp(x, y)$ from $V_\perp(s, u)$ expressed in curvilinear coordinates.

6.3 Potential in Cartesian coordinates

The split operator method explained in section 6.2 is implemented via a collection of C++ programs that use the whole potential as an input and evolve the particle on consecutive time steps. Thus, we need to define a finite region in the xy plane where the Fourier transform can be carried out. In order to simplify the notation and facilitate the calculations we will first rewrite the Schrödinger equation in **dimensionless units** so that the computation can be performed independently

from the real parameters of the system.

6.3.1 Schrödinger equation in dimensionless units

We will first perform a change of variable with respect to the three independent variables in the Schrödinger equation, i.e. the spatial variables x and y and the time variable t. The whole size of the system is clearly characterized by the radius R of the arc of the circle connecting the two straight sections. Similarly, the whole process is carried out in a total time T_f, so it becomes straightforward to introduce the following change of variables

$$\widetilde{x} = \frac{x}{R}, \qquad \widetilde{y} = \frac{y}{R}, \qquad \widetilde{t} = \frac{t}{T}. \tag{6.10}$$

Despite not knowing the exact functional for the potential $V_\perp(x, y)$, we know that it is quadratic on the spatial coordinates x and y, so we can rewrite the potential in dimensionless coordinates as

$$V_\perp(x, y) = \frac{1}{2} m\omega_0^2 f(x, y) = \frac{1}{2} m\omega_0^2 R^2 \widetilde{f}(\widetilde{x}, \widetilde{y}) \tag{6.11}$$

and the Schrödinger equation becomes (with $|\widetilde{\psi}\rangle = |\widetilde{\psi}(\widetilde{x},\widetilde{y},\widetilde{t})\rangle$) :

$$i\frac{\hbar}{T_f}\frac{\partial}{\partial\widetilde{t}}|\widetilde{\psi}\rangle = -\frac{\hbar^2}{2m}\frac{1}{R^2}\left[\frac{\partial^2}{\partial\widetilde{x}^2}+\frac{\partial^2}{\partial\widetilde{y}^2}\right]|\widetilde{\psi}\rangle + \frac{m\omega_0^2R^2}{2}\widetilde{f}(\widetilde{x},\widetilde{y})\,|\widetilde{\psi}\rangle \tag{6.12}$$

$$i\frac{\partial}{\partial\widetilde{t}}|\widetilde{\psi}\rangle = -\frac{T_f\cancel{\hbar}^{\prime}}{\cancel{\hbar}2mR^2}\left[\frac{\partial^2}{\partial\widetilde{x}^2}+\frac{\partial^2}{\partial\widetilde{y}^2}\right]|\widetilde{\psi}\rangle + \frac{mR^2\omega_0^2T_f}{2\hbar}\widetilde{f}(\widetilde{x},\widetilde{y})\,|\widetilde{\psi}\rangle \tag{6.13}$$

$$i\frac{\partial}{\partial\widetilde{t}}|\widetilde{\psi}\rangle = \frac{1}{2\widetilde{m}}\left[\frac{\partial^2}{\partial\widetilde{x}^2}+\frac{\partial^2}{\partial\widetilde{y}^2}\right]|\widetilde{\psi}\rangle + \frac{1}{2}\widetilde{m}\widetilde{\omega}^2\widetilde{f}(\widetilde{x},\widetilde{y})\,|\widetilde{\psi}\rangle\,, \tag{6.14}$$

where between (6.13) and (6.14) we have defined the dimensionless mass and the dimensionless frequency

$$\widetilde{m} = \frac{mR^2}{T_f\hbar}, \qquad\qquad \widetilde{\omega} = \omega_0 T_f. \tag{6.15}$$

Using the same argument we can define the dimensionless momentum $\widetilde{k}_0 = k_0 R$. In the remainder of the chapter we will use both the notations of (6.10) depending on the context.

We are now ready to describe the process that will produce the potential in Cartesian coordinates starting from the expression in curvilinear coordinates.

6.3.2 Conversion from curvilinear to Cartesian

In our case, we have a square region of the form $[\widetilde{x}_0,\widetilde{x}_1]\times[\widetilde{y}_0,\widetilde{y}_1]$ and we need to define a grid of sample points of size $n\times n$ included in this region fine enough to ensure the desired accuracy but at the same time the number of points cannot be excessively large, otherwise the split operation algorithm will be too time-

consuming.

With this in mind, every point can be written as a couple $(\widetilde{x}_i, \widetilde{y}_j)$ of the form

$$\begin{aligned} &(\widetilde{x}_i, \widetilde{y}_j) = (\widetilde{x}_0 + i\Delta\widetilde{x}, \widetilde{y}_0 + j\Delta\widetilde{y}) \quad \text{for} \quad i, j = 0, ..., n-1, \\ &\text{with} \qquad \Delta\widetilde{x} = \frac{\widetilde{x}_1 - \widetilde{x}_0}{n} \qquad \Delta\widetilde{y} = \frac{\widetilde{y}_1 - \widetilde{y}_0}{n}. \end{aligned} \tag{6.16}$$

Now we need to express the trapping potential in Cartesian coordinates, i.e. we need to assign to each point in the grid the corresponding value of the potential expressed in curvilinear coordinates. This problem has been solved recursively, so for each point $(\widetilde{x}_i, \widetilde{y}_j)$ we take its Euclidean distance from the curve $\vec{\mathbf{\Gamma}}(s)$ delineating the bottom of the trap:

$$d_{i,j} = min(\sqrt{(\widetilde{x}_i - \xi(\widetilde{s}))^2 + (\widetilde{y}_j - \eta(\widetilde{s}))^2}. \tag{6.17}$$

The potential relative to the point $(\widetilde{x}_i, \widetilde{y}_j)$ can then be easily defined as $\frac{1}{2}\widetilde{m}\widetilde{\omega}^2 d_{i,j}^2$ and the conversion process from curvilinear to Cartesian coordinates is represented in figure 6.1. The conversion has been performed using a collection of codes written using the Mathematica software suite [51].

The collection of n^2 triplets $(\widetilde{x}_i, \widetilde{y}_j, \frac{1}{2}\widetilde{m}\widetilde{\omega}^2 d_{i,j}^2)$ will be then stored into a data file that can be lately accessed by the C++ program to solve the Schrödinger equation. In our study, have chosen $\widetilde{x}_0 = \widetilde{y}_0 = -1.5$, $\widetilde{x}_1 = \widetilde{y}_1 = 2.5$. The number of sampling points will be discussed in section 6.5 as we have compared

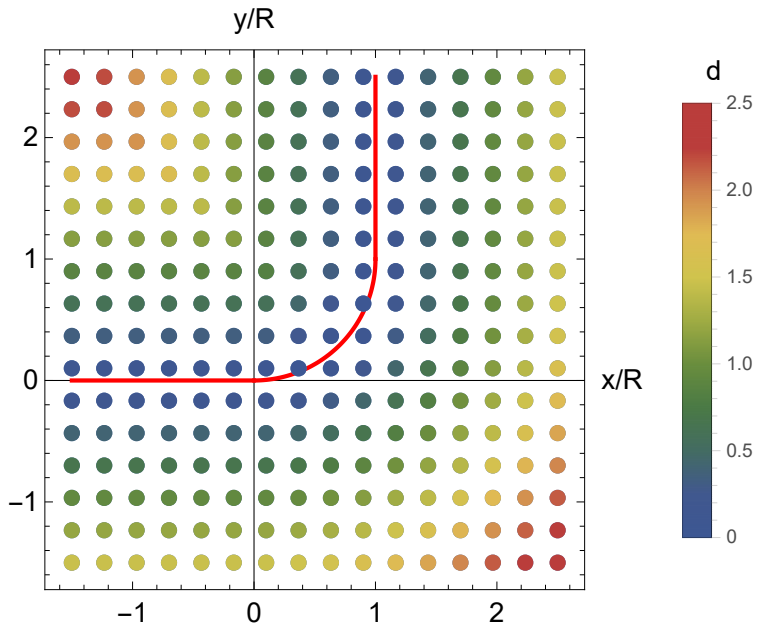


Figure 6.1: Outline of the process employed to build the potential in Cartesian coordinates: the grid is laid out (in this case we used 16 points in each dimension for simplicity) and to every point we associated its relative distance from the curve. The potential is easily obtained from the distance, via the usual formula.

the results obtained with a different number of sampling points.

In the next section we will give the definition of fidelity for this process as well as describing in detail all the parameters.

6.4 Fidelity

The fidelity of a protocol is a measure that quantifies the discrepancy between a reference, ideal, quantum state and the quantum state resulting from the application of that protocol.

For the process of a wave function moving along a waveguide, we assumed the initial state to be

$$\begin{aligned}\psi_{in} := \psi(\widetilde{x},\widetilde{y},\widetilde{t}_{in}) &= \frac{1}{\sqrt{\pi}}\left(\frac{1}{4\widetilde{\sigma}_y^2}\right)^{1/4}\left(\frac{\widetilde{\sigma}_x}{\widetilde{\sigma}_x^2+i\widetilde{t}_{in}/2\widetilde{m}}\right)^{1/2} \\ &\times \exp\left\{i\widetilde{k}_0\widetilde{x}_{in} - i\left(\widetilde{k}_0^2+\frac{1}{4\widetilde{\sigma}_y^2}\right)\frac{\widetilde{t}_{in}}{2\widetilde{m}} - \frac{(\widetilde{x}_{in}-\widetilde{x}_{in})^2}{4(\widetilde{\sigma}_x^2+i\widetilde{t}_{in}/2\widetilde{m})} - \frac{(\widetilde{y}_{in}-\widetilde{y}_0)^2}{4\widetilde{\sigma}_y^2}\right\}\end{aligned} \tag{6.18}$$

with $\widetilde{x}_{in} = -0.5$, $\widetilde{y}_{in} = 0$, $\widetilde{t}_f = 0$ and $\widetilde{\sigma}_y = \dfrac{1}{\sqrt{2\widetilde{m}\widetilde{\omega}}}$. We assumed a waveguide with transverse confining $\widetilde{\omega} = 20$ and a particle of mass $\widetilde{m} = 400$ and an initial longitudinal dispersion $\widetilde{\sigma}_x = 0.05$.We would like to stress out that ψ_{in} will be our initial wave function for every simulation in the remainder of the work, we will vary the $\widetilde{k}_0$ parameter only.

In the ideal case, the wave function would move along the curved section of the waveguide - the length of which we call L - retaining its Gaussian envelope in the transverse direction, while evolving as a free wave along the longitudinal axis. It would then leave the bent region and the final, ideal, wave function would be

$$\begin{aligned}\psi_f := \psi(\widetilde{x},\widetilde{y},\widetilde{t}_f) &= \frac{1}{\sqrt{\pi}}\left(\frac{1}{4\widetilde{\sigma}_y^2}\right)^{1/4}\left(\frac{\widetilde{\sigma}_x}{\widetilde{\sigma}_x^2+i\widetilde{t}_f/2\widetilde{m}}\right)^{1/2} \\ &\times \exp\left\{i\widetilde{k}_0\widetilde{y} - i\left(\widetilde{k}_0^2+\frac{1}{4\widetilde{\sigma}_y^2}\right)\frac{\widetilde{t}_f}{2\widetilde{m}} - \frac{(\widetilde{y}-\widetilde{y}_f)^2}{4(\widetilde{\sigma}_x^2+i\widetilde{t}_f/2\widetilde{m})} - \frac{(\widetilde{x}-\widetilde{x}_f)^2}{4\widetilde{\sigma}_y^2}\right\}\end{aligned} \tag{6.19}$$

where $\widetilde{x}_f = 1$, $\widetilde{y}_f = 1.5$ and the final time $\widetilde{t}_f$ will be evaluated classically, depending from the context. The form of (6.19) is nothing more than the final state we would expect from the evolution of the wave function along a straight

waveguide of length L, but in this case we have rotated it about $\pi/2$. The assumption we made for ψ_f can be better understood as a slow deformation of a completely straight waveguide of length L into a curved one. If the bending process is slow enough, the adiabatic theorem ensures that the wave function will stay unperturbed. This is the underlying idea of the definition of fidelity in these settings: we want to evalute the overlap between the resulting wave function obtained by the split operation method and the wave function that would result in the ideal case. The fidelity will then assume the form

$$F := |\langle \psi_{so} | \psi_f \rangle|^2 \tag{6.20}$$

where $|\psi_{so}\rangle$ is the wave function obtained numerically and $|\psi_f\rangle$ is the one from the ideal case. The situation is sketched in figure 6.2. Having defined the fidelity for this process and having set up all the different parameters, we are now ready to perform the numerical simulations and compare the performances of different shapes of waveguides as we increase the momentum of the incoming particle.

6.5 Results of numerical simulation

6.5.1 Circular bend

In order to have a reference case, we started by simulating a quantum waveguide, the shape of which is an arc of a circle. Assuming a circular bend of radius R, we obtained the potential in Cartesian coordinates following the procedure

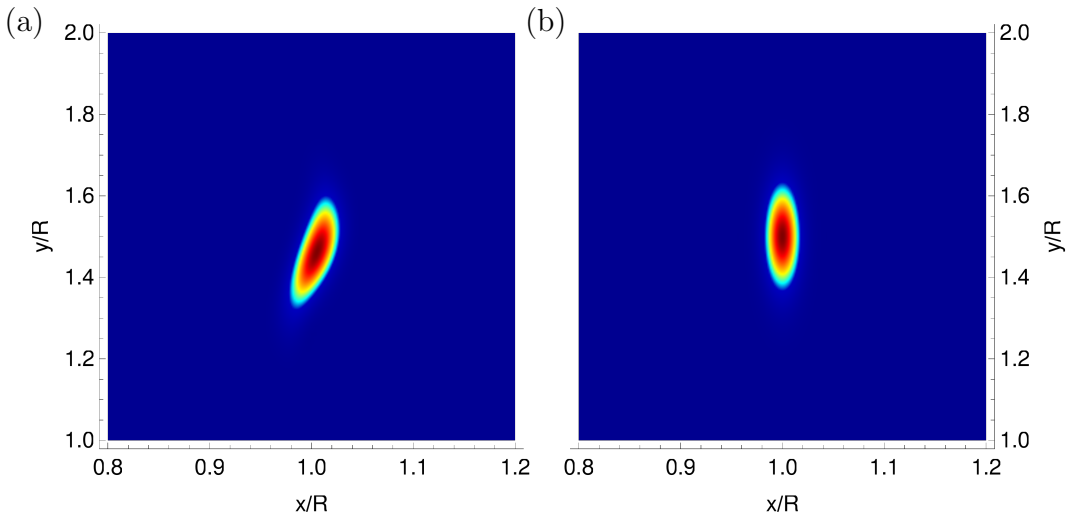


Figure 6.2: Example of comparison between a wave function obtained from a simulation (a) and the corresponding ideal wave function (b). For reference, the fidelity in this case is $F = 0.25$.

explained in section 6.3 and shown in figure 6.3. In this case we calculated the total time of the travel assuming constant velocity throughout the whole process. So, for a given $\widetilde{k}_0$, total time is simply evaluated as the ratio between the total length of the path and the velocity:

$$\widetilde{T} = \frac{L}{\widetilde{k}_0/\widetilde{m}} \quad \text{with} \quad L = 2d + \frac{\pi}{2}, \tag{6.21}$$

where $d = 0.5$ is the length of each straight section. For the ideal final wave function ψ_f (6.19), we will then use $\widetilde{t}_f = \widetilde{T}$.

At first we started with a grid composed of 1024×1024 sampling points and simulate the evolution of the wave function for different initial momenta. From

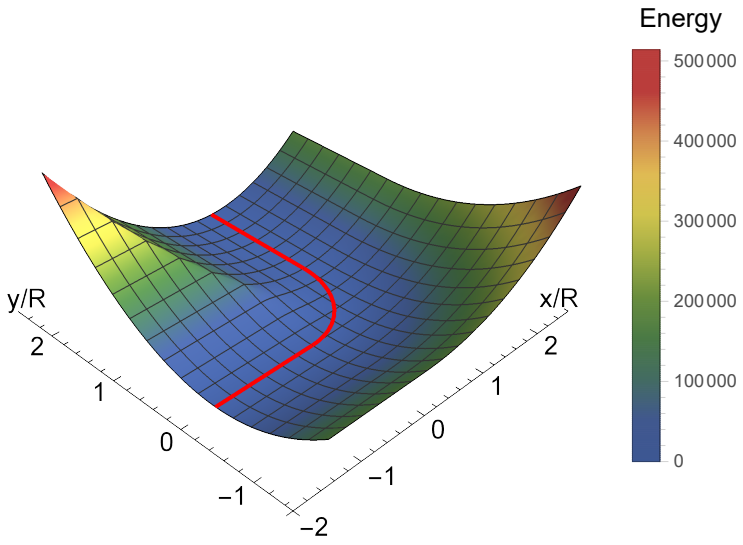


Figure 6.3: 3D depiction of the trapping potential of the circular bend which axis goes along an arc of a circle.

$\widetilde{k}_0 = 300$ we progressively increased this value by then up to 900 by steps of 10. The results of the simulation are shown in figure 6.4 and we can see the fidelity showing oscillating behaviour. Moreover, there is a dramatic drop in fidelity after $k_0 = 770$. This is quite suspect and it is probably connected to the number of sampling points we used. We have then decided to increase the number of points to a grid of 2048×2048 and evaluated the fidelities for different initial momenta around $k_0 = 770$. We then compared the results, as in figure 6.5. The fidelities are similar up to $k_0 = 770$ and for this reason we have decided, for the upcoming calculations, to reduce the maximum value of the momentum from 900 to 770 with a grid of 1024×1024 points as these values ensure the best trade-off between accuracy and time consumption. In the next section we will

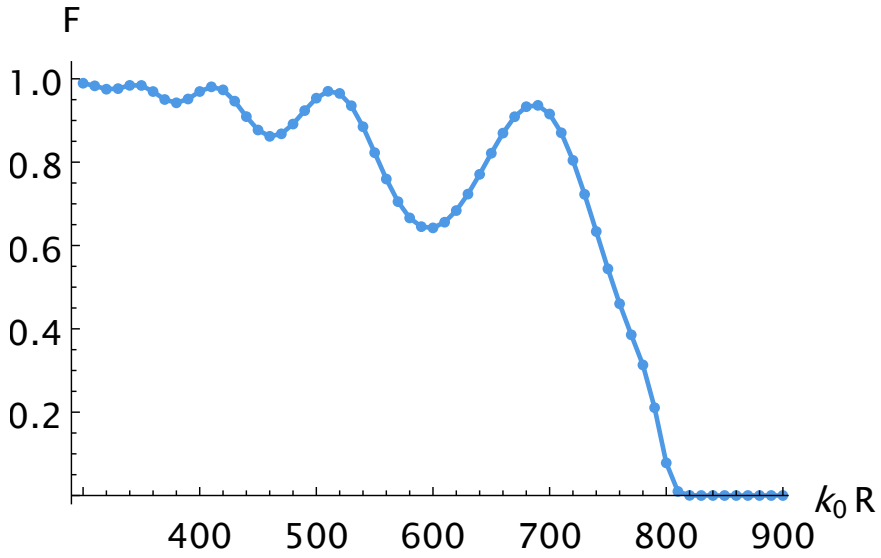


Figure 6.4: Fidelity F for the circular bend as the momentum of the incoming particle k_0 increases.

retrieve the curve that maximizes the fidelity given an initial momentum $\widetilde{k}_0$ for different curves we obtained using the approach explained earlier in chapter 5 .

6.5.2 Optimized quantum waveguide

Every curve is uniquely defined by the chosen polynomial P_n and by the parameters of the system. In particular, $\widetilde{k}_0$ and $\widetilde{\omega}$ affect the maximum transverse displacement of the particle trajectory at the middle of the curve and consequently the time $\widetilde{T}_c$ that the particle spend travelling in the curved section. So, for each $\widetilde{k}_0$ we have calculated both the corresponding $\widetilde{T}_c$ and the resulting curve $\vec{\mathbf{\Gamma}}_n$, from which we obtained the potential in Cartesian coordinates. The total

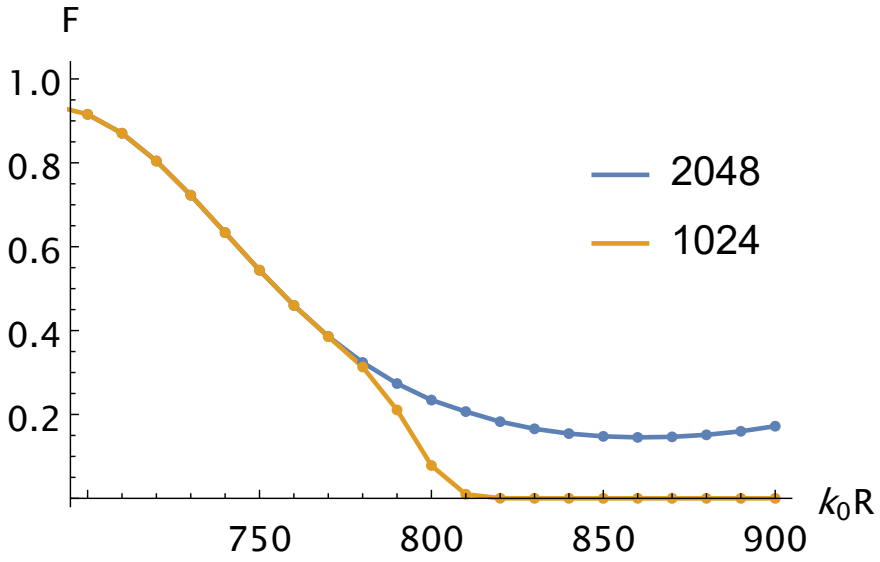


Figure 6.5: Fidelities calculated with a grid of 1024×1024 and 2048×2048 points respectively, as the momentum of the incoming particle $\widetilde{k}_0$ increases.

time $\widetilde{T}$ that will be used in the split operator method is, finally

$$\widetilde{T} = \frac{2d}{\widetilde{k}_0/\widetilde{m}} + \widetilde{T}_c. \tag{6.22}$$

Similarly to section 6.5.1, we will set $\widetilde{t}_f = \widetilde{T}$ to evaluate the ideal final wave function ψ_f.

Given the results of chapter 5, we have decided to run the simulation for different curves $\vec{\mathbf{\Gamma}}_n$ with n from 1 to 4 and for different initial momenta $\widetilde{k}_0$ to calculate the corresponding fidelities. The results are summarized in figure 6.6, where we can clearly see a big improvement in fidelity for the curves designed with the STA approach when compared to the fidelity of a waveguide where the bottom

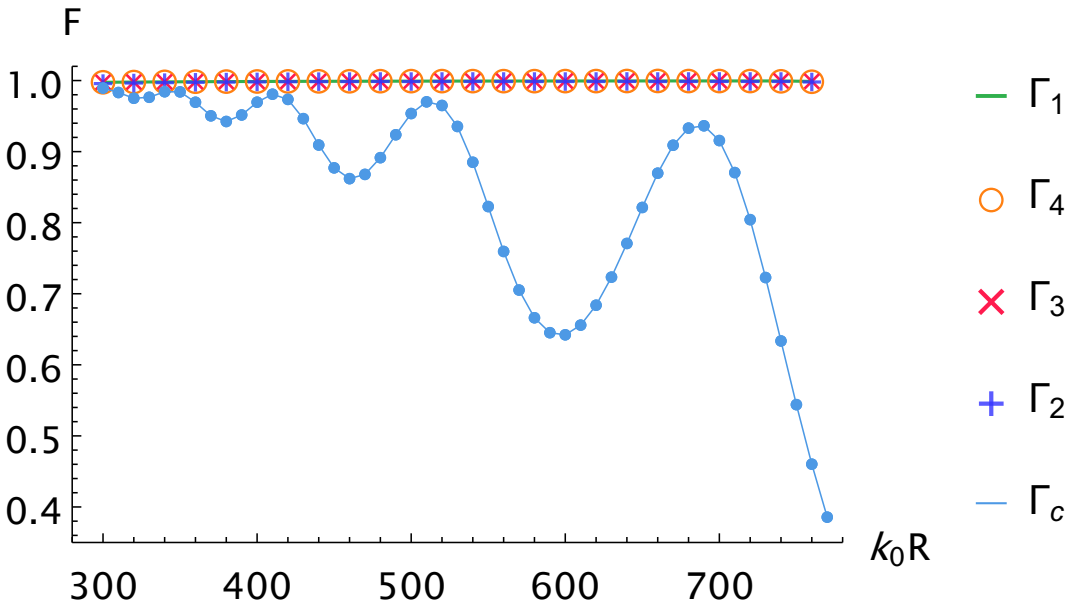


Figure 6.6: Fidelity F for different curves as the momentum $\widetilde{k}_0 = k_0 R$ increases. $\vec{\mathbf{\Gamma}}_c$ (light blue line) represents the arc of a circle, while $\vec{\mathbf{\Gamma}}_1$ (green solid line), $\vec{\mathbf{\Gamma}}_2$ (blue plus), $\vec{\mathbf{\Gamma}}_3$ (red cross), $\vec{\mathbf{\Gamma}}_4$ (orange circle) are the curves obtained from the polynomial P_1, P_2, P_3, P_4 respectively. The points overlap each other as the difference in fidelity is 10^{-5}.

of the harmonic trap follows an arc of a circle (light blue line). The fidelity of the designed curves $\vec{\mathbf{\Gamma}}_1$ to $\vec{\mathbf{\Gamma}}_4$ has been found to be greater than 0.998 for each different initial momentum $\widetilde{k}_0$, thus indicating that the shortcuts approach is very robust and gives a platform to design lossless wave guides that maximize transmission rates.

Considering the common traits that the different curves show, we have decided not to investigate the performances of the curves $\vec{\mathbf{\Gamma}}_5$ and $\vec{\mathbf{\Gamma}}_6$ as we believe the results would have not been significantly dissimilar.

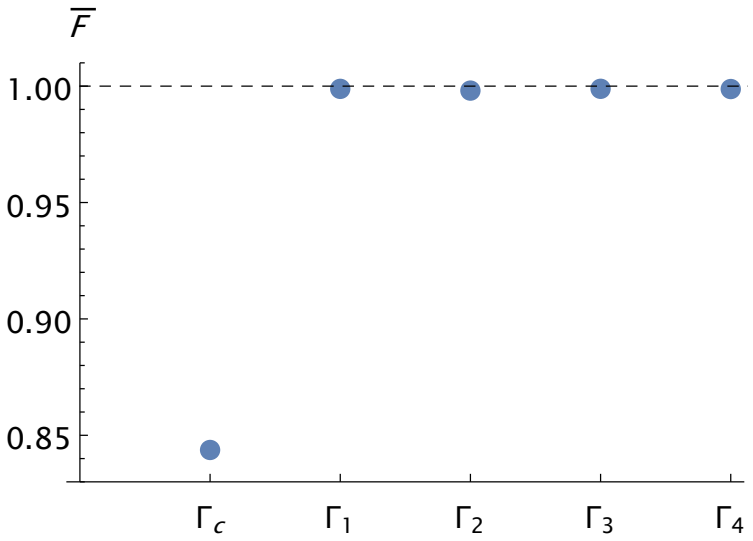


Figure 6.7: Average value of the fidelity $\overline{F}$ for the examined curves $\vec{\mathbf{\Gamma}}_c$, $\vec{\mathbf{\Gamma}}_1$, $\vec{\mathbf{\Gamma}}_2$, $\vec{\mathbf{\Gamma}}_3$, $\vec{\mathbf{\Gamma}}_4$. The dashed line corresponds to the value 1 and is set as a reference.

In order to evaluate the effectiveness of every curve, we have decided to average the fidelities of each curve for different initial momenta $\widetilde{k}_0$. This number, identified by $\overline{F}$, summarizes the overall stability of the curve and also gives us a measure to compare different shapes.

We can clearly see that the curves designed via shortcuts outperform the circular bend. Between the curves $\vec{\mathbf{\Gamma}}_n$ we cannot determine which one has the best performances, as the average fidelities are equal up to 10^{-5}, where the numerical uncertainty becomes prevailing. We believe that decreasing the value of the trapping frequency $\widetilde{\omega}$ can help highlighting the effects of the structure of the curve on the fidelity: in our settings the trapping frequency plays a dominant role and the small geometrical differences of the curves $\vec{\mathbf{\Gamma}}_n$ are suppressed by $\widetilde{\omega}$.

This concludes our study to the design of quantum waveguides using a STA-based approach. In the next chapter we will summarize the work done in this thesis and suggest some possible outlooks for future studies.

Chapter 7

Summary and future prospects

In this thesis we focused on applying a STA-based protocol to transport of quantum particle in quantum waveguides. In this chapter we will review our work and alongside we will provide outlooks that could sparkle further studies.

7.1 Conclusion

In the first chapters we reviewed the theoretical background and built the framework that helped us establishing the environment of our problem. We started by giving the definition of qubit and proceeded describing different methods to manipulate and control quantum states, effectively generating quantum waveguides by shining laser light. We then introduced the STA paradigm and presented two applications of this approach, namely counterdiabatic drive and Lewis-Reisenfeld-invariant-based inverse engineer, with the aim of applying these pro-

tocols specifically to quantum waveguides. We subsequntly concentrated toward quantum waveguides and we showed how the Hamiltonian for a general, bent waveguide changed according to the geometry of the system. This calculation helped highlighting the vital importance of the curvature function in the waveguide system.

We then proceeded and reviewed the paper that inspired this thesis [21], where a STA-based approach has been applied to a classical particle to retrieve the curve that would have met all the desired constraints. We have tested this protocol in classical settings and showed some possible extensions to this procedure testing the sensitivity of the obtained curves against different initial conditions. Finally, we gathered the results of the semi-classical approach and used them as the starting point to numerically simulate the evolution of a quantum particle moving inside bent quantum waveguides using the split operator method that has been used to compare the efficiency of different waveguide shapes. In particular we obtained remarkable results for the shapes obtained using the inverse engineer approach as opposed to the reference case (the arc of a circle). More specifically, we found that the inverse engineer waveguide shapes grant an average fidelity very close to 1, as opposed to the reference case where the average fidelity is ≈ 0.85.

In conlusion, we validate the inverse engineer approach proposed in [21] and improved upon that technique by changing the parameters governing the process to design bent quantum waveguides that have been shown to be robust and

efficient both in classical and quantum settings.

7.2 Outlooks

There are still plenty of possibilities one can investigate, starting from the results of this thesis.

An interesting study would be to have the harmonic trapping changing along the curve. In this case, instead of a constant frequency ω, we would have a function $\omega(s)$. We could connect the two straight ends with a simple arc of a circle and then inverse engineer the profile of the trapping frequency along the curve with the aim of minimizing the final transverse excitation. Of course this idea could also be extended to different curves, in particular the ones obtained inverse engineering the curvature as in chapter 5 with the hope that the two strategies would sinergies to produce waveguides that present a higher level of robustness.

Another promising prospect, this time relatoed to STA approaches to quantum waveguides, would be to use the Lagrange density technique [52–54] specializing it to curved geometry. We will give a brief overview in this section, while more details on this idea can be found in the appendix 7.2. The main idea is to write the Lagrangian as a functional of the wave function

$$\mathcal{L}(\vec{\boldsymbol{r}}, t, \psi, \psi^*), \tag{7.1}$$

and consequently the action integral in curvilinear coordinates

$$S := \int_0^T dt \int_{\mathbb{R}^2} dsdu(1 - u\gamma)\,\mathcal{L}. \tag{7.2}$$

Then, by making extra assumptions on the form of the wave function and imposing the small curvature approximation (again, more details in appendix 7.2), we are going to minimise the action integral (7.2) for a specific class of wave functions. This can be done by employing the **Euler - Lagrange** equations

$$\frac{\partial \mathcal{L}}{\partial q_i} - \frac{\mathrm{d}}{\mathrm{d}t}\frac{\partial \mathcal{L}}{\partial \dot{q}_i} = 0 \tag{7.3}$$

that can be used to calculate the desired curvature.

Lagrange density approach

Starting from the definition for the Lagrangian density in one dimension

$$\mathcal{L}(x,t,\psi,\psi^*) \doteqdot \frac{i\hbar}{2}\left(\psi\frac{\partial\psi^*}{\partial t} - \psi^*\frac{\partial\psi}{\partial t}\right) + \frac{\hbar^2}{2m}\left|\frac{\partial\psi}{\partial x}\right|^2 + V(x)|\psi|^2, \tag{4}$$

we can write the more general form as

$$\mathcal{L}(\vec{\boldsymbol{r}},t,\psi,\psi^*) = \frac{i\hbar}{2}\left(\psi\frac{\partial\psi^*}{\partial t} - \psi^*\frac{\partial\psi}{\partial t}\right) + \frac{\hbar^2}{2m}\left|\vec{\boldsymbol{\nabla}}\psi\right|^2 + V(\vec{\boldsymbol{r}})|\psi|^2 \tag{5}$$

with $\psi = \psi(t,\vec{\boldsymbol{r}})$.

In particular, we can apply this formula to $\mathbb{R}^2$ and move to curvilinear coordinates. The change of coordinates modifies the gradient operator

$$\left(\frac{\partial}{\partial x},\frac{\partial}{\partial y}\right) \longrightarrow \left(\frac{1}{1-u\gamma}\frac{\partial}{\partial s},\frac{\partial}{\partial u}\right) \tag{6}$$

and in turn

$$\left|\vec{\boldsymbol{\nabla}}\psi\right|^2 = \vec{\boldsymbol{\nabla}}\psi\cdot\vec{\boldsymbol{\nabla}}\psi^* = \left(\frac{1}{1-u\gamma}\frac{\partial\psi}{\partial s}, \frac{\partial\psi}{\partial u}\right)\cdot\begin{pmatrix}\frac{1}{1-u\gamma}\frac{\partial\psi^*}{\partial s}\\ \frac{\partial\psi^*}{\partial u}\end{pmatrix} = \frac{1}{(1-u\gamma)^2}\left|\frac{\partial\psi}{\partial s}\right|^2 + \left|\frac{\partial\psi}{\partial u}\right|^2. \tag{7}$$

Assuming the wave function is a stationary solution of the Schrödinger equation, we can write

$$\psi(s,u,t) \to e^{-\frac{iEt}{\hbar}}\phi(s,u), \tag{8}$$

so we have

$$\begin{aligned}&\frac{i\hbar}{2}\left(\psi\frac{\partial\psi^*}{\partial t} - \psi^*\frac{\partial\psi}{\partial t}\right) = \frac{i\hbar}{2}\left(e^{-\frac{iEt}{\hbar}}\phi\frac{iE}{\hbar}e^{\frac{iEt}{\hbar}}\phi^* - e^{\frac{iEt}{\hbar}}\phi^*\left(-\frac{iE}{\hbar}\right)e^{-\frac{iEt}{\hbar}}\phi\right)\\ &= \frac{i\hbar}{2}\left(\frac{2iE}{\hbar}\right)|\phi|^2 = -E|\phi|^2.\end{aligned} \tag{9}$$

Moreover,

$$\left|\vec{\boldsymbol{\nabla}}\psi\right|^2 = \left|\vec{\boldsymbol{\nabla}}\phi\right|^2. \tag{10}$$

The action integral is then defined as

$$S \doteqdot \int_0^T dt \int_{\mathbb{R}^2} dxdy\,\mathcal{L}. \tag{11}$$

We need to perform the coordinates transformation for the differential forms in the integral as well.

Given the transformation, the differential two form changes according to

$$dxdy = (1 - u\gamma)dsdu \tag{12}$$

and we can finally write the action integral in curvilinear coordinates as

$$\begin{aligned} S &= \int_0^T \int_{\mathbb{R}^2} dsdu \; - E|\phi|^2 + \frac{1}{(1-u\gamma)} \frac{\hbar^2}{2m} \left| \frac{\partial \psi}{\partial s} \right|^2 \\ &+ (1-u\gamma) \frac{\hbar^2}{2m} \left| \frac{\partial \psi}{\partial u} \right|^2 + (1-u\gamma) V_{ext}(s,u) |\psi|^2 \\ &= -ET + \int_0^T \int_{\mathbb{R}^2} dsdu \, \frac{1}{(1-u\gamma)} \frac{\hbar^2}{2m} \left| \frac{\partial \psi}{\partial s} \right|^2 \\ &+ (1-u\gamma) \frac{\hbar^2}{2m} \left| \frac{\partial \psi}{\partial u} \right|^2 + (1-u\gamma) V_{ext}(s,u) |\psi|^2 \end{aligned} \tag{13}$$

where the ET terms is obtained exploiting the normalization of the wave function and we can see that does not have any significant contribution to the calculation of (13) as it is just an overall constant factor and it will be neglected when evaluating the action integral. As a reminder, we recall from (4.29) that $V_{ext}(s,u) = V(s,u) + V_\perp(s,u)$ where

$$V(s,u) := -\frac{\gamma^2}{4(1-u\gamma)^2} - \frac{u\ddot{\gamma}}{2(1-u\gamma)^3} - \frac{5}{4} \frac{u^2 \dot{\gamma}^2}{(1-u\gamma)^4} \tag{14}$$

is the induced potential and

$$V_\perp(s,u) = \frac{1}{2}\omega^2 u^2 \tag{15}$$

is the harmonic confinement potential (we have tacitely assumed a trapping frequency changing along the curve, $\omega(s)$).

We now need to make an assumption for the wave function ansatz: the solution of the Hamiltonian in the straight segment is a travelling wave with Gaussian envelope along the transverse axis. It will be of the form

$$\phi_{str}(s,u) = \left(\frac{m\Omega(s)}{\pi\hbar}\right)^{\frac{1}{4}} exp\left[-\frac{m\Omega(s)u^2}{2\hbar} + i\kappa s\right] \tag{16}$$

where we would like to point out the fact that the $\Omega(s)$ is different from $\omega(s)$ of $V_\perp$, since we allow the wave function the freedom to react to the change of trapping frequency.

Moreover, we can note that (16) has an explicit dependence from s, so it can be written as a product of two different functions, each dependent from a distinct variable

$$\phi_{str}(s,u) = \left(\frac{m\Omega(s)}{\pi\hbar}\right)^{\frac{1}{4}} \upsilon(u)\sigma(s) \tag{17}$$

where

$$\upsilon(u) = e^{-\frac{m\Omega(s)u^2}{2\hbar}} \tag{18}$$

$$\sigma(s) = e^{i\kappa s} \tag{19}$$

The curvature will introduce mixing between s and u, hence the solution of the

curved Hamiltonian cannot be factored out, thus our ansatz will be

$$\phi(s,u) = \left(\frac{m\Omega(s)}{\pi\hbar}\right)^{\frac{1}{4}} exp\left[-\frac{m\Omega(s)u^2}{2\hbar} + if(s,u)\right]. \tag{20}$$

In this case $f(s,u)$ is an auxiliary function that reflects the symmetry breaking caused by the curvature.

Unsurprisingly, (13) is not analitically solvable, so we need to introduce some approximations that will help tackle the problem. Firstly, we impose the small curvature approximation, in other words we write $\gamma(s) = \lambda\zeta(s)$ and then write a series expansion in terms of λ. In this case we expand λ up to the second order

$$\gamma(s) \approx \lambda\zeta(s) + O(\lambda^2). \tag{21}$$

We also assume that the auxiliary function $f(s,u)$ could be separable to a certain degree, i.e. we set

$$f(s,y) = f_0(s) + uf_1(s) + u^2 f_2(s) \tag{22}$$

where $f_i(s)$ is another set of auxiliary functions.

Imposing these approximations helps us solving the action integral with respect to the u variable letting us obtaining a Lagrange functional of the type

$$\mathcal{L} = \mathcal{L}(\omega, f_0, f_1, f_2). \tag{23}$$

Now every argument of (23) can be used as an indipendent variable to obtain the **Euler - Lagrange** equations.

$$\frac{\partial \mathcal{L}}{\partial q_i} - \frac{\mathrm{d}}{\mathrm{d}t}\frac{\partial \mathcal{L}}{\partial \dot{q}_i} = 0. \tag{24}$$

We finally obtained a set of four differential equations that can be solved to calculate the resulting curvature.

Bibliography

[1] M.A. Nielsen and I.L. Chuang. *Quantum Computation and Quantum Information: 10th Anniversary Edition*. Cambridge University Press, 2010.

[2] Anargyros Papageorgiou and Joseph F. Traub. "Measures of quantum computing speedup". In: *Phys. Rev. A* 88 (2 Aug. 2013), p. 022316.

[3] Aram W. Harrow and Ashley Montanaro. "Quantum computational supremacy". In: *Nature* 549.7671 (Sept. 2017), pp. 203–209.

[4] Wolfgang Scherer. *Introduction*. Cham: Springer International Publishing, 2019, pp. 1–9.

[5] Pulak Ranjan Giri and Vladimir E. Korepin. "A review on quantum search algorithms". In: *Quantum Information Processing* 16.12 (Nov. 2017), p. 315.

[6] P. W. Shor. "Algorithms for quantum computation: discrete logarithms and factoring". In: (Nov. 1994), pp. 124–134.

[7] Benjamin Schumacher. "Quantum coding". In: *pra* 51.4 (Apr. 1995), pp. 2738–2747.

[8] Xiaolong Liu and Mark C. Hersam. “2D materials for quantum information science”. In: *Nature Reviews Materials* 4.10 (Oct. 2019), pp. 669–684.

[9] Charles H. Bennett et al. “Teleporting an unknown quantum state via dual classical and Einstein-Podolsky-Rosen channels”. In: *Phys. Rev. Lett.* 70 (13 Mar. 1993), pp. 1895–1899.

[10] M. A. Bashar et al. “A Review and Prospects of Quantum Teleportation”. In: *2009 International Conference on Computer and Automation Engineering*. Mar. 2009, pp. 213–217.

[11] S. Pirandola et al. “Advances in quantum teleportation”. In: *Nature Photonics* 9.10 (Oct. 2015), pp. 641–652.

[12] Charles H. Bennett and Stephen J. Wiesner. “Communication via one- and two-particle operators on Einstein-Podolsky-Rosen states”. In: *Phys. Rev. Lett.* 69 (20 Nov. 1992), pp. 2881–2884.

[13] X. Liu et al. “General scheme for superdense coding between multiparties”. In: *Physical Review A - PHYS REV A* 65 (Jan. 2002).

[14] T. Schaetz et al. “Quantum Dense Coding with Atomic Qubits”. In: *Phys. Rev. Lett.* 93 (4 July 2004), p. 040505.

[15] Sergei Slussarenko and Geoff J. Pryde. “Photonic quantum information processing: A concise review”. In: *Applied Physics Reviews* 6.4 (2019), p. 041303.

[16] Christoph Kloeffel and Daniel Loss. "Prospects for Spin-Based Quantum Computing in Quantum Dots". In: *Annual Review of Condensed Matter Physics* 4.1 (2013), pp. 51–81.

[17] D. Leibfried et al. "Quantum dynamics of single trapped ions". In: *Rev. Mod. Phys.* 75 (1 Mar. 2003), pp. 281–324.

[18] Kovařík H. Exner P. *Quantum Waveguides*. 2015.

[19] D. Guéry-Odelin et al. "Shortcuts to adiabaticity: Concepts, methods, and applications". In: *Rev. Mod. Phys.* 91 (4 Oct. 2019), p. 045001.

[20] Erik Torrontegui et al. "Chapter 2 - Shortcuts to Adiabaticity". In: *Advances in Atomic, Molecular, and Optical Physics*. Ed. by Ennio Arimondo, Paul R. Berman, and Chun C. Lin. Vol. 62. Advances In Atomic, Molecular, and Optical Physics. Academic Press, 2013, pp. 117–169.

[21] François Impens, Romain Duboscq, and David Guéry-Odelin. "Quantum Control beyond the Adiabatic Regime in 2D Curved Matter-Wave Guides". In: *Phys. Rev. Lett.* 124 (25 June 2020), p. 250403.

[22] Francesco Cataliotti et al. "Dynamics of a trapped Bose–Einstein condensate in the presence of a one-dimensional optical lattice". In: *J. Opt. B: Quantum Semiclass. Opt* 5 (Apr. 2003), pp. 1464–426655739.

[23] L. Isenhower et al. "Demonstration of a Neutral Atom Controlled-NOT Quantum Gate". In: *Phys. Rev. Lett.* 104 (1 Jan. 2010), p. 010503.

[24] Harry Levine et al. “Parallel Implementation of High-Fidelity Multiqubit Gates with Neutral Atoms”. In: *Phys. Rev. Lett.* 123 (17 Oct. 2019), p. 170503.

[25] I. I. Rabi. “Space Quantization in a Gyrating Magnetic Field”. In: *Phys. Rev.* 51 (8 Apr. 1937), pp. 652–654.

[26] Leonard Mandel and Emil Wolf. *Optical Coherence and Quantum Optics*. Cambridge University Press, 1995.

[27] Immanuel Bloch. “Ultracold quantum gases in optical lattices”. In: *Nature Physics* 1.1 (Oct. 2005), pp. 23–30.

[28] Kevin Henderson et al. “Experimental demonstration of painting arbitrary and dynamic potentials for Bose-Einstein condensates”. In: *New Journal of Physics* 11 (Feb. 2009).

[29] Thomas A Bell et al. “Bose–Einstein condensation in large time-averaged optical ring potentials”. In: *New Journal of Physics* 18.3 (Mar. 2016), p. 035003.

[30] M. Lacki, P. Zoller, and M. A. Baranov. “Stroboscopic painting of optical potentials for atoms with subwavelength resolution”. In: *Phys. Rev. A* 100 (3 Sept. 2019), p. 033610.

[31] G. Gauthier et al. “Direct imaging of a digital-micromirror device for configurable microscopic optical potentials”. In: *Optica* 3.10 (Oct. 2016), pp. 1136–1143.

[32] C Ryu and M G Boshier. "Integrated coherent matter wave circuits". In: *New Journal of Physics* 17.9 (Sept. 2015), p. 092002.

[33] Dustin Stuart and Axel Kuhn. "Single-atom trapping and transport in DMD-controlled optical tweezers". In: *New Journal of Physics* 20.2 (Feb. 2018), p. 023013.

[34] Xi Chen et al. "Fast Optimal Frictionless Atom Cooling in Harmonic Traps: Shortcut to Adiabaticity". In: *Phys. Rev. Lett.* 104 (6 Feb. 2010), p. 063002.

[35] M. Born and V. Fock. "Beweis des Adiabatensatzes". In: *Zeitschrift fur Physik* 51.3-4 (Mar. 1928), pp. 165–180.

[36] Mustafa Demirplak and Stuart A. Rice. "Adiabatic Population Transfer with Control Fields". In: *The Journal of Physical Chemistry A* 107.46 (2003), pp. 9937–9945.

[37] Mustafa Demirplak and Stuart A. Rice. "Assisted Adiabatic Passage Revisited". In: *The Journal of Physical Chemistry B* 109.14 (2005). PMID: 16851769, pp. 6838–6844.

[38] Mustafa Demirplak and Stuart A. Rice. "On the consistency, extremal, and global properties of counterdiabatic fields". In: *The Journal of Chemical Physics* 129.15 (2008), p. 154111.

[39] M V Berry. "Transitionless quantum driving". In: *Journal of Physics A: Mathematical and Theoretical* 42.36 (Aug. 2009), p. 365303.

[40] Xi Chen et al. "Shortcut to Adiabatic Passage in Two- and Three-Level Atoms". In: *Phys. Rev. Lett.* 105 (12 Sept. 2010), p. 123003.

[41] A Kiely and A Ruschhaupt. "Inhibiting unwanted transitions in population transfer in two- and three-level quantum systems". In: *Journal of Physics B: Atomic, Molecular and Optical Physics* 47.11 (May 2014), p. 115501.

[42] A Ruschhaupt et al. "Optimally robust shortcuts to population inversion in two-level quantum systems". In: *New Journal of Physics* 14.9 (Sept. 2012), p. 093040.

[43] Utkan Güngördü et al. "Dynamical invariants for quantum control of four-level systems". In: *Phys. Rev. A* 86 (6 Dec. 2012), p. 062312.

[44] H. R. Lewis and W. B. Riesenfeld. "An Exact Quantum Theory of the Time-Dependent Harmonic Oscillator and of a Charged Particle in a Time-Dependent Electromagnetic Field". In: *Journal of Mathematical Physics* 10.8 (1969), pp. 1458–1473.

[45] K. Lin and R. Jaffe. "Bound States and Threshold Resonances in Quantum Wires with Circular Bends". In: *Physical Review B* 54 (Jan. 1996).

[46] Iain J Clark and Anthony J Bracken. "Bound states in tubular quantum waveguides with torsion". In: *Journal of Physics A: Mathematical and General* 29.15 (Aug. 1996), pp. 4527–4535.

[47] S Schwartz et al. "One-dimensional description of a Bose–Einstein condensate in a rotating closed-loop waveguide". In: *New Journal of Physics* 8.8 (Aug. 2006), pp. 162–162.

[48] Adolfo del Campo, Malcolm G. Boshier, and Avadh Saxena. "Bent waveguides for matter-waves: supersymmetric potentials and reflectionless geometries". In: *Scientific Reports* 4.1 (June 2014), p. 5274.

[49] J. A. Fleck, J. R. Morris, and M. D. Feit. "Time-dependent propagation of high-energy laser beams through the atmosphere: II". In: *Applied physics* 14.1 (Sept. 1977), pp. 99–115.

[50] Shaik Qadeer, Mohammed Zafar Ali Khan, and Mohammed Yousuf khan. "Computation of Discrete Fourier Transform (FFT): A Review Article". In: *Proceeding of the Second International Conference on Microelectronics, Computing & Communication Systems (MCCS 2017)*. Ed. by Vijay Nath and Jyotsna Kumar Mandal. Singapore: Springer Singapore, 2019, pp. 381–390.

[51] Inc. Wolfram Research. "Mathematica, Version 12.2". In: (). Champaign, IL, 2020.

[52] Donald Kobe. "Lagrangian Densities and Principle of Least Action in Nonrelativistic Quantum Mechanics". In: (Jan. 2008).

[53] Peter Sigmund and George Basbas. "A Time-Dependent Analog of the Ritz Variational Principle in Nonrelativistic Quantum Mechanics". In: *Physica Scripta* 32 (Nov. 2006), p. 482.

[54] E. Deumens et al. "Time-dependent theoretical treatments of the dynamics of electrons and nuclei in molecular systems". In: *Rev. Mod. Phys.* 66 (3 July 1994), pp. 917–983.